

University of Dundee

A small-molecule PI3K α activator for cardioprotection and neuroregeneration

Gong, Grace Q.; Bilanges, Benoit; Allsop, Ben; Masson, Glenn R.; Robertson, Victoria; Askwith, Trevor

Published in:
Nature

DOI:
[10.1038/s41586-023-05972-2](https://doi.org/10.1038/s41586-023-05972-2)

Publication date:
2023

Licence:
CC BY

Document Version
Peer reviewed version

[Link to publication in Discovery Research Portal](#)

Citation for published version (APA):

Gong, G. Q., Bilanges, B., Allsop, B., Masson, G. R., Robertson, V., Askwith, T., Oxenford, S., Madsen, R. R., Conduit, S. E., Bellini, D., Fitzek, M., Collier, M., Najam, O., He, Z., Wahab, B., McLaughlin, S. H., Chan, A. W. E., Feierberg, I., Madin, A., ... Vanhaesebroeck, B. (2023). A small-molecule PI3K α activator for cardioprotection and neuroregeneration. *Nature*, 618, 159-168. <https://doi.org/10.1038/s41586-023-05972-2>

General rights

Copyright and moral rights for the publications made accessible in Discovery Research Portal are retained by the authors and/or other copyright owners and it is a condition of accessing publications that users recognise and abide by the legal requirements associated with these rights.

- Users may download and print one copy of any publication from Discovery Research Portal for the purpose of private study or research.
- You may not further distribute the material or use it for any profit-making activity or commercial gain.
- You may freely distribute the URL identifying the publication in the public portal.

Take down policy

If you believe that this document breaches copyright please contact us providing details, and we will remove access to the work immediately and investigate your claim.

1 Main body of text: 4618 words excluding references
2 Figures: 5 primary figures; 9 extended data figures, 2 Supplementary Figures
3 Tables: 9 supplementary tables
4 Videos: 4 supplementary videos

6 **A small molecule PI3K α activator for cardioprotection and neuroregeneration**

8 **Grace Q Gong¹, Benoit Bilanges¹, Ben Allsop², Glenn R Masson^{3,4}, Victoria Robertson⁵, Trevor Askwith², Sally Oxenford², Ralitsa R Madsen¹, Sarah E Conduit¹, Dom Bellini³, Martina Fitzek⁶, Matt Collier⁶, Osman Najam⁷, Zhenhe He⁷, Ben Wahab⁸, Stephen H McLaughlin³, AW Edith Chan⁹, Isabella Feierberg¹⁰, Andrew Madin¹¹, Daniele Morelli¹⁴, Amandeep Bhamra¹², Vanesa Vinciauskaite⁴, Karen E. Anderson¹³, Silvia Surinova¹², Nikos Pinotsis¹⁴, Elena Lopez-Guadamillas¹, Matthew Wilcox⁵, Alice Hooper², Chandni Patel², Maria A Whitehead¹, Tom D Bunney¹⁵, Len R Stephens¹³, Phillip T Hawkins¹³, Matilda Katan¹⁵, Derek M Yellon^{7,#}, Sean M Davidson^{7,#}, David M Smith^{16,#}, James B Phillips^{5,#}, Richard Angell^{2,8,#}, Roger L Williams^{3,#}, & Bart Vanhaesebroeck^{1✉}**

17 ¹Cell Signalling, Cancer Institute, University College London, UK.

18 ²Drug Discovery Group, Translational Research Office, University College London, London, UK.

19 ³Medical Research Council Laboratory of Molecular Biology, Cambridge, UK.

20 ⁴Division of Cellular Medicine, School of Medicine, University of Dundee, UK.

21 ⁵UCL Centre for Nerve Engineering, UCL School of Pharmacy, University College London, London, UK.

22 ⁶Hit Discovery, Discovery Sciences, R&D, AstraZeneca, Alderley Park, Cheshire, UK.

23 ⁷The Hatter Cardiovascular Institute, University College London, London, UK.

24 ⁸Medicines Discovery Institute, School of Biosciences, Cardiff University, Cardiff CF10 3AT, UK.

25 ⁹Wolfson Institute for Biomedical Research, University College London, London, UK.

26 ¹⁰Molecular AI, Discovery Sciences, R&D, AstraZeneca, Waltham MA, USA.

27 ¹¹Hit Discovery, Discovery Sciences, R&D, AstraZeneca, Cambridge, UK.

28 ¹²Proteomics Research Translational Technology Platform, Cancer Institute, University College London, London, UK.

30 ¹³Signalling Programme, Babraham Institute, Cambridge, UK.

31 ¹⁴Institute of Structural and Molecular Biology, Birkbeck College, London, UK.

32 ¹⁵Institute of Structural and Molecular Biology, Division of Biosciences, University College London, London, UK.

34 ¹⁶Emerging Innovations, Discovery Sciences, R&D, AstraZeneca, Cambridge, UK.

36 [#]*Joint senior authors*

37 [✉]*Corresponding author* e-mail: bart.vanh@ucl.ac.uk

39 **Main text**

41 **Abstract: Harnessing the potential beneficial effects of kinase signalling through the generation of**
42 **direct kinase activators remains an underexplored area of drug development¹⁻⁵. This also applies to**
43 **the PI 3-kinase (PI3K) signalling pathway, which has been extensively targeted by inhibitors for**
44 **conditions with PI3K overactivation, such as cancer and immune dysregulation. Here we report on**
45 **the discovery of UCL-TRO-1938 (further referred to as 1938), a small molecule activator of the PI3K α**
46 **isoform, a critical effector of growth factor signalling. 1938 allosterically activates PI3K α through a**
47 **unique mechanism, by enhancing multiple steps of the PI3K α catalytic cycle, and causes both local**
48 **and global conformational changes in the PI3K α structure. This compound is selective for PI3K α over**
49 **other PI3K isoforms and multiple protein and lipid kinases. It transiently activates PI3K signalling in**
50 **all rodent and human cells tested, resulting in cellular responses such as proliferation and neurite**
51 **outgrowth. In rodent models, acute treatment with 1938 provides cardioprotection from ischaemia**

52 reperfusion injury and, upon local administration, enhances nerve regeneration following nerve
 53 crush. This study identifies a unique chemical tool to directly probe PI3K α signalling and a novel
 54 approach to modulate PI3K activity, widening the therapeutic potential of targeting these enzymes,
 55 through short-term activation for tissue protection and regeneration. Our findings illustrate the
 56 potential of activating kinases for therapeutic benefit, a currently largely untapped area of drug
 57 development.

58 Introduction

59 Compared to the development of protein and lipid kinase inhibitors, efforts to generate
 60 pharmacological activators to harness the beneficial activities of some of these enzymes, such as in
 61 tissue regeneration and protection, wound healing, immune stimulation and metabolic sensitization,
 62 have been very limited¹⁻⁵.

63 Class IA PI3Ks signal downstream of tyrosine kinases, G protein-coupled receptors and small
 64 GTPases to regulate cell metabolism, growth, proliferation and migration. They consist of a p110 α , β
 65 or δ catalytic subunit and a p85 regulatory subunit (further referred to as PI3K α , PI3K β and PI3K δ),
 66 with a broad tissue distribution (p110 α , p110 β) or enriched in leukocytes (p110 δ)^{6,7}. Overactivation
 67 of class IA PI3Ks and their effectors AKT and mTORC1 in cancer and the immune system has driven
 68 extensive PI3K pathway inhibitor development⁶.

69 PI3K pathway *activation* could also be of therapeutic benefit in tissue protection and regeneration.
 70 PI3K inhibition dampens the protective effect of growth factors and other agents in models of
 71 cell/tissue damage⁸⁻¹¹. This includes protection from ischaemia-reperfusion injury (IRI) (such as in
 72 neurons following a stroke^{12,13} and in cardiomyocytes following myocardial infarction¹⁴), protection
 73 from ionising radiation¹⁵, enhancement of tissue/wound repair^{8,16} and neuro-
 74 protection/regeneration¹⁷⁻²⁰.

75 Genetic strategies of PI3K pathway activation tested in this context include expression of activated
 76 alleles of PI3K α ²¹ or AKT²², or deletion/knockdown of PTEN, a lipid phosphatase that downregulates
 77 PI3K signalling^{8,23}. Non-genetic PI3K pathway activators include p85-binding phospho-peptides^{17,24},
 78 the AKT-activating small molecule SC79^{25,26} and PTEN inhibitors^{8,27}. These agents have poor drug-like
 79 properties, obscure mechanisms of PI3K pathway activation, and poor selectivity for their target
 80 proteins.

81 A screen for PI3K α activators

82 We conducted an unbiased high throughput screen for small molecule activators of recombinant
 83 human p110 α /p85 α with liposomes mimicking the plasma membrane composition, enriched with 5%
 84 phosphatidylinositol(4,5)bisphosphate (PIP₂), the natural PI3K α substrate. Confirmed hits were
 85 screened by a fluorescence polarisation assay (an orthogonal assay for lipid kinase activity) and
 86 microscale thermophoresis (to test for direct PI3K α binding). Validated hits were investigated for the
 87 generation of phospho-S473-AKT (pAKT^{S473}) in the human A549 cell line. Subsequent medicinal
 88 chemistry cellular potency (as measured by pAKT^{S473} in A549) led to the generation of UCL-TRO-1938
 89 (Fig. 1a), further referred to as 1938.

90 1938 is an allosteric activator of PI3K α

91 1938 is a drug-like compound (MW <500, cLogP <5), with an EC₅₀ of ~60 μ M for PI3K α (assessed by *in*
 92 *vitro* lipid kinase activity) and a *K*_d for PI3K α of 36 \pm 5 μ M and 16 \pm 2 μ M (determined by surface plasmon
 93 resonance and by differential scanning fluorimetry, respectively; Extended Data Fig. 1a,b). 1938-
 94 stimulated PI3K α activity was fully inhibited by the nanomolar potency ATP-competitive PI3K α -
 95 selective inhibitor BYL719²⁸ (Fig. 1b, Extended Data Fig. 1c).

96 1938 activates PI3K α but not PI3K β or PI3K δ (Fig. 1c). This contrasts with activation of all class IA
 97 PI3K isoforms by pY (Extended Data Fig. 1d), a bis-phosphorylated phosphopeptide (based on a PDGF-
 98 receptor peptide phosphorylated on Tyr-740 and Tyr-751²⁹) that mimicks tyrosine-phosphorylated
 99 peptides in receptors and adaptor proteins that engage p85 α SH2 domains to release p85-mediated
 100
 101
 102

103 PI3K inhibition²⁹.

104 Like pY, 1938 increased the *k_{cat}* of PI3K α (Fig. 1d). Unlike pY, which did not affect the *K_m* of PI3K α
 105 for ATP, 1938 slightly decreased *K_m* at activator concentrations of 1 and 10 μ M, but not at 30 μ M (Fig.
 106 1d). 1938 also induced increased PI3K α binding to lipid membranes, to a maximum level of about half
 107 of that induced by pY (Fig. 1e).

108 Combination of a saturating concentration of pY with 1938 (Fig. 1f, left), led to synergistic PI3K α
 109 activation (Fig. 1f, right), indicating that 1938 activates PI3K α via a different mechanism or enhances
 110 activatory events beyond those induced by pY. This synergy is unlikely to involve changes in membrane
 111 binding, given that the combination of 1938 with pY did not further increase PI3K α membrane
 112 association beyond that induced by pY (Fig. 1e).

113 Oncogenic mutants of p110 α each activate p85 α /p110 α through different mechanisms²⁹. 1938
 114 activated the G106V, N345K and H1047R mutants to levels comparable with stimulation with pY.
 115 Although the E545K mutant was insensitive to pY stimulation, as previously shown²⁹, it could be
 116 further activated by 1938 (Fig. 1g). Co-stimulation using 1938 with pY also led to a synergistic
 117 activation of G106V and N345K, and additive activation of H1047R (Fig. 1g).

118 In summary, 1938 does not specifically mimic the mechanism of activation of any single oncogenic
 119 p110 α mutation tested, but instead it stimulates PI3K α by enhancing multiple events associated with
 120 natural and mutation-mediated PI3K α activation.

121

122 1938 changes the conformation of PI3K α

123 Class IA PI3K activation upon binding to phosphorylated tyrosine motifs in proteins occurs through the
 124 release of inhibitory interactions between p85 and p110, by: (1) release of p85 α -nSH2 and p85 α -iSH2
 125 from the p110 α -helical and p110 α -C2 domains, respectively; (2) movement of the N-terminal p85-
 126 binding domain in p110 α relative to the rest of the catalytic subunit and (3) interaction of the p110 α
 127 kinase domain with the lipid membrane²⁹.

128 HDX-MS of PI3K α incubated with 1938 revealed changes in protection that occurred mostly
 129 outside the ATP-binding site (Fig. 2a; Extended Data Fig. 2a-c; Supplementary Table 1). There was
 130 protection of the linker between the p110 α -RBD and p110 α -C2 domains, and of a small loop consisting
 131 of amino acids (AA) 1002-1016 of p110 α , suggesting that the latter region might be the 1938 binding
 132 site on p110 α (further referred to as the kinase/activator interface).

133 Increases in solvent exchange rate in several additional regions were also observed: the p85 α -
 134 nSH2 domain (AA326-333 and 371-380), the p85 α -iSH2 domain (AA555-570) and multiple regions in
 135 p110 α , namely (from N- to C-terminus): AA444-455 (interface between p85 α -iSH2 and p110 α -C2
 136 domains), AA532-551 (interface between p85 α -nSH2 and p110 α -helical domains), and AA848-859
 137 (ATP-binding site). These changes are compatible with the notion that 1938 activates PI3K α by
 138 disrupting inhibitory contacts at the p85 α -nSH2/p110 α -helical and p85 α -iSH2/p110 α -C2 domains,
 139 leading to decreased inhibition of p85 α on p110 α .

140 HDX-MS with BYL719 produced a characteristic ATP-competitive footprint on PI3K α , with strong
 141 protections of AA848-859 in the hinge between the N- and C-lobes of the kinase domain and the
 142 AA735-745 and AA767-781 regions adjacent to the ATP binding site (Extended Data Fig. 2a).

143 Combination of BYL719 and 1938 yielded a combined footprint that largely overlapped with that
 144 of each ligand separately bound to PI3K α , with the protections in the kinase hinge and the AA1002-
 145 1016 regions, along with exposures in the p110 α -C2 interface (Extended Data Fig. 2b), suggesting that
 146 PI3K α can accommodate both ligands simultaneously.

147 We next attempted to crystallize full-length p110 α /nSH2-p85 α in the presence of 1938. Despite
 148 obtaining PI3K α crystals, no 1938 was visible, either upon co-crystallisation or upon compound
 149 soaking into preformed crystals (PDB:7PG5). Co-crystallisation of PI3K α with 1938 and BYL719 resulted
 150 in crystals in which only density for BYL719 was visible (PDB:7PG6; Supplementary Table 2a).

151 We next used a deletion variant of p110 α (p110 α AA105-1048)³⁰ in which the p85 adaptor-
 152 binding domain (AA1-104) and a C-terminal membrane binding motif in the kinase domain (AA1049-
 153 1068) were deleted. This construct lacks catalytic activity but, in contrast to wild-type p110 α , is stable

154 in the absence of p85³⁰. Co-crystallisation with 1938 did not yield crystals, however, soaking
 155 preformed crystals with 1938 revealed density for 1938 (Fig. 2b-d; Extended Data Fig. 2d). Crystals
 156 diffracted to 2.4 Å for apo (PDB:8BFU), and 2.6 Å for 1938-bound p110α (PDB:8BFV; Supplementary
 157 Table 2b). The bound 1938 is in a pocket surrounded by residues E365, I459, L540, D603, C604, N605,
 158 Y641 of p110α and, in agreement with HDX-MS protection, S1003, L1006, G1007 and F1016 (Fig. 2c;
 159 Extended Data Fig. 2e). The core pyridine nitrogen in 1938 is predicted to be sufficiently basic to be
 160 predominantly protonated at physiological pH (Marvin Sketch 21.14, pKa calculator plug-in, Chemaxon
 161 Ltd, Váci út 133. 1138 Budapest, Hungary), and this NH⁺ makes key interactions with the side chain of
 162 D603. The acetylated indoline of 1938 sits in a pocket comprised of L1006, F1016 and I459, and makes
 163 face-to-edge interactions with F1016. Binding of 1938 induces F1016 to move away from the pocket
 164 in order to accommodate the ligand. The piperazine is surrounded by E365 and L540, and points out
 165 towards solvent.

166 1938 induced global conformational shifts in the p110α crystal structure (Fig. 2d; Video S1), with
 167 the C2 and helical domains moving away from the kinase domain, the AA1002-1016 kinase/activator
 168 interface moving away from the helical domain and the α-helix AA1016-1026 moving toward the
 169 active site (Fig. 2d; Video S1). This 1016-1026 helix is structurally analogous to a region in the PI3K-like
 170 protein kinases (PIKKs) known as the PIKK regulatory domain (PRD). In PIKKs, this region can block
 171 substrate interaction with the activation loop. In PI3Kα, the PRD-analogous region interacts with the
 172 substrate-binding activation loop (AA933-957). The AA940-954 activation loop region is disordered in
 173 both the apo and 1938-bound structures, however, in the structure of PIP₂ bound to PI3Kα
 174 (PDB:4OVV³¹) and in our own apo p110α/niSH2 structure (PDB:7PG5), the activation loop is fully
 175 ordered and packed against the PRD-analogous helix. Activation loop residues K942 and R949 are
 176 important for recognizing PIP₂³², suggesting that a component of the mechanism of action of 1938 is
 177 to cause repositioning of the activation loop to facilitate productive phosphotransfer to PIP₂. In
 178 addition, 1938 binding causes pivoting of the helical domain to bring the ATP-binding loop and the N-
 179 lobe of the kinase domain toward the ATP-binding pocket (Fig. 2d; Video S1). This helical domain
 180 pivoting to close the ATP pocket is analogous to a closing of the N-lobe relative to the C-lobe that
 181 accompanies RHEB-mediated activation of mTORC1 caused by conformational change of the FAT
 182 domain³³. The COSMIC database³⁴ shows that several cancer-associated mutations in *PIK3CA* occur
 183 at sites adjacent to the activator-binding pocket (Fig. 2d; Video S1), including two of the most common
 184 cancer-associated mutants E542K and E545K that are known to relieve inhibition of p110α by the
 185 p85α-nSH2 domain²⁹. Therefore, it is possible that 1938 weakens the inhibitory effects of p85α on
 186 p110α, contributing to enzyme activation. Key components of the compound binding mode are
 187 confirmed by preliminary structure-activity relationship (SAR) analysis of our small molecule scaffold
 188 (Supplementary Table 3).

189 Based on the crystal structure and SAR data, we performed mutagenesis to generate 1938-
 190 resistant p110α-mutants, as follows: D603K, D603A, 603DCN_AAA605 triple-mutant, D603A/F1016S
 191 double-mutant, L1006R, F1016S, and the L1006R/F1016S double-mutant. All mutants were resistant
 192 to activation by 1938 but could be activated by pY (Extended Data Fig. 2f).

193 Comparison of the p110α/1938 crystal structure with that of p110β (PDB:2Y3A) and p110δ
 194 (PDB:6PYU) indicates that these PI3Ks cannot accommodate 1938 at the homologous site due to side-
 195 chains that occlude the analogous volume in which 1938 binds to p110α (Fig. 2e), explaining the high
 196 selectivity of 1938 for p110α.

197

198 **1938 induces PI3Kα signalling in cells**

199 PI3Kα phosphorylates PIP₂ in the plasma membrane to PtdIns(3,4,5)P₃ (or PIP₃), which can be
 200 converted by 5-phosphatases to PtdIns(3,4)P₂.

201 In MEFs, 1938 increased PIP₃ levels within 30 sec, as assessed by mass spectrometry (MS)³⁵,
 202 maxing at 5 min and maintained at this maximum level for up to 40 min (Fig. 3a). At the 2 min time
 203 point, the PIP₃ levels induced by 1938 were comparable to those induced by insulin, but lower than
 204 those induced by PDGF. The observation of different PIP₃ levels induced by insulin and PDGF is in line

205 with the notion that PI3K α is the sole mediator of PIP₃ production downstream of insulin^{36,37}, whereas
 206 PDGF activates both PI3K α and PI3K β , with PI3K β contributing substantially to PDGF-stimulated PIP₃-
 207 generation in MEFs³⁸. In the same experiment as in Fig. 3a, a PI(3,4)P₂ signal was detected in MEFs
 208 upon PDGF stimulation but not with 1938 (at 5 μ M; Extended Data Fig. 3a). This is consistent with a
 209 higher threshold of PI(3,4)P₂ detection compared to PIP₃ by MS (due primarily to background
 210 contamination³⁹), together with the lower PI3K activation by 1938 compared to a high dose of PDGF,
 211 as is also illustrated by the experiments below.

212 When tested at different doses at a fixed 2 min time point, PIP₃ induction by 1938 in MEFs had an
 213 EC₅₀ of \sim 5 μ M, plateauing around 10 μ M, at a substantial lower level of PIP₃ to that induced by PDGF
 214 at 1 or 3 ng/ml (Fig. 3b). These maximal 1938-induced PIP₃ levels are below those required to give rise
 215 to sufficient PI(3,4)P₂ to be detectable by MS, a conclusion also supported by the observation that
 216 substantial levels of PIP₃ induced by lower doses of PDGF (e.g. 0.5 ng/ml) also did not give rise to
 217 PI(3,4)P₂ levels detectable by MS (Extended Data Fig. 3b). Similar to what was observed for MEFs,
 218 stimulation of A549 cells for 2 min with a dose range of 1938 revealed that the PIP₃ response to 1938
 219 maxed out at 10 μ M (Fig. 3c). A strong PIP₃ response was also observed with insulin in A549, with no
 220 PIP₃ induced by PDGF, in line with the absence of the PDGF receptor in epithelial cells, including in
 221 A549⁴⁰.

222 Live imaging of A549 cells expressing a fluorescent biosensor for PIP₃⁴¹ showed acute plasma
 223 membrane-associated PIP₃ production upon 1938 addition, which could be fully and acutely
 224 neutralized by BYL719 (Fig. 3d; Video S2,S3). This PIP₃ signal was not seen in PI3K α -KO A549 (Fig. 3d;
 225 Video S4). In HeLa cells, 1938 also induced an acute and BYL719-sensitive burst of PIP₃ (Fig. 3d),
 226 followed by the generation of membrane-associated PI(3,4)P₂ (Fig. 3d), with a timing in line with the
 227 known mechanism of PIP₃ conversion to PI(3,4)P₂ by 5-phosphatases⁴²⁻⁴⁴ and similar kinetics of
 228 PIP₃/PI(3,4)P₂ production in insulin-stimulated HeLa cells⁴¹. The small increases in signal upon addition
 229 of agonists (Fig. 3d) represent a non-specific response to medium addition in HeLa cells (Extended
 230 Data Fig. 3c).

231 Treatment with 1938 for 15 min increased pAKT^{S473} levels in a concentration-dependent manner
 232 in PI3K α -WT MEFs, with an EC₅₀ of \sim 2-4 μ M (Fig. 3e), with no pAKT^{S473} signal in 1938-stimulated PI3K α -
 233 KO MEFs⁴⁵ (Fig. 3e). The latter cells still respond to insulin, but in a PI3K β -dependent manner, as shown
 234 by sensitivity of insulin-stimulated pAKT^{S473} to the PI3K β -selective inhibitor TGX-221 (Fig. 3e).
 235 Expression in PI3K α -KO MEFs of WT PI3K α restored 1938-mediated pAKT^{S473} stimulation (Extended
 236 Data Fig. 2f), while none of the p110 α -mutants resistant to 1938-activation in *in vitro* kinase assays
 237 showed a response to 1938, as assessed by pAKT^{S473} induction (Extended Data Fig. 3d). 1938 treatment
 238 of A549 and MCF10A also led to a BYL719-sensitive increase in pAKT^{S473} (Extended Data Fig. 3e,f).

239 A dose titration of 15 min stimulation with 1938 and insulin in A549 cells revealed that in these
 240 cells, 1938 can activate the PI3K pathway as measured by pAKT^{S473} generation, beyond pathway
 241 activation by saturating doses of insulin, namely \sim 200% of E_{max} of 1 μ M insulin at doses of 5-10 μ M
 242 1938 (Fig. 3f). The induction of pAKT^{S473} in A549 and MCF10A by 1938 (5 μ M) was rapid (5 min; Fig. 3g;
 243 Extended Data Fig. 3f,g), reaching peak activation at 30 min and persisting for few hours before
 244 returning to levels slightly above baseline 24h or 48h later (Fig. 3g; Extended Data Fig. 3e). Similar
 245 observations were made for mTORC1 pathway activation, as measured by phosphorylation of S6^{S240/44}
 246 and 4EBP1^{S65} (Extended Data Fig. 3g). Interestingly, the kinetics of Akt/mTORC1 pathway activation
 247 was overall similar to that induced by insulin (Fig. 3g; Extended Data Fig. 3e,g), suggesting that 1938-
 248 mediated PI3K pathway activation is subject to the endogenous cellular feedback mechanisms within
 249 in the PI3K signalling pathway⁴⁶.

250 In summary, 1938 activates both proximal and distal signalling in a dose- and PI3K α -dependent
 251 manner in rodent and human cells, demonstrating its ability to directly activate PI3K α signalling in
 252 cells.

253

254 **Unbiased assessment of 1938 signalling**

1938 contains a pyridine core, a scaffold of multiple kinase inhibitors. A key feature of many kinase inhibitors is their ability to form mono-, bi- or tridentate H-bonding with the hinge region between the N- and C-lobes of kinase domains. The key interaction usually involves the inhibitor accepting a H-bond from the backbone amide in the hinge in the ATP-binding site. As mentioned above, the core pyridine nitrogen in 1938 is predicted to be sufficiently basic and predominantly protonated at physiological pH, which is likely to render this NH⁺ unable to form the donor-acceptor motif characteristic of standard kinase inhibitors. In order to gain insight into possible kinase inhibitory effects of 1938, we tested its impact in a panel of 133 protein kinases and 7 lipid kinases (Supplementary Tables 4-6; Extended Data Fig. 4). At 1 μM of 1938, 13 protein kinases were inhibited between 25-50%, with the LCK and BRK protein kinases inhibited by 58% and 56%, respectively. It is important to note that the *in vitro* kinase assays with LCK and BRK were performed in the presence of 50 and 75 μM ATP, respectively. If 1938 were to act as an ATP-competitive inhibitor for these kinases, the inhibition by 1938 in cells is expected to be significantly lower, given that the ATP concentration in cells is 1-10 mM, i.e. ≥200x higher than tested in the kinase counterscreen. Overall, these data indicate that in cells, 1938 is unlikely to inhibit any of the kinases in the panel tested.

1938 did not affect the activity of the other PI3K isoforms in the panel (PI3Kβ, PI3Kγ, PI3Kδ, PI3K-C2α and Vps34) or the PI3K-related kinases PI4Kβ, mTOR and DNA-PK (Extended Data Fig. 4; Supplementary Table 4). In separate *in vitro* assays, 1938 did not affect the activity of the PI3K-related kinases ATM (Extended Data Fig. 5) and mTORC1 [Extended Data Fig. 5; tested as the mTOR/RAPTOR/LST8 complex; note that mTOR activity in the ThermoFisher screen (Extended Data Fig. 4) was tested on baculovirus-expressed human mTOR/FRAP1 (AA1360-2549).

We next investigated the impact of 1938 on cell signalling using phosphoproteomics. Serum-starved PI3Kα-WT and PI3Kα-KO MEFs were treated for 15 min or 4h with 1938 or insulin (Extended Data Fig. 6a,b), with phosphosites exhibiting >2-fold up- or downregulation relative to DMSO and adjusted p-value <0.05 defined as significantly regulated. We quantified 10,611 phosphosites from 3,093 proteins (Supplementary Table 7) of which 9100, 1420 and 91 were pSer, pThr and pTyr residues, respectively (Extended Data Fig. 6a). In line with the data shown in Fig. 3e, 1938 had little signalling impact in PI3Kα-KO MEFs (Fig. 4a,b; Extended Data Fig. 6b), with Paxillin (pPXN^{S322}) the only phosphosite altered (downregulated upon 15 min treatment but not affected by 4h stimulation; Fig. 4a).

In PI3Kα-WT MEFs, 1938 induced differential phosphorylation of 27 and 50 peptides at 15 min and 4h, respectively (Fig. 4a,b; Extended Data Fig. 6c; Supplementary Table 7). Most of these were upregulated and included the PI3K pathway components pAKT1S1^{T247} (PRAS40) and pGSK3β^{S9} (Fig. 4a; Extended Data Fig. 6c; Supplementary Table 8). Approximately half of the 1938-controlled phosphosites have been reported in PhosphoSitePlus⁴⁷ to be regulated by insulin, IGF-1, PI3K or AKT, with some linked to regulation by mTOR or PDK1 (Fig. 4a-c; Supplementary Table 8), indicating that 1938 activates the canonical PI3K pathway. Notably, some phosphosites upregulated by 1938 in PI3Kα-WT MEFs, including top hits such as pSPECC1L^{S923}, pMSN^{S384} and pMAPK3^{Y205}, have not been previously linked to PI3K signalling as per PhosphoSitePlus⁴⁷ (Fig. 4a; Supplementary Table 8), highlighting the utility of 1938 to uncover novel pathways potentially downstream of PI3Kα.

Compared to treatment with vehicle, insulin induced differential phosphorylation of 11 and 18 sites at 15 min and 4 h, respectively, in PI3Kα-WT MEFs (Fig. 4a; Extended Data Fig. 6d), with substantial overlap in phosphosites regulated by 1938 and insulin at both time points (Fig. 4d). The majority of phosphosites upregulated by insulin at both timepoints were similar to the sites upregulated by 15 min 1938 treatment, whereas 4h treatment with 1938 induced phosphorylation of a larger set of sites (Fig. 4a,d), which might be due to a threshold effect, with a higher level of pAKT induced by 1938 compared to insulin at the concentrations of ligands tested (Extended Data Fig. 6b).

302

303 1938 induces cell proliferation

304 In PI3Kα-WT but not in PI3Kα-KO MEFs, 24h treatment with 1938 dose-dependently increased
305 metabolic activity, with an EC₅₀ of ~0.5 μM (Fig. 5a), and a decrease in ATP levels in both PI3Kα-WT

306 and PI3K α -KO MEFs at concentrations >7.5 μ M, indicative of PI3K α -independent effects of 1938 at
307 these doses (Fig. 5a). Upon 48h and 72h incubation, these non-PI3K α -dependent 1938 effects were
308 observed from 2-4 μ M onwards (Extended data Fig. 7a).

309 In PI3K α -WT but not in PI3K α -KO MEFs, 1938 induced cell cycle progression (Fig. 5b) and an
310 increase in cell number (Extended Data Fig. 7b), which could be fully neutralised by co-treatment with
311 BYL719. Unlike 1938, insulin did not induce cell cycle progression and an increase in cell number (Fig.
312 5b, Extended Data Fig. 7b), providing further evidence for a differential cellular impact of insulin and
313 1938 at the doses tested, as suggested by our proteomics data (Fig. 4a,d).

314

315 **1938 provides cardioprotection**

316 Myocardial infarction is responsible for significant morbidity and mortality in patients with coronary
317 artery disease. Despite the development of new anti-platelet and anti-thrombotic agents, timely
318 reperfusion by percutaneous coronary intervention via catheterisation remains fundamental to heart
319 tissue salvage. Paradoxically, such reperfusion also causes IRI, tissue damage that occurs following the
320 restoration of blood supply after a period without^{14,48}, and is also observed in intra-arterial device-
321 based treatment of stroke^{12,13}. Finding ways to reduce IRI is vital to improving the long-term outcome
322 of patients with myocardial infarction^{14,48} and stroke^{12,13}. Ischaemic preconditioning, an experimental
323 method of protecting the heart from IRI, leads to the activation of kinases including PI3K/AKT as part
324 of the so-called Reperfusion Injury Salvage Kinase pathway¹¹, a cardioprotective signalling pathway
325 induced by most cardioprotective agents⁴⁹, including insulin, the canonical activator of PI3K α ^{36,37,50}.
326 Using PI3K α inhibitors, we previously showed that PI3K α activation is both necessary and sufficient
327 for cardioprotection provided by ischaemic preconditioning or insulin⁵¹.

328 In *ex vivo* perfused rat hearts, 1938 was found to be a fast-acting agonist which, upon
329 administration during the first 15 min of reperfusion, provided substantial tissue protection from IRI.
330 This was evidenced by increased tissue survival and reduced infarct size (Fig. 5c), associated with an
331 increase in generation of pAKT^{S473} (Fig. 5d; Extended data Fig. 7c). 1938 also provided significant
332 cardioprotection in an *in vivo* IRI model in mice, with a corresponding pAKT^{S473} increase in the hearts
333 (Fig. 5e; Extended data Fig. 7d). Given the observed rapid PI3K α activation observed in both models,
334 it could be envisaged that therapeutic application of a direct PI3K α activator to a patient undergoing
335 emergency coronary revascularization following myocardial infarction could be cardioprotective, and
336 practically feasible in the clinical setting.

337

338 **1938 stimulates nerve regeneration**

339 PI3K pathway activation has been linked to neuroprotection and neuroregeneration^{9,10,17-19,22,23,25}, with
340 a positive role for PI3K α recently demonstrated in axonal regeneration using genetic approaches²⁰.
341 There are currently no therapeutic agents used routinely to stimulate neuronal regeneration such as
342 for injury to peripheral nerves, the spinal cord or optic nerves.

343 In a dose-dependent manner, 1938 significantly increased neurite outgrowth in dissociated adult
344 rat dorsal root ganglion (DRG) cultures, an *in vitro* model for neuroregeneration, with higher 1938
345 concentrations doubling the total length of neurites measured at 72h (Fig. 5f). In the presence of low,
346 biologically-inactive doses of 1938 (such as 10⁻⁹ M), BYL719 inhibited neurite outgrowth, and partially
347 reduced the increase in neurite outgrowth induced by 1938 concentrations above 10⁻⁷ M (Fig. 5f).

348 We next tested 1938 in the rat sciatic nerve crush model of peripheral nerve injury and
349 regeneration (Fig. 5g). Exploratory experiments showed pAKT induction upon direct injection of 1938
350 or bathing of exposed sciatic nerves in a 1938 solution (Extended Data Fig. 8a), indicating that 1938
351 leads to PI3K pathway activation in this tissue when delivered locally. Immediately after the nerve
352 crush (Fig. 5g, *i-ii*), 1938 was delivered via a single intraneural injection into the proximal crush site
353 (Fig. 5g, *iii*) and via a minipump implanted adjacent to the nerve (Fig. 5g, *iv*), loaded with 1938 solution,
354 for continuous delivery for the duration of the experiment. Analyses were conducted 3 weeks after
355 injury.

356 Electrophysiological recordings from the *tibialis anterior* muscle during nerve stimulation

357 proximal to the injury site showed a greater electrophysiological recovery upon 1938-treatment, as
358 indicated by an increased motor unit number estimation (MUNE) (Fig. 5h) and greater compound
359 muscle action potential (CMAP) recovery (Fig. 5i). This correlated with histological analyses which
360 showed an increase in 1938-treated animals in the number of choline acetyltransferase (ChAT)-
361 positive motor axons (Fig. 5j); assessed in distal nerve sections from the common peroneal branch of
362 the sciatic nerve, close to the point of re-innervation of the *tibialis anterior* muscle (indicated in Fig.
363 5g, v, i.e. approximately 25 mm from the injury site), with neurites grouped within normal fascicular
364 nerve architecture (Extended Data Fig. 8b).

365 Histological analysis further showed innervation of a proportion of neuromuscular junctions
366 (NMJs) in the *tibialis anterior* muscles (Fig. 5k), with the characteristic normal distribution of post-
367 synaptic acetylcholine receptors and axons (Extended Data Fig. 8c).

368 Analysis after 21 days is an early time point in terms of regeneration, with low level initial re-
369 innervation of muscle expected in untreated animals. The histological detection of motor axons in the
370 distal nerve and NMJs corresponds with improved electrophysiological reinnervation of the *tibialis*
371 *anterior* muscle. Histological analysis of nerve sections closer to the point of injury (3 and 6 mm distal
372 to the crush site) showed equivalent numbers of neurofilament- and ChAT-positive axons in treatment
373 and control groups (Fig. 5l). This indicates that the improved functional muscle re-innervation
374 associated with 1938 treatment is due to an acceleration of natural neuronal regeneration rather than
375 an increase in the overall number of regenerating neurites.

376

377 Discussion

378 Here we report on a small molecule to directly and allosterically activate PI3K α , providing a chemical
379 tool to investigate the consequences of direct PI3K α activation in basic and translational studies. This
380 reagent will facilitate controlled studies to gain a better quantitative understanding of PI3K α
381 signalling⁵² and to delineate PI3K α -specific signalling in cells. Our data also reveal the potential of
382 PI3K α -activating compounds like 1938 for use in tissue protection and regeneration, widening the
383 possible therapeutic range of modulating this enzyme. However at present, we cannot exclude that
384 some of the regenerative effects of 1938 *in vivo* are contributed by non-target-dependent effects, a
385 challenge for any pharmacological modulator, especially at the first stages of development.

386 1938 is an allosteric activator of wild-type and all oncogenic PI3K α mutants tested. 1938 binds
387 outside the ATP-binding site, and weakens the inhibitory effects of p85 α on p110 α , contributing to
388 enzyme activation. Its ability to induce conformational changes that do not fully overlap with those
389 observed in PI3K α activation by natural ligands (pY) or oncogenic *PIK3CA* mutations, indicates a unique
390 mechanism of activation. The AA1016-1026 p110 α helix, which is analogous to the PIKK regulatory
391 domain (PRD) of PI3K-like protein kinases such as mTOR and ATM, acts as a transmission between the
392 kinase/activator interface and the kinase active site. Binding of 1938 shifts this PRD-like loop to
393 potentially reposition the activation loop and facilitate productive phospho-transfer to PIP₂. The
394 helical domain also pivots to bring the ATP-binding loop (AA772-776) and the N-lobe of the p110 α
395 kinase domain toward the ATP-binding site for better phospho-transfer.

396 Our data indicate that *transient* PI3K activation using 1938 allows to effectively boost endogenous
397 protective and regenerative signalling. PI3K α signalling induced by 1938 and insulin showed similar
398 kinetics in cells, including downregulation upon prolonged exposure, indicating that 1938-driven
399 PI3K α signalling remains subject to endogenous feedback mechanisms⁴⁶. Such short-lived PI3K
400 signalling is likely to differ from the *sustained* impact on signalling provided by constitutive oncogenic
401 *PIK3CA* activation. Mutant *PIK3CA* on its own is a weak driver oncogene, with mice constitutively
402 expressing the *Pik3ca*^{H1047R} hot-spot mutation not developing cancer within a year^{53,54}. Similarly,
403 people with rare mosaic genetic activation of *PIK3CA* are not predisposed to cancer in adulthood,
404 although it has to be noted that *PIK3CA* mutations in these patients are present in different tissues
405 than the tissue types with somatic *PIK3CA* mutations in sporadic cancer⁵⁵. Taken together, these data
406 make it less likely that short-term and transient pharmacological PI3K α activation would induce or
407 promote cancer.

408 In general, our work illustrates the potential of activating kinases for therapeutic benefit, a
 409 currently largely unexplored area of drug development.

410

411 Main text References

412

- 413 1 Cowan-Jacob, S. W., Jahnke, W. & Knapp, S. Novel approaches for targeting kinases: allosteric
 414 inhibition, allosteric activation and pseudokinases. *Future medicinal chemistry* **6**, 541-561
 415 (2014). <https://doi.org:10.4155/fmc.13.216>
- 416 2 Astl, L., Tse, A. & Verkhivker, G. M. Interrogating Regulatory Mechanisms in Signaling Proteins
 417 by Allosteric Inhibitors and Activators: A Dynamic View Through the Lens of Residue
 418 Interaction Networks. *Adv Exp Med Biol* **1163**, 187-223 (2019). [https://doi.org:10.1007/978-
 419 981-13-8719-7_9](https://doi.org:10.1007/978-981-13-8719-7_9)
- 420 3 Simpson, G. L., Hughes, J. A., Washio, Y. & Bertrand, S. M. Direct small-molecule kinase
 421 activation: Novel approaches for a new era of drug discovery. *Curr Opin Drug Discov Devel* **12**,
 422 585-596 (2009).
- 423 4 Fang, Z., Grutter, C. & Rauh, D. Strategies for the selective regulation of kinases with allosteric
 424 modulators: exploiting exclusive structural features. *ACS Chem Biol* **8**, 58-70 (2013).
 425 <https://doi.org:10.1021/cb300663j>
- 426 5 Mobitz, H., Jahnke, W. & Cowan-Jacob, S. W. Expanding the Opportunities for Modulating
 427 Kinase Targets with Allosteric Approaches. *Curr Top Med Chem* **17**, 59-70 (2017).
 428 <https://doi.org:10.2174/1568026616666160719165314>
- 429 6 Vanhaesebroeck, B., Perry, M. W. D., Brown, J. R., Andre, F. & Okkenhaug, K. PI3K inhibitors
 430 are finally coming of age. *Nat Rev Drug Discov* **20**, 741-769 (2021).
 431 <https://doi.org:10.1038/s41573-021-00209-1>
- 432 7 Fruman, D. A. *et al.* The PI3K Pathway in Human Disease. *Cell* **170**, 605-635 (2017).
 433 <https://doi.org:10.1016/j.cell.2017.07.029>
- 434 8 Borges, G. A. *et al.* Pharmacological PTEN inhibition: potential clinical applications and effects
 435 in tissue regeneration. *Regen Med* **15**, 1329-1344 (2020). [https://doi.org:10.2217/rme-2019-
 436 0065](https://doi.org:10.2217/rme-2019-0065)
- 437 9 Matsuda, S. *et al.* Effective PI3K modulators for improved therapy against malignant tumors
 438 and for neuroprotection of brain damage after tumor therapy (Review). *International journal
 439 of oncology* **49**, 1785-1790 (2016). <https://doi.org:10.3892/ijo.2016.3710>
- 440 10 Koh, S. H. & Lo, E. H. The Role of the PI3K Pathway in the Regeneration of the Damaged Brain
 441 by Neural Stem Cells after Cerebral Infarction. *J Clin Neurol* **11**, 297-304 (2015).
 442 <https://doi.org:10.3988/jcn.2015.11.4.297>
- 443 11 Hausenloy, D. J. & Yellon, D. M. New directions for protecting the heart against ischaemia-
 444 reperfusion injury: targeting the Reperfusion Injury Salvage Kinase (RISK)-pathway. *Cardiovasc
 445 Res* **61**, 448-460 (2004). <https://doi.org:10.1016/j.cardiores.2003.09.024>
- 446 12 Catanese, L., Tarsia, J. & Fisher, M. Acute Ischemic Stroke Therapy Overview. *Circ Res* **120**,
 447 541-558 (2017). <https://doi.org:10.1161/CIRCRESAHA.116.309278>
- 448 13 Bala, F. *et al.* Infarct Growth despite Successful Endovascular Reperfusion in Acute Ischemic
 449 Stroke: A Meta-analysis. *AJNR Am J Neuroradiol* (2021). <https://doi.org:10.3174/ajnr.A7177>
- 450 14 Heusch, G. Myocardial ischaemia-reperfusion injury and cardioprotection in perspective. *Nat
 451 Rev Cardiol* **17**, 773-789 (2020). <https://doi.org:10.1038/s41569-020-0403-y>
- 452 15 Chauhan, A. *et al.* PTEN inhibitor bpV(HOpic) confers protection against ionizing radiation.
 453 *Scientific reports* **11**, 1720 (2021). <https://doi.org:10.1038/s41598-020-80754-8>
- 454 16 Iosifidis, T. *et al.* Aberrant cell migration contributes to defective airway epithelial repair in
 455 childhood wheeze. *JCI insight* **5** (2020). <https://doi.org:10.1172/jci.insight.133125>
- 456 17 Arnes, M., Romero, N., Casas-Tinto, S., Acebes, A. & Ferrus, A. PI3K activation prevents
 457 Abeta42-induced synapse loss and favors insoluble amyloid deposit formation. *Mol Biol Cell*
 458 **31**, 244-260 (2020). <https://doi.org:10.1091/mbc.E19-05-0303>

- 459 18 Cuesto, G. *et al.* Phosphoinositide-3-kinase activation controls synaptogenesis and
460 spinogenesis in hippocampal neurons. *J Neurosci* **31**, 2721-2733 (2011).
461 <https://doi.org:10.1523/JNEUROSCI.4477-10.2011>
- 462 19 Asua, D., Bougamra, G., Calleja-Felipe, M., Morales, M. & Knafo, S. Peptides Acting as Cognitive
463 Enhancers. *Neuroscience* **370**, 81-87 (2018).
464 <https://doi.org:10.1016/j.neuroscience.2017.10.002>
- 465 20 Nieuwenhuis, B. *et al.* PI 3-kinase delta enhances axonal PIP3 to support axon regeneration in
466 the adult CNS. *EMBO molecular medicine* **12**, e11674 (2020).
467 <https://doi.org:10.15252/emmm.201911674>
- 468 21 Prakoso, D. *et al.* Gene therapy targeting cardiac phosphoinositide 3-kinase (p110alpha)
469 attenuates cardiac remodeling in type 2 diabetes. *Am J Physiol Heart Circ Physiol* **318**, H840-
470 H852 (2020). <https://doi.org:10.1152/ajpheart.00632.2019>
- 471 22 Chen, S. *et al.* Neuroprotective Role of the PI3 Kinase/Akt Signaling Pathway in Zebrafish. *Front*
472 *Endocrinol (Lausanne)* **8**, 21 (2017). <https://doi.org:10.3389/fendo.2017.00021>
- 473 23 Ohtake, Y., Hayat, U. & Li, S. PTEN inhibition and axon regeneration and neural repair. *Neural*
474 *Regen Res* **10**, 1363-1368 (2015). <https://doi.org:10.4103/1673-5374.165496>
- 475 24 Derossi, D., Williams, E. J., Green, P. J., Dunican, D. J. & Doherty, P. Stimulation of mitogenesis
476 by a cell-permeable PI 3-kinase binding peptide. *Biochem Biophys Res Commun* **251**, 148-152
477 (1998). <https://doi.org:10.1006/bbrc.1998.9444>
- 478 25 Jo, H. *et al.* Small molecule-induced cytosolic activation of protein kinase Akt rescues ischemia-
479 elicited neuronal death. *Proc Natl Acad Sci U S A* **109**, 10581-10586 (2012).
480 <https://doi.org:10.1073/pnas.1202810109>
- 481 26 Zheng, K. *et al.* Activation of Akt by SC79 protects myocytes from oxygen and glucose
482 deprivation (OGD)/re-oxygenation. *Oncotarget* **8**, 14978-14987 (2017).
483 <https://doi.org:10.18632/oncotarget.14785>
- 484 27 Spinelli, L., Lindsay, Y. E. & Leslie, N. R. PTEN inhibitors: an evaluation of current compounds.
485 *Advances in biological regulation* **57**, 102-111 (2015).
486 <https://doi.org:10.1016/j.jbior.2014.09.012>
- 487 28 Furet, P. *et al.* Discovery of NVP-BYL719 a potent and selective phosphatidylinositol-3 kinase
488 alpha inhibitor selected for clinical evaluation. *Bioorg Med Chem Lett* **23**, 3741-3748 (2013).
489 <https://doi.org:10.1016/j.bmcl.2013.05.007>
- 490 29 Burke, J. E., Perisic, O., Masson, G. R., Vadas, O. & Williams, R. L. Oncogenic mutations mimic
491 and enhance dynamic events in the natural activation of phosphoinositide 3-kinase p110alpha
492 (PIK3CA). *Proc Natl Acad Sci U S A* **109**, 15259-15264 (2012).
493 <https://doi.org:10.1073/pnas.1205508109>
- 494 30 Chen, P. *et al.* Engineering of an isolated p110alpha subunit of PI3Kalpha permits
495 crystallization and provides a platform for structure-based drug design. *Protein Sci* **23**, 1332-
496 1340 (2014). <https://doi.org:10.1002/pro.2517>
- 497 31 Maheshwari, S. *et al.* Kinetic and structural analyses reveal residues in phosphoinositide 3-
498 kinase alpha that are critical for catalysis and substrate recognition. *J Biol Chem* **292**, 13541-
499 13550 (2017). <https://doi.org:10.1074/jbc.M116.772426>
- 500 32 Pirola, L. *et al.* Activation loop sequences confer substrate specificity to phosphoinositide 3-
501 kinase alpha (PI3Kalpha). Functions of lipid kinase-deficient PI3Kalpha in signaling. *J Biol Chem*
502 **276**, 21544-21554 (2001). <https://doi.org:10.1074/jbc.M011330200>
- 503 33 Yang, H. *et al.* Mechanisms of mTORC1 activation by RHEB and inhibition by PRAS40. *Nature*
504 **552**, 368-373 (2017). <https://doi.org:10.1038/nature25023>
- 505 34 Tate, J. G. *et al.* COSMIC: the Catalogue Of Somatic Mutations In Cancer. *Nucleic Acids Res* **47**,
506 D941-D947 (2019). <https://doi.org:10.1093/nar/gky1015>
- 507 35 Clark, J. *et al.* Quantification of PtdInsP3 molecular species in cells and tissues by mass
508 spectrometry. *Nat Methods* **8**, 267-272 (2011). <https://doi.org:10.1038/nmeth.1564>

- 509 36 Foukas, L. C. *et al.* Critical role for the p110alpha phosphoinositide-3-OH kinase in growth and
510 metabolic regulation. *Nature* **441**, 366-370 (2006). <https://doi.org/10.1038/nature04694>
- 511 37 Knight, Z. A. *et al.* A pharmacological map of the PI3-K family defines a role for p110alpha in
512 insulin signaling. *Cell* **125**, 733-747 (2006). <https://doi.org/10.1016/j.cell.2006.03.035>
- 513 38 Tsolakos, N. *et al.* Quantitation of class IA PI3Ks in mice reveals p110-free-p85s and isoform-
514 selective subunit associations and recruitment to receptors. *Proc Natl Acad Sci U S A* **115**,
515 12176-12181 (2018). <https://doi.org/10.1073/pnas.1803446115>
- 516 39 Malek, M. *et al.* PTEN Regulates PI(3,4)P2 Signaling Downstream of Class I PI3K. *Mol Cell* **68**,
517 566-580 e510 (2017). <https://doi.org/10.1016/j.molcel.2017.09.024>
- 518 40 Gerber, D. E. *et al.* Stromal platelet-derived growth factor receptor alpha (PDGFRalpha)
519 provides a therapeutic target independent of tumor cell PDGFRalpha expression in lung cancer
520 xenografts. *Mol Cancer Ther* **11**, 2473-2482 (2012). <https://doi.org/10.1158/1535-7163.MCT-12-0431>
- 521
522 41 Goulden, B. D. *et al.* A high-avidity biosensor reveals plasma membrane PI(3,4)P2 is
523 predominantly a class I PI3K signaling product. *J Cell Biol* **218**, 1066-1079 (2019).
524 <https://doi.org/10.1083/jcb.201809026>
- 525 42 Liu, Y. & Bankaitis, V. A. Phosphoinositide phosphatases in cell biology and disease. *Prog Lipid*
526 *Res* **49**, 201-217 (2010). <https://doi.org/10.1016/j.plipres.2009.12.001>
- 527 43 Majerus, P. W. & York, J. D. Phosphoinositide phosphatases and disease. *J Lipid Res* **50 Suppl**,
528 S249-254 (2009). <https://doi.org/10.1194/jlr.R800072-JLR200>
- 529 44 Ramos, A. R., Ghosh, S. & Erneux, C. The impact of phosphoinositide 5-phosphatases on
530 phosphoinositides in cell function and human disease. *J Lipid Res* **60**, 276-286 (2019).
531 <https://doi.org/10.1194/jlr.R087908>
- 532 45 Foukas, L. C., Berenjeno, I. M., Gray, A., Khwaja, A. & Vanhaesebroeck, B. Activity of any class
533 IA PI3K isoform can sustain cell proliferation and survival. *Proc Natl Acad Sci U S A* **107**, 11381-
534 11386 (2010). <https://doi.org/10.1073/pnas.0906461107>
- 535 46 Rozengurt, E., Soares, H. P. & Sinnet-Smith, J. Suppression of feedback loops mediated by
536 PI3K/mTOR induces multiple overactivation of compensatory pathways: an unintended
537 consequence leading to drug resistance. *Mol Cancer Ther* **13**, 2477-2488 (2014).
538 <https://doi.org/10.1158/1535-7163.MCT-14-0330>
- 539 47 Hornbeck, P. V. *et al.* PhosphoSitePlus, 2014: mutations, PTMs and recalibrations. *Nucleic*
540 *Acids Res* **43**, D512-520 (2015). <https://doi.org/10.1093/nar/gku1267>
- 541 48 Hausenloy, D. J. & Yellon, D. M. Myocardial ischemia-reperfusion injury: a neglected
542 therapeutic target. *The Journal of clinical investigation* **123**, 92-100 (2013).
543 <https://doi.org/10.1172/JCI62874>
- 544 49 Hausenloy, D. J. & Yellon, D. M. Preconditioning and postconditioning: united at reperfusion.
545 *Pharmacol Ther* **116**, 173-191 (2007). <https://doi.org/10.1016/j.pharmthera.2007.06.005>
- 546 50 Jonassen, A. K. *et al.* Insulin administered at reoxygenation exerts a cardioprotective effect in
547 myocytes by a possible anti-apoptotic mechanism. *Journal of molecular and cellular cardiology*
548 **32**, 757-764 (2000). <https://doi.org/10.1006/jmcc.2000.1118>
- 549 51 Rossello, X. *et al.* The role of PI3Kalpha isoform in cardioprotection. *Basic Res Cardiol* **112**, 66
550 (2017). <https://doi.org/10.1007/s00395-017-0657-7>
- 551 52 Madsen, R. R. & Vanhaesebroeck, B. Cracking the context-specific PI3K signaling code. *Sci*
552 *Signal* **13** (2020). <https://doi.org/10.1126/scisignal.aay2940>
- 553 53 Kinross, K. M. *et al.* An activating Pik3ca mutation coupled with Pten loss is sufficient to initiate
554 ovarian tumorigenesis in mice. *The Journal of clinical investigation* **122**, 553-557 (2012).
555 <https://doi.org/10.1172/JCI59309>
- 556 54 Berenjeno, I. M. *et al.* Oncogenic PIK3CA induces centrosome amplification and tolerance to
557 genome doubling. *Nature communications* **8**, 1773 (2017). <https://doi.org/10.1038/s41467-017-02002-4>
- 558

559 55 Madsen, R. R., Vanhaesebroeck, B. & Semple, R. K. Cancer-Associated PIK3CA Mutations in
 560 Overgrowth Disorders. *Trends Mol Med* **24**, 856-870 (2018).
 561 <https://doi.org/10.1016/j.molmed.2018.08.003>

562

563 **Main figure legends**

564

565 **Fig. 1 | Biochemical mechanism of PI3K α activation by 1938.** **a**, Structure of UCL-TRO-1938 (referred
 566 to in the text as 1938). **b**, Effect of the PI3K α -selective inhibitor BYL719 on 1938-activated PI3K.
 567 Enzyme activity in the presence of 1938 only was considered 100%. **c**, Selectivity of 1938 for PI3K α
 568 over PI3K β and PI3K δ . **d**, Enzyme kinetics (calculated using kcat function in Prism 8) upon ATP titration
 569 on PI3K α with or without 1938 and pY. **e**, Membrane binding of PI3K α shown as FRET signal (I-I₀). I,
 570 fluorescence intensity at 520 nm, I₀, fluorescence intensity at 520 nm in the absence of enzyme. **f**,
 571 Effect of 1938 on PI3K α catalytic activity in the presence of a saturating dose of pY. **g**, Effect of 1938
 572 on the catalytic activity of oncogenic mutants of PI3K α . Data shown as n=2 independent experiments
 573 (**b,e**). Data shown as mean \pm SEM, n=6 (**c**, left), n=4 (**c**, right), n=3. (**d,f,g**) experiments. Kinetic values
 574 in **d** shown as mean \pm SD. Statistical analysis performed with two way ANOVA, Tukey's multiple
 575 comparisons test (**c**) or Dunnett's multiple comparisons test (**g**); one way ANOVA, Dunnett's multiple
 576 comparisons test (**f**). ****P<0.0001.

577

578 **Fig. 2 | Structural mechanism of PI3K α activation by 1938.** **a**, Structural changes induced by 1938 as
 579 assessed by HDX-MS in full-length p110 α /p85 α , highlighted on the structure of p110 α (gray)/niSH2-
 580 p85 α (green) (pdb:4ZOP). Selection threshold for significant peptides: a-b difference \geq 2.5%, Da
 581 difference \geq 0.25, p-value <0.05 (unpaired t-test). **b**, Sigma-weighted density map in blue (2mFo-DFc)
 582 for the 1938 ligand (magenta) in the p110 α crystal structure. Yellow dashes show predicted H-bonds.
 583 **c**, Crystal structure of 1938 bound to p110 α ; 1938 (magenta), activation loop (yellow), loop 1002-1016
 584 (kinase/activator interface, slate), predicted H-bonds (yellow dashes). **d**, Comparison of the 1938-
 585 bound p110 α with apo-p110 α . The 1938-bound structure is shown in cartoon representation, while
 586 the apo-model is shown as a superimposed red α trace. 1938 shown as magenta blob, PRD-like helix
 587 shown in purple. Yellow spheres mark the sites of cancer-associated mutations from the COSMIC
 588 database that are near the 1938-binding site (only mutations with >10 reports are shown). Regions
 589 showing decreased HDX-MS protection for the common helical domain mutations are colored orange.
 590 PIP₂ substrate (slate) has been modelled in the active based on 4OVV. A region of the activation loop
 591 (thick worm representation, slate) has been taken from 7PG5 since it is disordered in the 1938-bound
 592 structure. Slate spheres represent residues important for PIP₂ recognition (K942 and R949). Chocolate
 593 spheres represent residues essential for phosphate transfer (K776, H917 and H936). A bound ATP
 594 (blue) has been modelled based on PDB ID 1E8X. The ATP binding loop is coloured yellow. Phosphates
 595 in PIP₂ and ATP are shown in red. **e**, Comparison of 1938-binding pocket in p110 α with homologous
 596 regions in p110 β and p110 δ .

597

598 **Fig. 3 | 1938 activates PI3K α signalling in cells.** All cells were serum-starved overnight. **a**, Time-
 599 dependent PIP₃ generation in MEFs stimulated with 1938, PDGF or insulin. Data shown as mean \pm SD,
 600 n=number of experiments. **b**, Dose-dependent PIP₃ generation by 2 min stimulation with the indicated
 601 agonists in MEFs (mean \pm SD, n=3 experiments except no DMSO (n=1)) and **c**, A549 cells (n=2
 602 experiments). **d**, Total internal fluorescence (TIRF) microscopy of 3-phosphoinositide reporter-
 603 expressing A549 or HeLa cells treated with DMSO, 1938 and BYL719. Thick lines specify medians;
 604 n=number of single cells. A549: PIP₃ reporter-expressing PI3K α -WT or PI3K α -KO cells, with data from
 605 one experiment. HeLa: PIP₃- or PI(3,4)P₂-reporter cells, with PIP₃ and PI(3,4)P₂ data representative of
 606 2 and 4 experiments, respectively. Shown below is a representative TIRF image of a PI3K α -WT A549
 607 cell, imaged 3 min before 1938 addition; 3 min after 1938 addition at t=27 min, and 3 min after BYL719
 608 addition at t=87 min. Scale bar: 11 μ m. **e**, pAKT^{S473} induction by 15 min treatment with different doses
 609 of 1938 in PI3K α -WT and PI3K α -KO MEFs. BYL719 (BYL), TGX-221 (TGX) and Parsaclisib (Pars) were

610 used at 0.5 μ M, 0.2 μ M and 0.05 μ M, respectively. Blot representative of n=3 experiments. **f**, pAKT^{S473}
 611 induction (measured by ELISA) in A549 by a 1938 dose titration or insulin. Data shown as mean \pm SEM
 612 (n=3 experiments). **g**, Time course analysis of insulin- or 1938-induced PI3K/AKT/mTORC1 signalling in
 613 A549, n=2 experiments. Quantification of pAKT^{S473}/vinculin signal ratio, expressed relative to
 614 treatment with DMSO only.

615

616 **Fig. 4 | Phosphoproteomic analysis of PI3K α -WT and PI3K α -KO MEFs** stimulated with 1938 (5 μ M) or
 617 insulin (100 nM) for 15 min or 4h (n=4 independent experiments). **a**, Heat map: phosphosites
 618 significantly altered by stimulation relative to DMSO treatment. Green boxes, significantly upregulated
 619 phosphosites; magenta boxes, significantly downregulated phosphosites; white crosses: phosphosites
 620 not detected in a comparison. **b**, Volcano plot of phosphosites differentially regulated by 1938 (5 μ M)
 621 in PI3K α -WT or PI3K α -KO MEFs, relative to DMSO-treated cells of the same genotype. Note that the
 622 PI3K α -WT volcano plots have been reproduced in enlarged format with labeling of individual proteins
 623 and phosphosities in **Extended Data Fig. 6c**. **c**, Venn diagram showing overlap of the number of
 624 phosphosites significantly regulated by 1938 in PI3K α -WT MEFs with sites that have been identified
 625 previously and are annotated in PhosphoSitePlus⁴⁷ as regulated by insulin, IGF-1, LY294002 (pan-PI3K
 626 inhibitor) or MK2206 (AKT inhibitor). **d**, Venn diagrams showing the overlapping number of
 627 phosphosites regulated by 1938 and insulin in PI3K α -WT MEFs.

628

629 **Fig. 5 | 1938 induces biological responses in cultured cells, explanted tissues and model organisms.**
 630 **a,b**, MEFs were serum-starved overnight, followed by 24h stimulation in serum-free medium with
 631 1938+BYL719, insulin, or culture medium containing 10% FBS, followed by measurement of: **a**,
 632 metabolic activity (ATP content assessed by CellTiter-Glo[®]), **b**, cell cycle progression (EdU
 633 incorporation). (**a,b**) show 2 independent experiments. Gating strategies for (**b**) shown in
 634 **Supplementary Fig. 2**. **c**, *Left*, Representative tetrazolium-stained slices of isolated rat hearts
 635 (Langendorff model) subjected to 45 min global ischaemia, followed by 2h reperfusion, with
 636 administration of DMSO (0.1%) or 1938 (5 μ M) during the first 15 min of perfusion. *Right*, infarct size
 637 measured at the end of the 2h reperfusion, in *ex vivo* hearts administered DMSO (n=6) or 1938 (n=6).
 638 Unpaired Student's t-test. **d**, pAKT^{S437} in *ex vivo* hearts administered DMSO (n=6), 1938 (n=6) or insulin
 639 (n=2). 1-way ANOVA with Tukey post-test. **e**, Impact of 1938 on *in vivo* heart IRI in mice. *Left*, infarct
 640 size measured following 40 min ischaemia and 2h reperfusion, with DMSO (n=7) or 1938 (n=8)
 641 administered 15 min prior to reperfusion. Unpaired Student's t-test. *Right*, pAKT^{S437} in hearts
 642 administered DMSO (n=4) or 1938 (n=4). Unpaired Student's t-test. Data in **c-e** shown as mean \pm SEM
 643 (n=independent experiment). **f**, Neurite length in DRG cultures stimulated with 1938+BYL719 for 72h,
 644 with representative images of neurons stained with anti- β -III tubulin at 72h. Data represent
 645 mean \pm SEM of n=3 independent experiments. **g**, Sciatic nerve crush injury (*i*), arrowhead in (*ii*) shows
 646 resulting lesion. Injury was followed by (*iii*) direct injection proximal to the injury, of a single dose of
 647 dH₂O or 1938 (5 μ M in sterile H₂O) and (*iv*) minipump implantation for continuous delivery of dH₂O or
 648 1938 (100 μ M in sterile H₂O) for 21 days. **h**, Motor unit number estimation (MUNE) recordings from
 649 the *tibialis anterior* (TA) muscle. **i**, Compound muscle action potential (CMAP) recordings in the TA
 650 muscle following nerve stimulation proximal to the crush site (percentage of the contralateral side). **j**,
 651 Total number of choline acetyltransferase (ChAT)-positive motor axons in distal common peroneal
 652 nerve cross-sections. **k**, Proportion of neuromuscular junctions (NMJs) re-innervated by axons at the
 653 target TA muscle, revealed by α -bungarotoxin (α -BTX) and neurofilament (NF) staining. **l**,
 654 Quantification of total axons (neurofilament) and motor axons (ChAT) in the sciatic nerve at 3 and 6
 655 mm distal to the injury site. For all experiments in **h-l**: n=5 animals per group, error bars are SD. Two-
 656 tailed Student's t-tests. All data are from the 21 day endpoint.

657

658 **METHODS**

659

660 Compound UCL-TRO-1938 is available from <https://www.cancertools.org/> catalog No. 161068.

661

662 **HTS**

663 A HTS for human p110 α /p85 α (referred to as PI3K α) of 450,000 small molecules in the AstraZeneca
664 screening library was performed using the ADP-Glo™ kinase assay. To enable the HTS, the PI3K α ADP-
665 Glo™ kinase assay was miniaturised into 1536-well format. Reagent stability and compatibility with
666 low volume dispensing technology were optimised to ensure conformity with HTS conditions. The HTS
667 was performed in single point at room temperature using white 1536-well plates (Corning #3729).
668 DMSO-solubilised compounds were acoustically dispensed to assay ready plates using an Echo 555
669 (Labcyte) yielding a final compound concentration of 10 μ M for most compounds (with some low MW
670 compounds screened at 10 μ M) and a final DMSO concentration of 1%. The reaction mixture
671 contained 750 nl enzyme, 750 nl substrate. Final concentrations of reaction buffer, PI3K α , liposomes
672 and ATP used were unchanged. PI3K α was incubated for 3 h at room temperature with 500 μ M ATP
673 and liposomes that mimic the plasma membrane lipid composition, enriched with 5% PtdIns(4,5)P₂
674 substrate, using the ADP-Glo™ assay (Promega) to measure ADP production. Compound responses
675 were normalised to DMSO control, and 6000 hit compounds with activity >3x standard deviation of
676 the DMSO control were re-screened in duplicate, using the assay described above. The final assay hit
677 rate was 0.53%. The HTS experimental procedure and data analysis were performed at AstraZeneca
678 using proprietary processes.

679 Confirmed hits with near neighbour molecules were subsequently screened in a 10-point
680 concentration response curve using a bis-phosphorylated phosphopeptide (a PDGF-receptor-derived
681 peptide phosphorylated on Tyr-740 and Tyr-751, hereafter referred to as pY peptide²⁹) to mimic
682 receptor tyrosine kinase binding to p85 α as a positive control.

683 Confirmed hits and near neighbour compounds were subsequently screened using an orthogonal
684 fluorescence polarisation biochemical activity assay in 10-point concentration response curves.
685 Biophysical confirmation of PI3K α binding of selected hits was assayed by microscale thermophoresis,
686 and hits that bound PI3K α investigated for cellular activity using the A549 human lung carcinoma cell
687 line, measuring the generation of phospho-S473-AKT (further referred to as pAKT^{S473}) by automated
688 Wes western blotting or ELISA. Routine compound profiling of novel compounds was performed using
689 the ADP-Glo™ *in vitro* kinase assay and ELISA for pAkt generated in A549 cells.

690

691 **Lipid substrate preparation for HTS**

692 A plasma membrane-like composition of liposomes was prepared by combining L- α -
693 phosphatidylinositol-4,5-bisphosphate (Brain, Porcine, Avanti #840046X), L- α -phosphatidylserine
694 (Brain, Porcine, Avanti 840032C), L- α -phosphatidylethanolamine (Brain, Porcine, Avanti #840022C) L-
695 α -phosphatidylcholine (Brain, Porcine, Avanti #840053C), cholesterol (Ovine Wool, Avanti #700000P)
696 and sphingomyelin (Brain, Porcine, Avanti #860062C) in a 5:20:45:15:10:5 ratio while in organic
697 solvent (primarily a chloroform:methanol:water (9:3:1) mixture). Methanol was titrated into the
698 mixture until components were in solution. The liposome solution was then placed on a rotatory
699 evaporator flushed with nitrogen gas, and solvent was evaporated at 250 mbar using a 25°C water
700 bath, until a translucent film of lipids was observed. The container was flushed with nitrogen before
701 being placed under vacuum for a further 16 h. Lipid buffer (20 mM HEPES pH 7.5, 100 mM KCl, 1 mM
702 EGTA pH 8.0) was then added, and the flask vortexed until the lipids were in suspension. The flask was
703 then bath-sonicated for 2 min, before being aliquoted into 250 ml plastic flasks. These fractions were
704 freeze-thawed 11 times using liquid nitrogen and a 42°C water bath. Liposomes were then extruded
705 using the Avestin LF-50 liposome extrusion apparatus. Liposomes were extruded with nitrogen gas at
706 a pressure of 150 psi. 50 ml aliquots of liposome solution were initially extruded through a 0.4 μ m
707 filter, followed by five passes through a 0.25 μ m filter. Liposome solutions were then flash frozen in
708 liquid nitrogen and stored at -80°C.

709 **Lipid substrate preparation for post-HTS ADP-Glo™ kinase assay**

710 Liposomes were prepared by mixing lipid components dissolved in chloroform and then evaporating
711 the solvent under a stream of nitrogen gas. The remaining lipid film was dried under a vacuum for 2
712 h, then resuspended in liposome buffer (20 mM HEPES, 100 mM KCl, 1 mM EGTA, pH 7.5). The lipid
713 solution was vortexed for 3 min and sonicated in a water bath for 2 min at room temperature. The
714 clarified solution was then subjected to 11 freeze-thaw cycles of snap freezing in liquid nitrogen
715 followed by thawing in a 42°C water bath. Liposomes were created by extruding 11 times through a
716 100 nm filter, snap frozen in liquid nitrogen and stored at -80°C.

717

718 **PI3K protein expression and purification**

719 Full-length human p110 α was expressed either in a complex with full-length human p85 α (for HTS,
720 biochemistry and HDX-MS) or with p85-niSH2 (amino acids 307-593) (for crystallography). A p110 α
721 construct (AA 105-1048)³⁰ lacking the adaptor binding domain and lipid binding surface was also used
722 for crystallography

723 Expression and purification of wild-type p110 α (Cambridge MRC Laboratory for Molecular Biology
724 (LMB-MRC) plasmid number OP831) in a complex with full-length p85 α (LMB-MRC plasmid OP809)
725 was performed as described²⁹. The oncogenic mutants G106V (LMB-MRC plasmid JB35), N345K (LMB-
726 MRC plasmid OP661) and E545K (LMB-MRC plasmid OP663) were also purified using this protocol.
727 Briefly, 10 litres of *Spodoptera frugiperda* (Sf9) cell culture at a density of 1.0×10^6 cells/ml were co-
728 infected with a p85 α -encoding virus [LMB-MRC plasmid OP809]. and a virus encoding p110 α with an
729 N-terminal 6xHis tag followed by a tobacco etch virus (TEV) protease site [LMB-MRC plasmid OP831].
730 After a 48 h infection at 27°C, cells were harvested and washed with PBS. Cell pellets were then
731 resuspended in Lysis Buffer (20 mM Tris pH 8.0, 300 mM NaCl, 5% glycerol, 10 mM Imidazole pH 8.0,
732 2 mM β -mercaptoethanol, 1 EDTA-free protease inhibitor tablet (Roche) per 50 ml of buffer) and
733 sonicated at 4°C for 7 min in 15 sec intervals followed by a 15 sec wait. Cell lysate was then centrifuged
734 at 45,000 g for 45 min at 4°C. Supernant was then filtered using a 0.45 μ M filter before being passed
735 over 2 x 5 ml HisTrap FF (Cytiva) Columns (equilibrated in NiNTA Buffer [20 mM Tris pH 8.0, 300 mM
736 NaCl, 5% glycerol, 10 mM imidazole (pH 8.0), 2 mM β -mercaptoethanol]) at a 3 ml/min flow rate.
737 Columns were then washed using a 20 mM imidazole wash, and protein was eluted in a gradient to
738 NiNTA B Buffer (20 mM Tris pH 8.0, 300 mM NaCl, 5% glycerol, 200 mM imidazole (pH 8.0), 2 mM β -
739 mercaptoethanol). PI3K α containing fractions were then pooled and diluted 1:2 with Salt Dilution
740 Buffer (20 mM Tris pH 8.0, 1 mM DTT) to reduce NaCl concentration to 100 mM. This solution was then
741 passed over a HiTrap Heparin (Cytiva) Column (equilibrated in Hep A Buffer (20 mM Tris pH 8.0, 100
742 mM NaCl, 2 mM β -mercaptoethanol)) at a rate of 3 ml/min. PI3K α was eluted using a gradient to HEP
743 B Buffer (20 mM Tris pH 8.0, 1 M NaCl, 2 mM β -mercaptoethanol). Protein containing fractions were
744 then pooled and concentrated to 8 mg/ml, before being loaded onto a Superdex 200 16/60 column,
745 equilibrated in Gel Filtration Buffer (20 mM HEPES pH 7.4, 100 mM NaCl, 2 mM TCEP), run at 1 ml/min
746 at 4°C. PI3K α -containing fractions were pooled and concentrated to 2.5 mg/ml before being flash-
747 frozen in liquid nitrogen and stored at -80°C.

748 Expression and purification of full-length human p110 α (carrying the M232K and L233K mutations
749 used in the structure determination for PDB ID 4JPS^{28,56}), in complex with human p85 α -niSH2 (amino
750 acids 307-593), was performed as follows. Sf9 insect cells were cultured in Insect-XPRESS with L-
751 Glutamine medium (Lonza BE12-730Q) at 27°C and infected with baculovirus encoding both p110 α
752 and p85 α -niSH2 [LMB-MRC plasmid GM129] at a density of $1.6-1.8 \times 10^6$ cells/ml. The culture was
753 incubated for 48 h after infection, and cells were collected and washed with PBS, flash-frozen in liquid
754 N₂ and stored at -80°C. For purification, cell pellets were resuspended in 100 ml of lysis buffer (20 mM
755 Tris, 150 mM NaCl, 5% glycerol, 2 mM β -mercaptoethanol, 0.02% CHAPS, pH 8.0) containing EDTA-
756 free Protease inhibitor tablets (Roche, 1 tablet per 50 ml of solution) and 500 μ l DNase I. The
757 suspension was sonicated for 10 min on ice, with 10 sec on and 10 sec off. The lysate was then
758 centrifuged at 35,000 rpm for 45 min using a Ti45 rotor at 4°C. The samples were loaded onto a
759 StrepTrap (Cytiva) column in S300 buffer (20 mM Tris, 300 mM NaCl, 5% glycerol, 2 mM TCEP, pH 8.0).
760 Once the protein was loaded, the column as washed with buffer A (20 mM Tris, 100 mM NaCl, 5%

761 glycerol, 1 mM TCEP, pH 8.0). The column was eluted using a gradient from 1-100% buffer B (buffer A
762 containing 5 mM *d*-Desthiobiotin). Fractions of the p110 α /p85 α -niSH2 peak were pooled and TEV
763 protease (0.8 mg/ml) was added at the ratio of 1:10 and left at 4°C to cleave overnight. Protein was
764 loaded onto a 5 ml HiTrap Heparin HP column (Cytiva) washed with buffer A, and eluted with a
765 gradient of 1-100% buffer C (20 mM Tris, 1 M NaCl, 1 mM TCEP, pH 8.0). The fractions were collected,
766 concentrated and loaded on a Superdex 200 26/60 HiLoad gel filtration column (Cytiva) and eluted in
767 20 mM Tris, 200 mM NaCl, 2 mM TCEP, 1% betaine, 1% ethylene glycol and 0.02% CHAPS, pH 7.2. The
768 peak fractions were pooled and concentrated to 10-13 mg/ml using Amicon Ultra-15 Centrifugal filters
769 100K (Millipore), as measured by a NanoDrop at 280 nm. The protein was then flash-frozen in liquid
770 nitrogen and stored at -80°C. Purity of protein was checked using SDS-PAGE.

771 Expression and purification of truncated human p110 α (105-1048) were performed as follows. Sf9
772 insect cells (9 L) were cultured in Insect-XPRESS with L-Glutamine medium (Lonza BE12-730Q) at
773 27°C and infected with baculovirus encoding the p110 α subunit [LMB-MRC plasmid OP798] at a
774 density of 1.6×10^6 cells/ml. The culture was incubated for 48 h after infection, cells were collected,
775 flash-frozen in liquid N₂ and stored at -80°C. For purification, cell pellets were resuspended in 360 ml
776 of lysis buffer (20 mM Tris, 150 mM NaCl, 5% glycerol, 1 mM TCEP, pH 8.0) containing EDTA-free
777 Protease inhibitor tablets (1 tablet per 50 ml of solution), 0.5 mM PEFA and 36 μ l of Piece[®] Universal
778 Nuclease For Cell Lysis. The suspension was sonicated for 5 min on ice, with 10 sec on and 10 sec off.
779 The lysate was then centrifuged at 35,000 rpm for 35 min using a Ti45 rotor at 4°C. The samples were
780 filtered through a 5 μ m filter and loaded onto a StrepTrap (Cytiva) column equilibrated in lysis buffer.
781 Once the sample was loaded, the column was washed with 20 mM Tris, 300 mM NaCl, 5% glycerol, 1
782 mM TCEP, pH 8.0, and then with 20 mM Tris, 150 mM NaCl, 5% glycerol, 1 mM TCEP, pH 8.0. Then 5
783 ml TEV solution at 0.14 mg/ml was added onto the column and left at 4°C to cleave overnight. Protein
784 was loaded onto a 5 ml HiTrap Heparin HP column (Cytiva) equilibrated in 20 mM Tris, 150 mM NaCl,
785 5% glycerol, 1 mM TCEP, pH 8.0, and eluted with a gradient of 1-100% of 20 mM Tris, 1 M NaCl, 1 mM
786 TCEP, pH 8.0. The fractions were collected, concentrated and loaded on a Superdex 200 16/60 HiLoad
787 gel filtration column (Cytiva) and eluted in 50 mM Tris, 100 mM NaCl, 2% ethylene glycol, and 1 mM
788 TCEP, pH 8.0. The peak fractions were pooled and concentrated to 5.83 mg/ml using Amicon Ultra-15
789 Centrifugal filters 50K (Millipore), as measured by a NanoDrop at 280 nm. The protein was then flash-
790 frozen in liquid nitrogen and stored at -80°C. Purity of protein was checked using SDS-PAGE.

791 Expression and purification of mutants resistant to 1938 were performed as follows. Sf9 insect
792 cells (1.5 L) were cultured in Insect-XPRESS with L-Glutamine medium (Lonza BE12-730Q) at 27°C and
793 co-infected with baculovirus encoding the regulatory p85 α -subunit [LMB-MRC plasmid OP809] and
794 the catalytic subunit p110 α -D603K [LMB-MRC plasmid OP895], D603A [OP900], 603DCN_AAA605
795 [OP894], D603A/F1016S [OP901] L1006R [OP897], F1016S [OP898], L1006R/F1016S [OP899] at a
796 density of 1.6×10^6 cells/ml. The culture was incubated for 47 h after infection, cells were collected,
797 flash-frozen in liquid N₂ and stored at -80°C. For purification, cell pellets were resuspended in 50 ml
798 of lysis buffer (20 mM Tris, 150 mM NaCl, 5% glycerol, 1 mM TCEP, pH 8.0) containing EDTA-free
799 Protease inhibitor tablets (1 tablet per 50 ml of solution), 0.5 mM PEFA and 5 μ l of Piece[®] Universal
800 Nuclease For Cell Lysis. The suspension was sonicated for 3 min on ice, with 10 sec on and 10 sec off.
801 The lysate was then centrifuged at 35,000 rpm for 35 min using a Ti45 rotor at 4°C. The samples were
802 filtered through a 5 μ m filter and loaded onto a StrepTrap (Cytiva) column equilibrated in lysis buffer.
803 Once the sample was loaded, the column was washed with 20 mM Tris, 300 mM NaCl, 5% glycerol, 1
804 mM TCEP, pH 8.0, and then with 20 mM Tris, 150 mM NaCl, 5% glycerol, 1 mM TCEP, pH 8.0. Then 5
805 ml TEV solution at 0.14 mg/ml was added onto the column and left at 4°C to cleave overnight. Protein
806 was loaded onto a 5 ml HiTrap Heparin HP column (Cytiva) equilibrated in 20 mM Tris, 150 mM NaCl,
807 5% glycerol, 1 mM TCEP, pH 8.0, and eluted with a gradient of 1-100% of 20 mM Tris, 1 M NaCl, 1 mM
808 TCEP, pH 8.0. The fractions were collected, concentrated and loaded on a Superdex 200 16/60 HiLoad
809 gel filtration column (Cytiva) and eluted in 20 mM HEPES pH 7.5, 150 mM NaCl, 1 mM TCEP. The peak
810 fractions were pooled and concentrated using Amicon Ultra-4 Centrifugal filters 50K (Millipore). The

811 protein was then flash-frozen in liquid nitrogen and stored at -80°C . Purity of protein was checked
812 using SDS-PAGE.

813 Full-length human p110 β /p85 α and p110 δ /p85 α were cloned and expressed in a similar manner.
814 Briefly, 5 litres of *Spodoptera frugiperda* (Sf9) cell culture at a density of 1.0×10^6 cells/ml were co-
815 infected with both a p85 α -encoding virus and a virus encoding p110 β / δ with an N-terminal Strep-tag
816 followed by a tobacco etch virus (TEV) protease site (plasmid OP832 for p110 β , plasmid OP833 for
817 p110 δ and plasmid of OP809 for p85 α). After a 48 h infection at 27°C , cells were harvested and washed
818 with PBS. Cell pellets were then resuspended in Lysis Buffer (20 mM Tris pH 8.0, 150 mM NaCl, 5%
819 glycerol, 2 mM β -mercaptoethanol, 1 EDTA-free protease inhibitor tablet (Roche) per 50 ml of buffer)
820 and sonicated at 4°C for 7 min in 15 sec intervals followed by a 15 sec wait. Cell lysate was then
821 centrifuged at 45,000 *g* for 45 min at 4°C . Supernatant was then filtered using a $0.45 \mu\text{m}$ filter before
822 being passed over 1 x 5 ml StrepTap No 1 (GE Healthcare) Columns (equilibrated in 100S Buffer [20
823 mM Tris pH 8.0, 100 mM NaCl, 5% glycerol, 1 mM TCEP]) at a 3 ml/min flow rate. Column was then
824 washed using 70 ml 100S Buffer, followed by 80 ml S300 Buffer (20 mM Tris pH 8.0, 300 mM NaCl, 5%
825 glycerol, 1 mM TCEP) followed by 50 ml S100 Buffer. 5 ml of 0.1 mg/ml His6TEV protease (p30) in S100
826 Buffer was injected onto the column and was incubated at 4°C for 4 h. The column was then attached
827 to a Heparin column, and the purification protocol proceeded as for PI3K α .

828

829 **Fluorescence polarization assay**

830 PIP $_3$ production was measured using a fluorescence polarization assay (#K-1100; Echelon Biosciences,
831 Salt Lake City, UT, USA) and carried out in 384-well microtitre plates. PI3K α , liposomes and ATP were
832 all diluted in the reaction buffer (20 mM HEPES, 50 mM NaCl, 50 mM KCl, 3 mM MgCl $_2$, 1 mM EGTA, 1
833 mM TCEP, pH 7.4) and added to the microtitre plate at a final reaction concentration of 10 nM PI3K α ,
834 75 $\mu\text{g/ml}$ liposomes and 10 μM ATP. The reaction was carried out for 45 min at room temperature and
835 quenched with the PIP $_3$ detector and TAMRA probe, before being read in a Hidex Sense platereader
836 using $\lambda 544 \pm 20$ and $\lambda 590 \pm 20$ polarizing filters. Data was normalised to the TAMRA probe alone and
837 TAMRA plus detector for minimum and maximum PIP $_3$ production, respectively.

838

839 **Microscale thermophoresis**

840 MST experiments were performed using an automated Monolith NT.115 (NanoTemper Technologies,
841 Munich, Germany). Fluorescence labelling of PI3K α with the NT647 dye was performed in accordance
842 with manufacturer protocol using the RED-NHS protein labelling Kit (NanoTemper Technologies,
843 Munich, Germany). PI3K α was diluted to a final concentration of 2.5 nM in reaction buffer (20 mM
844 HEPES, 100 mM NaCl, 0.1% Tween-20 and 2 mM TCEP, pH 7.4). Compounds were serially diluted in
845 neat DMSO and added to the enzyme to a final concentration of 3% DMSO. Premium treated
846 capillaries, IR laser powers of 80% and LED intensity of 10% were used. Data was analysed with the
847 NanoTemper Analysis software with ΔF_{norm} values ($\Delta F_{\text{norm}} = F_{\text{hot}}/F_{\text{cold}}$) used to define compound binding.

848

849 **ADP-GloTM kinase assay**

850 Kinase reactions were performed with ADP-Glo kinase assay kit (Promega Corporation). The enzyme,
851 substrate and compounds were diluted in reaction buffer (20 mM HEPES, 50 mM NaCl, 50 mM KCl, 3
852 mM MgCl $_2$, 1 mM EGTA, 1 mM TCEP, pH 7.4). Final concentrations of PI3K α and PI3K δ used were 25
853 nM and 50 nM for PI3K β . Liposomes (5% brain PI(4,5)P $_2$, 20% brain phosphatidylserine, 45% brain
854 phosphatidylethanolamine, 15% brain phosphatidylcholine, 10% cholesterol, 5% sphingomyelin
855 (Avanti Polar Lipids)) were used at a final concentration of 1 mg/ml.

856 For the HTS, the reaction mixture contained 0.75 μl enzyme, 15 nl compound and/or pY and 0.75
857 μl of liposome substrate mixed with ATP. The pY sequence was
858 ESDGG(pY)MDMSKDESID(pY)VPMLDMKGDIKYADIE (GL Biochem, Shanghai Ltd). ATP was used at a
859 final concentration of 500 μM unless otherwise stated. The final DMSO concentration in the assay was
860 1%. The experiments were performed at room temperature for 3 h using 1536-well white-polystyrene
861 plates (Corning #3729) before addition of 2 μl of ADP-Glo R1 to terminate the reaction. The plate was

862 incubated for 40 min, followed by addition of 4 μ l of ADP-Glo R2 and incubated further for 60 min in
863 the dark. Luminescence was read using a EnVision (PerkinElmer) plate reader. All analyses were
864 performed using Genedata Screener.

865 For re-screening of HTS hits and routine compound profiling, the reaction mixture contained 2 μ l
866 PI3K enzyme, 2 μ l compound and/or pY and 2 μ l of liposome substrate mixed with ATP. ATP was used
867 at a final concentration of 500 μ M for PI3K α and PI3K β and at 200 μ M for PI3K δ , unless otherwise
868 stated. The final DMSO concentration in the assay was 1%. The experiments were performed at room
869 temperature for 3 h using 384 white-polystyrene plates (Corning #3824) before addition of 6 μ l of
870 ADP-Glo R1 to terminate the reaction. The plate was incubated for 45 min, followed by addition of 12
871 μ l of ADP-Glo R2 and incubated further for 60 min in the dark. Luminescence was read using a Sense
872 (Hidex) plate reader. Compound data were corrected to the no enzyme DMSO negative control and
873 expressed as a percentage of the internal positive control (1 μ M pY), equivalent to maximal activation
874 (E_{max}). All analyses were performed using GraphPad Prism 7.

875 For characterisation of the effects of 1938 on *in vitro* PI3K enzymology, all reactions were
876 performed at room temperature with 384 white-polystyrene plates (Corning #3574). The final DMSO
877 concentration in the assay was between 0.5%-1.8%. The reaction mixture contained 2 μ l PI3K enzyme,
878 2 μ l compound and/or pY and 2 μ l of liposome substrate mixed with ATP. ATP was used at a final
879 concentration of 200 μ M, unless otherwise stated. The enzyme and compounds were pre-incubated
880 for 10 min prior to addition of substrate. The reaction was allowed to proceed for up to 45 min at
881 room temperature, before addition of 6 μ l of ADP-Glo R1 to terminate the reaction. The plate was
882 incubated for 60 min, followed by addition of 12 μ l of ADP-Glo R2 and incubated further for 60 min in
883 the dark. Data was expressed as velocity (nmol of ADP generated/nmol of enzyme/sec). ADP-ATP
884 standard curves were performed according to the manufacturer's instructions. Luminescence was
885 read using a PHERAstar[®] plate reader with software version 5.41, and analyses were performed using
886 GraphPad Prism 8/9.

887

888 **FRET membrane binding assay**

889 Membrane binding assays were performed as previously published²⁹. Briefly, liposomes were
890 prepared with 5% (w/v) brain PtdIns(4,5)P₂, 20% brain phosphatidylserine, 35% brain
891 phosphatidylethanolamine, 15% brain phosphatidylcholine, 10% cholesterol, 5% sphingomyelin, and
892 10% dansyl-phosphatidylserine (Avanti Polar Lipids). PI3K α was used at a final concentration of 0.5
893 μ M. Protein solutions were preincubated with 10 μ M pY or compounds for 10 min before addition of
894 liposomes. Liposomes were used at a final concentration of 50 μ g/ml. The reaction mixture contained
895 5 μ l enzyme, 2 μ l compound and 3 μ l liposomes, all diluted in 30 mM HEPES, 50 mM NaCl, pH 7.4. The
896 reaction was allowed to proceed for 10 min at room temperature with 384 black-polystyrene plates
897 (Corning #3544) on an orbital shaker at 200 rpm. FRET signals were measured using PHERAStar (BMG)
898 with a 280 nm excitation filter with 350 nm and 520 nm emission filters to measure Dansyl-PS FRET
899 emissions, respectively. FRET signal shown as I-I₀, where I is the intensity at 520 nm, and I₀ is the
900 intensity at 520 nm for the solution in the absence of protein.

901

902 **Surface Plasmon Resonance**

903 SPR was performed with a Biacore T200, using CM7-sensor chips (Cytiva). Both reference control and
904 analyte channels were equilibrated in HBS-P (Cytiva) supplemented with 5% (v/v) DMSO at 20°C. Full
905 length p110 α /p85 α was immobilised onto the chip surface *via* amide coupling using the supplied kit
906 (Cytiva) to reach an RU value of approximately 25,000 RU. Serial dilutions (1:2) of 1938 starting from
907 500 μ M were injected over the chip for 60 s at 30 μ L/min, with a 60 sec dissociation time. The data
908 were double-referenced to the response on a blank but similarly modified flow channel and a buffer-
909 only injection was subtracted. Any differences in the DMSO concentrations between the sample and
910 buffer were corrected using the in-built solvent correction protocol. After reference and buffer signal
911 correction, sensogram data were fitted using Prism 9.4.1 (GraphPad Software Inc). The responses at

912 equilibrium (R_{eq}) of the were then fitted to a 1:1 binding model with a linear non-specific phase to
 913 determine K_d :

$$914 \quad R_{eq} = \left(\frac{C R_{max}}{C + K_d} \right) + DC + B \quad (1)$$

915 where C is the analyte concentration and R_{max} is the maximum response at saturation, D is a non-
 916 specific response and B is the background resonance. Data were replotted correcting for the linear
 917 non-specific response. The binding was performed in triplicate.

918

919 **Differential Scanning Fluorimetry**

920 Thermal denaturation was followed using intrinsic protein fluorescence measured with the
 921 NanoTemper Prometheus NT48 instrument (Nanotemper Technologies, München, Germany).
 922 Samples in HBS-P (Cytiva) supplemented with 5% (v/v) DMSO containing 3 μ M full length p110 α /p85 α
 923 and a 1:2 dilution series of 1938 (from 440 μ M to 13.8 nM) were loaded into standard capillaries and
 924 heated at 2 $^{\circ}$ C/min from 15 to 95 $^{\circ}$ C. The first derivative of the fluorescence emission ratio 350/330
 925 nm were analyzed using the PR.ThermControl v2.3.1 (NanoTemper), to define the T_m . Independent
 926 experiments using the same protein and compound stocks were performed in triplicate. Data were
 927 fitted using Prism 9.4.1 (GraphPad Software Inc). Dissociation constants were calculated using fits to
 928 a single-site ligand depletion model:

$$929 \quad T = T_0 + \frac{(T_1 - T_0) \{ ([C_T] + [P_T] + [K_D]) - \sqrt{([C_T] + [P_T] + [K_D])^2 - 4[C_T][P_T]} \}}{2[P_T]} \quad (2)$$

930 where T_0 and T_1 are the T_m in the absence of titrating compound and at saturation respectively, $[P_T]$
 931 and $[C_T]$ are the total concentrations of protein and compound respectively and K_D is the dissociation
 932 constant.

933

934 **HDX-MS**

935 Sample preparation: HDX-MS experiments were carried out as described previously⁵⁷. Briefly, 4 μ M
 936 PI3K α was incubated with in the absence of compound or with 250 μ M 1938, or 5 μ M BYL719, or both
 937 in a 2.5% DMSO-containing Protein Dilution Buffer (50 mM Tris pH 7.5, 150 mM NaCl, 2 mM DTT). 5
 938 μ l PI3K α either with or without compound was then incubated with 45 μ l D2O Buffer (50 mM Tris pH
 939 7.5, 150 mM NaCl, 5 mM DTT, 2.5% DMSO with or without 125 μ M 1938/ 2.5 μ M BYL719, 90.6% D2O)
 940 for 5 timepoints (0.3 sec/3 sec/30 sec/300 sec/3000 sec, with the 0.3 sec timepoint being a 3 sec
 941 timepoint conducted at 0 $^{\circ}$ C) before being quenched with 20 μ l ice-cold Quench Solution (8 M
 942 Guanidinium Chloride, 0.8% Formic Acid), and being rapidly snap-frozen in liquid nitrogen prior to
 943 storage at -80 $^{\circ}$ C. In total, three biological replicates, i.e. three separate protein preparations, each
 944 with exchange experiments carried out in triplicate were conducted. Data presented in the manuscript
 945 is a single biological replicate. Data acquisition and analysis were as follows: Each sample was thawed
 946 and injected onto an M-Class Acquity UPLC with HDX Technology (Waters) kept at 0.1 $^{\circ}$ C. Proteins were
 947 digested in-line using an Enzymate Pepsin Column (Waters, #186007233) at 15 $^{\circ}$ C for 2 min at 200
 948 μ l/min. Peptic peptides were then eluted onto an Acquity UPLC BEH C18 Column (Waters, #186002346)
 949 equilibrated in Pepsin-A buffer (0.1% formic acid) and separated using a 5-35% gradient of Pepsin-B
 950 buffer (0.1% formic acid, 99% acetonitrile) over 7 min at a flowrate of 40 μ l/min. Data were collected
 951 on a Waters Cyclic IMS, with an electrospray ionisation source, from 50-2000 m/z. Data were collected
 952 in the HDMSe mode. A single pass of the cyclic IMS was conducted. A "blank" sample of protein
 953 dilution buffer with quench was run between samples, and carry-over of peptides was routinely
 954 monitored. Five replicates were used to identify non-deuterated peptides. Criteria used to include
 955 peptides in the HDX-MS dataset were: minimum intensity 5000, minimum sequence length 5,
 956 maximum sequence length 25, a minimum of 3 fragment ions, a minimum of 0.1 products per amino
 957 acid, a minimum score of 6.62, a maximum MH+ Error of 10 ppm, identification in at least two datasets
 958 with a retention time RSD of less than 10%. Data was analysed using Protein Lynx Global Server
 959 (Waters) and DynamX (Waters). All peptides were manually inspected for EX1 kinetics and sufficient
 960 quality of the peptide envelope. Data quality, experiment design, and reporting of data meets the

961 criteria as determined by the HDX-MS community⁵⁸. Uptake files were created using Baryonyx. Data
962 are available via ProteomeXchange with identifier PXD037721.

963

964 ***In vitro* kinase profiling, mTORC1 and ATM kinase assays**

965 133 protein kinases and 7 lipid kinases were counterscreened, with 1988 used at 1 μ M, using the
966 Adapta, Lantha and Z-LYTE assays (SelectScreen Kinase Profiling Service; Thermofisher – experimental
967 details of these assays can be found here:
968 [https://www.thermofisher.com/uk/en/home/industrial/pharma-biopharma/drug-discovery-](https://www.thermofisher.com/uk/en/home/industrial/pharma-biopharma/drug-discovery-development/target-and-lead-identification-and-validation/kinasebiology/kinase-activity-assays.html)
969 [development/target-and-lead-identification-and-validation/kinasebiology/kinase-activity-](https://www.thermofisher.com/uk/en/home/industrial/pharma-biopharma/drug-discovery-development/target-and-lead-identification-and-validation/kinasebiology/kinase-activity-assays.html)
970 [assays.html](https://www.thermofisher.com/uk/en/home/industrial/pharma-biopharma/drug-discovery-development/target-and-lead-identification-and-validation/kinasebiology/kinase-activity-assays.html) . The tree representation in KinMap⁵⁹ generated courtesy of Cell Signaling Technology, Inc.
971 (www.cellsignal.com). mTORC1 (mTOR/RAPTOR/LST8) protein complex and ATM kinase and
972 substrates were produced as previously described^{57,60}. Screening of 1938 was conducted using
973 SuperSep Phos-Tag 50 μ mol/l 100 x 100 x 6.6 mm 17-well (192-18001/199-18011) gels. For ATM assays,
974 100 nM ATM was incubated for 30 min at 30°C with 5 μ M GST-p53 and 1 mM ATP, in the absence or
975 presence of 200 μ M 1938 in ATM Kinase Buffer (50 mM HEPES pH 7.5, 100 mM NaCl, 10% glycerol, 2
976 mM Trichloroethylene, 5 mM MgCl₂). As a positive control for ATM activation, the same reaction was
977 carried out with 100 nM ATM/5 μ M GST-p53/1 mM ATP in the presence of 100 nM Mre11-Rad50-
978 Nbs1 (MRN) complex, a known activator of ATM⁶¹. For mTORC1 assays, 50 nM mTORC1 complex
979 (mTOR/LST8/RAPTOR) was incubated for 3 h at 30°C with 15 μ M 4E-BP1, 10 mM MgCl₂ and 250 μ M
980 ATP, in the absence or presence of 200 μ M 1938. As a ‘positive’ control, a higher concentration (150
981 nM) of mTORC1 complex (mTOR/LST8/RAPTOR) was incubated for 3 h at 30°C with 15 μ M 4E-BP1, 10
982 mM MgCl₂ and 250 μ M ATP. Kinase reactions were quenched by addition of SDS-PAGE Loading Buffer
983 (as per manufacturer’s instructions) and freezing at -20°C before being run on the Phos-tag gels at 150
984 V for 90 min. Gels were then stained using InstantBlue™ Coomassie, and quantified using BioRad
985 Image Lab Software. Kinase assays were carried out in triplicate.

986

987 **Co-crystallisation of p110 α /p85 α niSH2-compound complexes**

988 All crystallisation experiments were performed at a temperature of 20°C. An initial screen of
989 approximately 2000 conditions was performed using the LMB robotic crystallization setup⁶².
990 p110 α /p85 α niSH2 was either pre-incubated with 100 μ M of BYL719 for 1 h, or pre-incubated with
991 100 μ M BYL719 for 1 h followed by incubation with 500 μ M 1938 for 1 h. Sitting drops were set up by
992 mixing 100 nl of reservoir with 100 nl of protein solution (10 mg/ml) in 96-well MRC-plates. Initial
993 crystals were obtained in 0.2 M KSCN, 0.1 M sodium cacodylate pH 6.5, and between 8-30% of PEG
994 2K, PEG 4K, PEG 5K and PEG 6K (w/v), or in 80 mM KSCN, 30% PEG 1K (w/v), 150 mM MES, pH 6.0. For
995 optimisation, the crystallisation was set in a sparse matrix layout by varying the concentrations PEG
996 and KSCN in hanging drops by mixing 1 μ l of 5.5 mg/ml protein with 1 μ l of reservoir. The best
997 diffracting crystals were obtained in a condition containing 10% PEG 5K MME (w/v), 160 mM KSCN,
998 100 mM sodium cacodylate pH 6.5 for both the apo and PI3K α /NVP-BYL719 structures. Crystals were
999 also soaked between 1-20 h in 10 mM 1938. Before data collection, harvested crystals were immersed
1000 in a solution containing the precipitant mixture and 15% 2-methyl-2,4-pentanediol (MPD) and cryo-
1001 cooled in liquid nitrogen.

1002

1003 **Crystallisation of p110 α -compound complexes**

1004 All crystallisation experiments were performed at 18°C. An initial screen of approximately 2300
1005 conditions was performed using the LMB robotic crystallization setup⁶². p110 α was either pre-
1006 incubated with 500 μ M of 1938 or 1% DMSO for 1 h. Sitting drops were set up by mixing 100 nl of
1007 reservoir with 100 nl of protein solution (5.8 mg/ml) in 96-well MRC-plates. Crystals for apo were
1008 obtained from the Morpheus II screen, in 12.5% (w/v) PEG 4K, 20% (v/v) 1,2,6-hexanetriol, 40 mM
1009 Polyamines, 0.1 M MOPSO/bis-tris pH 6.5; and in 12.5% (w/v) PEG 4K, 20% (v/v) 1,2,6-hexanetriol, 90
1010 mM LiNaK, 0.1 M MOPSO/bis-tris pH 6.5. For optimisation with 1938, crystallisation was set up in 96-
1011 well MRC-plates by varying the concentrations of PEG, 1,2,6-hexanetriol and polyamine or LiNaK in

1012 sitting drops by mixing either 200 nl of 5.8 mg/ml protein with 200 nl of reservoir, or 500 nl of 5.8
1013 mg/ml protein with 500 nl of reservoir. Crystals only formed under apo conditions. Crystals were then
1014 soaked for 1.5-2 h in 20 mM 1938 (20% DMSO). For data collection, crystals for apo were obtained in
1015 conditions containing 12.5% (w/v) PEG 4K, 20% (v/v) 1,2,6-hexanetriol, 90 mM LiNaK, 0.1 M
1016 MOPSO/bis-tris pH 6.5 and crystals soaked with 1938 were obtained in conditions containing 12.5%
1017 (w/v) PEG 4K, 20% (v/v) 1,2,6-hexanetriol, 50 mM Polyamines, 0.1 M MOPSO/bis-tris pH 6.5.
1018 Harvested crystals were cryo-cooled in liquid nitrogen prior to data collection.

1019

1020 **Crystal data collection and refinement for p110 α /p85 α niSH2**

1021 All datasets were collected at 100 K. A crystal of the native PI3K was measured at the i03 beam-line
1022 (Diamond Light Source, UK), while the crystal of the PI3K/BYL719 structure was collected at the PetraIII
1023 P13 beam-line (EMBL-Hamburg/DESY, Germany)⁶³. The native data set was indexed, processed and
1024 scaled using the XDS package⁶⁴ and integrated by AIMLESS⁶⁵, while the PI3K/BYL719 was processed by
1025 XDS. Both crystals belonged to the P2₁2₁2₁ space group with a solvent content 50.4 % corresponding
1026 to one complex (containing one catalytic and one regulatory subunit) in the asymmetric unit. The
1027 native PI3K structure was determined by molecular replacement using MOLREP⁶⁶ and the PI3K
1028 structure with PDB ID 4JPS as a search model. The molecular replacement solution was then used as
1029 a starting model for refinement using the high-resolution native data-set of PI3K. After several
1030 iterations of rigid-body, maximum-likelihood and TLS refinement using the PHENIX suite⁶⁷, manual
1031 building and model inspection using COOT⁶⁸, the final model converged to a final Rwork/Rfree of
1032 0.1964/0.2456 at a maximum resolution of 2.20 Å. The PI3K model covers the catalytic subunit
1033 residues 3-313, 322-501, 523-864 and 871-1065 and the regulatory subunit residues 326-591. This
1034 structure was used as a starting model for the PI3K/BYL719 structure which after refinement
1035 converged to a final Rwork/Rfree of 0.1873 / 0.2403 at a maximum resolution of 2.50 Å. Data collection
1036 and refinement statistics are summarised in [Supplementary Table 2a](#).

1037

1038 **Crystal data collection and refinement for p110 α 105-1048**

1039 X-ray diffraction for single crystals of p110 α 105-1048 alone and soaked with 1938 were collected at
1040 the i04 and i24 beamlines, respectively (Diamond Light Source, UK). Images were processed using
1041 automated image processing with Xia2 (Ref.⁶⁹). Both crystals belong to the P2₁2₁2₁ space group. Initial
1042 phases were obtained with molecular replacement, using Phaser in the CCP4 suite, with an initial
1043 model from PDB entry 4TUU. Models were manually adjusted to the densities, using COOT⁶⁸, and the
1044 structures were refined firstly with REFMAC⁷⁰ and with PHENIX⁶⁷ at later stages. A 3D model was built
1045 for 1938 from its chemical structure, using AceDRG in CCP4, and this model agreed well with the
1046 density in the 1938-soaked crystal. The final model converged to a final Rwork/Rfree of 0.24/0.28 at a
1047 maximum resolution of 2.41 Å for p110 α -apo, and Rwork/Rfree of 0.23/0.27 at a maximum resolution
1048 of 2.57 Å for p110 α -1938. Representations of the complex were prepared using PyMOL and Chimera.
1049 Data collection and refinement statistics are summarised in [Supplementary Table 2b](#). Geometry of
1050 1938 was checked using MOGUL 1.8.5 ([Supplementary Table 9](#)).

1051

1052 **Western blot analysis using enhanced chemiluminescence (ECL) detection**

1053 Unless otherwise indicated, western blotting was performed with ECL detection. For time course
1054 studies, A549 cells were seeded at 250,000 cells per well in 6-well plates in RPMI (10% FBS + 1 mM
1055 Na-Pyruvate + 1% P/S) and allowed to adhere overnight. The next day they were serum-starved for 4
1056 h prior to treatment with 100 nM insulin or 5 μ M 1938, for the indicated time (5 min to 48 h) at 37°C,
1057 5% CO₂. For 1938 titration assays in MEFs, cells were seeded at 150,000 cells per well in 6-well plates
1058 and allowed to adhere overnight. The next day they were serum-starved for 4 h prior to treatment
1059 with insulin (1 μ M), 1938 (0.2 to 30 μ M, final DMSO concentration of 1.5%) or inhibitors (final DMSO
1060 concentration of \leq 1.5%) for 15 min at 37°C, 5% CO₂. Cells were washed twice with cold PBS and lysed
1061 using cold RIPA buffer (25 mM Tris.HCl pH 7.6, 150 mM NaCl, 1% NP-40, 1% sodium deoxycholate, 0.1%
1062 SDS supplemented with protease/phosphatase inhibitor cocktail from Merck). To remove cell debris,

1063 homogenates were spun at 13,000 rpm for 15 min at 4°C and the supernatant fraction recovered.
1064 Protein concentration was determined by colorimetric assay (BCA assay, Promega). Protein extracts
1065 were resolved by SDS-PAGE, transferred to nitrocellulose membranes, and incubated overnight at 4°C
1066 with specific antibodies as follows: anti-vinculin (Sigma #V9131) and the following antibodies from Cell
1067 Signaling Technology (CST): pAKT-S473 (CST #9271), pS6-S240/44 (CST #2215), pPRAS40-T246 (CST
1068 #2640) and total S6 (CST #2317). Primary antibodies were used at 1:1000 dilution except anti-vinculin
1069 (1:10000). Secondary antibodies are also from Cell Signalling Technology: Anti rabbit IgG, HRP linked
1070 Antibody (CST #7074S), Anti mouse IgG, HRP linked Antibody (CST #7076S). Raw and uncropped blots
1071 are shown in [Supplementary Fig. 1](#).

1072 **Western blot analysis using Wes™**

1073 A549 cells were seeded at 200,000 cells per well in 24-well plates in DMEM (10% FBS + 1% P/S) and
1074 allowed to adhere overnight. The next day, cells were washed once with PBS before addition of serum-
1075 free DMEM for 24 h. On the day of treatment, cells were incubated in fresh serum-free DMEM prior
1076 to treatment. 15 min pre-treatment with either PI3K α inhibitor (BYL719, 500 nM) or 0.1% DMSO was
1077 performed prior to 1938 addition for 15 min at 37°C, 5% CO₂. Following incubation, cells were washed
1078 and lysed in RIPA buffer (Thermo), supplemented with protease and phosphatase inhibitors (Roche).
1079 The lysate was collected and centrifuged at 15,000 rpm for 15 min at 4°C, supernatant collected and
1080 stored at -80°C. Western blotting was performed by Wes™ (ProteinSimple) according to the
1081 manufacturer's instructions. Antibodies for pAKT-S473 (CST #4060) and total AKT (CST #9272) were
1082 used at 1:50; antibody to β -actin (CST #4970) was used at 1:100. Raw and uncropped blots are shown
1083 in [Supplementary Fig. 1](#).

1084 **Detection of AKT phosphorylation by ELISA**

1085 A549 cells were seeded at 50,000 cells per well in 96-well plates in DMEM (10% FBS + 1% P/S). The
1086 next day cells were washed once with PBS before addition of serum-free DMEM for 24 h. On the day
1087 of treatment, cells were incubated in fresh serum-free DMEM prior to treatment. Compounds
1088 solubilised to 10 mM in DMSO were diluted 1:3 in an 8-point concentration response curve in DMSO.
1089 Concentration response curves were diluted in serum-free DMEM by transfer into intermediate plates
1090 using a BRAVO liquid handler (Agilent). Intermediate plates were then used to treat cell plates using
1091 the BRAVO liquid handler. Compound concentration response curves had a top concentration of 50
1092 μ M and a final well concentration of 0.5% DMSO. Cell plates were treated for 15 min at 37°C, 5% CO₂
1093 before being washed with ice-cold PBS and lysed in lysis buffer 6 (R&D Systems #895561) and freezing
1094 at -80°C. Levels of pAKT^{S473} were determined using the phospho-AKT (S473) pan-specific Duoset IC
1095 ELISA (R&D Systems #DYC887BE) in 96-well white high-binding plates (Corning #3922) according to
1096 manufacturer's instructions. Endpoint luminescence was measured using a Sense (Hidex) platereader.
1097 Compound data were corrected to the negative DMSO control and expressed as a percentage the
1098 internal insulin control (1 μ M), equivalent to the maximal activation (E_{max}) induced by insulin. Data
1099 were transformed and EC₅₀ data were determined by variable slope (4 parameters) non-linear
1100 regression using Prism 7 (Graphpad).

1101

1102 **Cell culture**

1103 Immortalised PI3K α -WT and PI3K α -KO MEFs were generated and described previously⁴⁵. MEFs were
1104 cultured in DMEM containing 10% FBS and 1% penicillin-streptomycin and starved in serum-free
1105 DMEM with 1% penicillin-streptomycin at 37°C and 5% CO₂. A549 cells were cultured either in DMEM
1106 Glutamax (Gibco #31966021) supplemented with 10% FBS and 1% penicillin-streptomycin, or in RPMI
1107 1640 medium supplemented with 10% FBS, 1 mM sodium pyruvate and 1% penicillin-streptomycin.
1108 For starvation experiments, A549 cells were incubated in serum-free RPMI containing 1 mM sodium
1109 pyruvate and 1% penicillin-streptomycin. All cell cultures were regularly tested to be negative for
1110 Mycoplasma.

1111

1112

1113 **Plasmid vectors**

1114 Flag-*PIK3R1* (a kind gift of Neil Vasan), *PIK3CA*-WT and mutant *PIK3CA* (D603K, L1006R, F1016S and
 1115 L1006R/F1016S) were cloned into pcDNA3.4TOPO. pcDNA3-eGFP was used as a control for
 1116 transfection efficiency and is available on Addgene repository upon request (Plasmid #13031). The
 1117 mutations in *PIK3CA* were introduced by site-directed mutagenesis according to published commercial
 1118 protocols using NEBuilder HiFi DNA Assembly Master Mix (NEB E2621). For each mutation, a pair of
 1119 primers were designed to incorporate a mutation within the gene, with the resulting PCR products
 1120 containing a 20 bp overlap and the desired mutations. The DpnI-treated and purified PCR products
 1121 were combined with the linearized vector and treated with the NEBuilder HiFi DNA Assembly Master
 1122 Mix. Following transformation, single colonies were grown and purified with QIAprep spin Miniprep
 1123 kit (Qiagen 27106). All plasmids were sequenced for verification.

1124 **Transient transfection of WT and mutant *PIK3CA* constructs in MEFs**

1125 eGFP, Flag-*PIK3R1*, *PIK3CA*-WT and mutant *PIK3CA* (D603K, L1006R, F1016S, L1006R/F1016S) plasmids
 1126 were used for transient transfection. *Pik3ca*-KO MEFs cells were seeded at 70-80% confluency in 6-
 1127 well plate at 100,000 cells per well. The next day, fibroblasts was transfected using Lipofectamine™
 1128 3000 Transfection Reagent (ThermoFisher) as follows: 2.5 µg of plasmid DNA cocktail (containing
 1129 equimolar amount 1:1 of *PIK3CA*:*PIK3R1* plasmids) were mixed in Opti-MEM medium (ThermoFisher)
 1130 with 5 µl P3000 reagent. The diluted DNA mix was then added to a premix containing 7.5 µl
 1131 Lipofectamine 3000 in Opti-MEM in 1:1 ratio. After 10 min incubation, the DNA-lipid complex was
 1132 added to the cells and incubated for 48 h before treatment. All cells were serum starved for 4 h before
 1133 treatment with 5 µM of 1938 or DMSO and lysed in RIPA buffer.

1134 **Generation of *PIK3CA*-null A549 cells by CRISPR/Cas9 gene targeting**

1135 Generation of pooled *PIK3CA*-null A549 cells was outsourced to Synthego Corporation. Briefly, the
 1136 *PIK3CA* gene was targeted with synthetic ribonucleoprotein (RNP) complexes including the following
 1137 single guide RNA (sgRNA) sequence: 5'-*CUCUACUAUGAGGUGAAUUG*-3'. This sequence is located
 1138 within *PIK3CA* exon 3 and covers the coding sequence preceding the p110α RAS binding domain, with
 1139 the Cas9 cut site corresponding to amino acids 156/157 of p110α). In parallel, control cultures were
 1140 exposed to the Cas9 protein without sgRNA, henceforth referred to as "WT cultures". Single-cell clones
 1141 were established from both WT and targeted cultures by limiting dilution, thereby ensuring seeding
 1142 of maximum 1 cell per well of a 96-well plate. To promote recovery, subcloned cells in 96-wells were
 1143 cultured in a 1:1 mixture of standard A549 complete medium and conditioned medium. Conditioned
 1144 medium was prepared from WT cultures 2 days post-passaging by centrifuging the medium at 1000g
 1145 for 10 min, followed by 0.22 µm PES filtration and storage at 4°C (-80°C for storage exceeding 2 weeks).
 1146 The medium was replenished every 2-3 days, as gently as possible to prevent cells from dislodging.
 1147 Once cells reached sub-confluence, they were expanded to 24-well plates and 25 cm² flasks, followed
 1148 by genotyping and cell banking.

1149 For genotyping, genomic DNA was extracted from replicas of the cells cultured in 24-well plates
 1150 using 50 µl QuickExtract solution (Cambridge Bioscience #QE0905T) and the following thermocycling
 1151 conditions: 68°C for 15 min, 95°C for 10 min, 4°C HOLD. The edited locus was amplified by standard
 1152 PCR using GoTAQ G2 MasterMix (2X) (Promega #M7822) with 2 µl QuickExtract-processed genomic
 1153 DNA and the following primers: F 5'-*TCTACAGAGTCCCTGTTTGC*-3'; R 5'-
 1154 *AGCACTCAACTATATCTTGTCAGT*-3'. Annealing and extension were performed at 55°C for 30 sec and
 1155 72°C for 30 sec, respectively. The PCR reactions were cleaned up with ExoSAP-IT Express (Thermo
 1156 Fisher Scientific #75001.1.ML) according to the manufacturer's instructions, at 37°C for 30 min
 1157 followed by 80°C for 1 min. The cleaned-up reactions were submitted for Sanger sequencing (Eurofins
 1158 Genomics). Subsequent analyses of the Sanger sequencing traces were performed using Synthego's
 1159 open-source ICE tool⁷¹. Next, all predicted knock-out (KO) clones were validated by Western blotting
 1160 for the *PIK3CA* protein using two complementary antibodies (CST #4249 and CST #4255; each used at
 1161
 1162

1163 1:1000 dilution in 1X TBS/T with 3% BSA). Clones with confirmed loss of p110 α expression were kept
1164 for further experimental studies.

1165 The A549 clones used for the TIRF experiments (Fig. 3d) were *PIK3CA*-WT clone 9 and *PIK3CA*-KO
1166 clone 12. The DNA sequencing traces and p110 α Western blots of these A549 clones are shown in
1167 Extended Data Fig. 9. The *PIK3CA*-KO clone 12 shows a +1 bp insertion, resulting in a frameshift and
1168 the generation of a premature stop codon as shown in Extended Data Fig. 9 left panel.

1169

1170 **Mass spectrometry-based phosphoproteomics**

1171 PI3K α -WT and PI3K α -KO MEFs, grown in 15 cm dishes, were serum-starved overnight in DMEM with
1172 1% penicillin-streptomycin and stimulated by the addition of 0.05% DMSO, 5 μ M 1938 in final 0.05%
1173 DMSO or 100 nM insulin (Sigma #15016) for 15 min or 4 h. Cells were lysed in 500 μ l urea lysis buffer
1174 [50 mM triethylammonium bicarbonate, 8 M urea, cOMplete™, EDTA-free protease inhibitor cocktail
1175 (1:50 dilution) (Roche #11873580001), 1 PhosSTOP tablet (Roche #4906845001) per 10 ml of lysis
1176 buffer, 1 mM sodium orthovanadate] and lysates sonicated until clear for ~10 min with cooling breaks
1177 on ice. Protein concentration was measured using a BCA protein assay (Pierce #23227). 300 μ g of
1178 protein was reduced with 5 mM Tris(2-carboxyethyl)phosphine hydrochloride (Sigma #C4706) at 37°C
1179 for 20 min and alkylated using 10 mM 2-chloroacetamide (Sigma #22790) for 20 min at room
1180 temperature in the dark. Proteins were digested with LysC (#129-02541; FUJIFILM Wako Chemicals,
1181 Osaka, Japan) for 3.5 h at 30°C. Samples were then diluted with 50 mM triethylammonium bicarbonate
1182 (Sigma #T7408) to reduce the urea concentration to 1.5 M, followed by an overnight peptide digestion
1183 with trypsin (Promega #V5113) at 37°C. Digest reactions were quenched by the addition of 10%
1184 trifluoroacetic acid (EMD Millipore #302031-M) to a final pH of 2.0. Sample desalting was performed
1185 using 35-350 μ g C18 columns (HMM S18V; The Nest Group, Inc., Southborough, MA, USA) according
1186 to the manufacturer's specifications. TiO₂ (Hichrome Titansphere TiO₂, 10 μ m capacity, 100 mg, GL
1187 Sciences #5020-75010) was used for phosphoenrichment. Following peptide loading onto TiO₂, the
1188 beads were sequentially washed with 1 M glycolic acid (Sigma #124737)/80% acetonitrile/5%
1189 trifluoroacetic acid, followed by 80% acetonitrile/0.2% trifluoroacetic acid and 20% acetonitrile before
1190 elution with 5% ammonium hydroxide. Enriched samples were desalted using 7-70 μ g C18 columns
1191 (HUM S18V; The Nest Group, Inc., Southborough, MA, USA) according to the manufacturer's
1192 specifications. Dried phosphopeptide samples were stored at -80°C and resuspended in 10% formic
1193 acid immediately prior to analysis. nLC-MS/MS was performed on a Q-Exactive Orbitrap Plus
1194 interfaced to a NANOSPRAY FLEX ion source and coupled to an Easy-nLC 1000 (Thermo Scientific). Fifty
1195 percent of each sample was analysed as 10 μ l injections. Peptides were separated on a 27 cm fused
1196 silica emitter, 75 μ m diameter, packed in-house with Reprosil-Pur 200 C18-AQ, 2.4 μ m resin (Dr.
1197 Maisch, Ammerbuch-Entringen, Germany) using a linear gradient from 5% to 30% acetonitrile/0.1%
1198 formic acid over 180 min, at a flow rate of 250 nl/min. Peptides were ionised by electrospray ionisation
1199 using 1.9 kV applied immediately prior to the analytical column via a microtee built into the nanospray
1200 source with the ion transfer tube heated to 320°C and the S-lens set to 60%. Precursor ions were
1201 measured in a data-dependent mode in the orbitrap analyser at a resolution of 70,000 and a target
1202 value of 3e6 ions. The ten most intense ions from each MS1 scan were isolated, fragmented in the
1203 HCD cell, and measured in the Orbitrap at a resolution of 17,500.

1204

1205 **Peptide identification, quantification and statistical analysis of phosphoproteomics data**

1206 Raw data were analysed with MaxQuant⁷² (version 1.5.5.1) where they were searched against the
1207 mouse UniProt database (<http://www.uniprot.org/>, downloaded 04/12/2018) using default settings.
1208 Carbamidomethylation of cysteines was set as fixed modification, and oxidation of methionines,
1209 acetylation at protein N-termini, phosphorylation (on S, T or Y) were set as variable modifications.
1210 Enzyme specificity was set to trypsin with maximally 2 missed cleavages allowed. To ensure high
1211 confidence identifications, peptide-spectral matches, peptides, and proteins were filtered at a less
1212 than 1% false discovery rate (FDR). Label-free quantification in MaxQuant was used with a LFQ
1213 minimum ratio count of 2, Fast LFQ selected and the 'skip normalisation' option selected. The 'match

1214 between runs' feature was selected with a match time window of 0.7 min and an alignment time
1215 window of 20 min. The MaxQuant 'phospho(STY)Sites.txt' output file was reformatted by merging
1216 each protein accession and gene name with its corresponding phosphosite to obtain an
1217 'Annotated_PhosphoSite.txt'. This file, together with the MaxQuant 'evidence.txt' output file and an
1218 experimental design 'annotation.csv' file, was further processed by removing contaminants and
1219 reversed sequences, and the removal of phosphosites with 0 or 1 valid values across all runs. High
1220 experimental reproducibility was observed, as evidenced by an average Pearson Correlation
1221 Coefficient of $r=0.862$ for biological replicates (Extended Data Fig. 6e). Quantified phosphopeptides
1222 were analysed within the model-based statistical framework MSstats⁷³ (version 3.20.0, run through
1223 RStudio (version 1.2.5042, R version 4.0.0)). Data were log₂ transformed, quantile normalised, and a
1224 linear mixed-effects model was fitted to the data. The group comparison function was employed to
1225 test for differential abundance between conditions. p-values were adjusted to control the FDR using
1226 the Benjamini-Hochberg procedure⁷⁴. The mass spectrometry proteomics data have been deposited
1227 to the ProteomeXchange Consortium via the PRIDE⁷⁵ partner repository with the dataset identifier
1228 PXD027993. Reviewer account details: Username: reviewer_pxd027993@ebi.ac.uk; Password:
1229 FSaiKH6M)

1230

1231 **Quantification of phosphoinositide species by mass spectrometry**

1232 A549 cells ($5 \cdot 10^5$) or wild-type MEFs ($3 \cdot 10^5$) were plated in complete media onto 3.5 cm dishes or 60
1233 mm dishes respectively for 24 h, prior to FCS-free starvation media for 16 h. MEFs, in addition, were
1234 supplemented with arachidonic acid in the FCS-free starvation media as previously described⁷⁶. Cells
1235 were stimulated with indicated doses of 1938, PDGF-BB, insulin, or DMSO vehicle control
1236 (corresponding to DMSO amounts in 30 μ M 1938) for the indicated time points at 37°C, 5% CO₂.
1237 Reactions were terminated in 600 μ l ice-cold 1 M HCl and cells scraped and resuspended, then divided
1238 into two equal samples in eppendorfs. Samples were processed and extracted for C38:4:PI(3,4,5)P₃,
1239 or PIP₂ regio-isomer C38:4-PI(3,4)P₂/PI(4,5)P₂ analysis by mass spectrometry, essentially as described³⁹,
1240 with the exception that the following internal standards (ISDs, all synthesized by the Biological
1241 Chemistry Department at the Babraham Institute, Cambridge) were also included: d6-stearoyl-
1242 arachidonoyl (C18:0/C20:4) -PI (74.8 ng), -PI(4)P (925 ng) and -PI(4,5)₂/PI(3,4)P₂ (prepared as a 1:1 mix,
1243 100 ng total PIP₂). The data are shown as response ratios, calculated by normalizing the multiple
1244 reaction monitoring (MRM)-targeted lipid integrated response area to that of a known amount of
1245 relevant internal standard. To account for any cell input variability, PIP₃ response ratios were
1246 normalized to C38:4-PI response ratios; while PI(3,4)P₂ response ratios were normalised to PI(4,5)P₂
1247 response ratios. Data shown are mean \pm SD for $n \geq 3$, except for non-DMSO control in MEF PIP₃
1248 measurements where $n=1$.

1249

1250 **Total internal fluorescence (TIRF) microscopy of phosphoinositide reporters**

1251 Phosphoinositide reporters used were GFP-PH-ARNO^{1303E}x2 (PIP₃ reporter⁴¹) and mCherry-cPH-
1252 TAPP1x3 (PI(3,4)P₂ reporter⁴¹). TIRF microscopy allows selective imaging of the small cell volume,
1253 including the plasma membrane, directly adjacent to the coverslip onto which cells have been seeded.
1254 HeLa or A549 cells were seeded in Matrigel-coated (Corning #354230; diluted in Opti-MEM at 1:50) 8-
1255 well chamber slides (glass bottom, 1.55 refractive index; Thermo Fisher Scientific #155409) at a density
1256 of 5,000 cells/well. The following day, cells were transfected with 50 ng (A549) or 10 ng (HeLa) PIP₃
1257 reporter plasmid (GFP-PH-ARNO^{1303E}x2)⁴¹ using FuGENE® HD Transfection Reagent (Promega #E2311),
1258 at a 3:1 Fugene:DNA ratio according to the manufacturer's instructions. To ensure low yet uniform
1259 expression of the reporters in HeLa cells, and to aid in the identification of the critical TIRF angle for
1260 imaging, these cells were also co-transfected with 200 ng iRFP-tagged Paxillin plasmid (generated by
1261 conventional restriction enzyme-based subcloning from an mCherry-Paxillin plasmid, Addgene
1262 #50526). In separate experiments, HeLa cells were also transfected with 10 ng or 50 ng of the PI(3,4)P₂
1263 reporter mCherry-cPH-TAPP1x3 (Ref.⁴¹); the use of 50 ng of this reporter enabled easier visualisation

1264 in the TIRF field, however the kinetics of the response remained unchanged and results from both
1265 experiments were pooled.

1266 Following another 24 h post-transfection, cells were switched to 150 μ l serum-free Fluorobrite™
1267 DMEM (Thermo Fisher Scientific #A1896701; supplemented with L-glutamine (2 mM) and 1%
1268 penicillin-streptomycin for 3 h prior to time-lapse imaging on a 3i Spinning Disk Confocal microscope
1269 fitted with a sCMOS Prime95B (Photometric) sensor for TIRF, with full temperature (37°C) and CO₂
1270 (5%) control throughout the acquisitions. A 100X 1.45 NA plan-apochromatic oil-immersion TIRF
1271 objective was used to deliver the laser illumination beam (40-50% power) at the critical angle for TIRF
1272 and for acquisition of the images by epifluorescence (300-500 msec exposure) using single bandpass
1273 filters (445/20 nm and 525/30 nm). Acquisition was performed in sequential mode, without binning,
1274 using Slidebook 6.0 and an acquisition rate of 2 or 3 min as indicated. Individual treatments were
1275 added at the specified times at 2x to 5x concentration in the same imaging medium, ensuring correct
1276 final concentration and sufficient mixing with the existing medium solution. BYL719 (Advanced
1277 ChemBlocks Inc #R16000) was used at a concentration of 0.5 μ M.

1278 Image analyses of total reporter intensities were performed with the Fiji open source image
1279 analysis package⁷⁷. The region of interest (ROI) corresponding to the footprint of the individual cell
1280 across time points were defined using minimal intensity projection to select only pixels present across
1281 all time points, following prior subtraction of camera noise (rolling ball method, radius = 500 pixels)
1282 and xy drift correction, intensity levels over time were measured. These analyses were performed with
1283 a custom-written Fiji/ImageJ macro. A second macro was used to generate scaled images, with
1284 normalisation of all pixels to pre-treatment average intensity ($F_t/F_{baseline}$). All other quantifications
1285 were performed using the open source software R/RStudio. The values plotted in Fig. 3d (iii) represent
1286 mean \pm SEM, following signal scaling to minimum and maximum values of the normalised fluorescence
1287 intensity for each time point ($F_{n(t)}$). All raw images, macros and R analysis scripts are provided via the
1288 Open Science Framework (https://osf.io/gzxfm/?view_only=8de666831f5b444087a0ab7c6cf3a636).
1289

1290 **CellTiter-Glo® cell assay**

1291 MEFs were seeded at 5000 cells per well in 96-well plates in DMEM supplemented with 10% FBS and
1292 1% P/S, and allowed to attach overnight. The next day, cells were serum starved for 4 h prior to
1293 compound treatment in fresh serum-free DMEM. Compounds solubilised in DMSO were diluted 1:2 in
1294 a 12-point concentration response curve in DMSO. Intermediate plates were prepared by transferring
1295 4 μ l of compounds in DMSO into 96 μ l of serum-free DMEM media. This was then used to treat cell
1296 plates by transferring 12.5 μ l of solution from the intermediate plate into 87.5 μ l of serum-free DMEM
1297 in the cell plates. Compound concentration response curves had a top concentration of 30 μ M and a
1298 final well concentration of 0.5% DMSO. Cell plates were incubated for 24 h, 48 h or 72 h at 37°C, 5%
1299 CO₂, followed by determination of cell survival using the CellTiter-Glo® reagent according to
1300 manufacturer's instructions (Promega #G7571). Endpoint luminescence was measured using
1301 CLARIOstar (BMG). Compound data were analyzed using GraphPad Prism 8.
1302

1303 **Measurement of cell proliferation by crystal violet staining**

1304 MEFs were seeded at 5000 cells per well in 96-well plates in DMEM supplemented with 10% FBS and
1305 1% P/S, and allowed to attach overnight. The next day, cells were serum-starved for 5 h prior to
1306 compound addition in fresh serum-free DMEM. After different time points, cells were rapidly washed
1307 with distilled H₂O before fixed and stained in a solution of 0.5% crystal violet (Sigma-Aldrich #C0775)
1308 in 20% methanol (v:v) as described⁷⁸. Briefly, after 20 min incubation at room temperature on a
1309 rocking platform, fixed and stained cells were washed 3 times with distilled H₂O and plates air-dried
1310 overnight. 200 μ l methanol was next added to each well and the plates were incubated at room
1311 temperature for 20 min on a bench rocker, followed by measurement of optical density at 570 with a
1312 plate reader.
1313

1314 **Measurement of cell cycle progression by Edu staining**

1315 The Click-IT EdU protocol was used according to manufacturer instructions (Sigma-Aldrich #BCK-
1316 FC488-50). Briefly, MEFs were seeded at 50,000 cells per well in 6-well plates in DMEM supplemented
1317 with 10% FBS and 1% P/S, and allowed to attach overnight. The next day, cells were serum-starved for
1318 5 h prior to compound addition for 24 h in fresh serum-free DMEM. Cells were then pulsed for 3 h
1319 with 10 μ M EdU, followed by collection by trypsinization and fixation with 3.7% FA in PBS for 15 min
1320 in the dark, washed in 3% BSA and permeabilized in 1x saponin-based permeabilization buffer for 20
1321 min in the dark. EdU was then detected using the FAM-azide assay cocktail for 30 min in the dark. Cells
1322 were washed twice in 1x saponin-based permeabilization buffer followed by analysed with flow
1323 cytometer (Novocyte Advanteon flow cytometer, Agilent). Gating strategy for flow cytometry is shown
1324 in **Supplementary Fig. 2**.

1325

1326 **Langendorff perfused heart preparation in rats**

1327 The Langendorff *ex vivo* perfused rat heart was used as an experimental model of IRI⁷⁹. The animal
1328 experiments were conducted within the terms of the UK Animals (Scientific Procedures) Act 1986,
1329 under Project Licence number PPL 70/8556 (Protection of the Ischaemic and Reperfused Myocardium).
1330 All procedures conform to the guidelines from Directive 2010/63/EU of the European Parliament on
1331 the protection of animals used for scientific purposes. Male Sprague–Dawley rats were bred at a
1332 central animal unit in University College London and used at a weight of 250–350 g. Rats were
1333 anaesthetised by intraperitoneal injection of sodium pentobarbitone (60 mg/kg) (Animalcare, York,
1334 UK). Hearts were quickly excised via a clamshell thoracotomy and the aorta cannulated and
1335 retrogradely perfused on a Langendorff apparatus with a modified Krebs–Henseleit buffer (118 mM
1336 NaCl, 25 mM NaHCO₃, 11 mM D-glucose, 4.7 mM KCl, 1.22 mM MgSO₄·7H₂O, 1.21 mM KH₂PO₄ and
1337 1.84 mM CaCl₂·2H₂O, 37°C, pH 7.35–7.45, gassed with 95% O₂/5% CO₂) with a gravity-fed perfusion
1338 pressure of 70–80 mm Hg according to standard methods⁷⁹. The temperature of the heart was
1339 maintained at 37.0 \pm 0.5°C. All hearts were made globally ischaemic by stopping flow for 45 min and
1340 then reperfused for 2 h. The heart was perfused during the first 15 min of reperfusion with modified
1341 Krebs–Henseleit buffer containing either 1938 (5 μ M) or insulin (1 μ M) or an equivalent volume of
1342 vehicle (DMSO, final concentration 0.1 %). At the end of the protocol, hearts were frozen at -20°C
1343 before being sectioned into 5 transverse slices and stained for viable tissue by immersion in 1%
1344 triphenyl-tetrazolium chloride at 37°C for 15 min. Following fixation in 10% formalin for 24 h, the
1345 sections were digitally scanned for analysis. Analysis of infarct size (IS) as a proportion of area at risk
1346 (AAR) was calculated via planimetry using imageJ software (version 1.45, National Institutes of Health,
1347 USA).

1348 Alternatively, after 15 min reperfusion, perfusion was stopped and hearts were freeze-clamped
1349 in liquid nitrogen and frozen at -80°C. Tissues were incubated in lysis buffer (100 mM Tris.HCl pH 7.4,
1350 300 mM NaCl, 0.5% IGEPAL with 1x Halt protease inhibitor cocktail (#78429; Thermo Scientific,
1351 Loughborough, UK), 1x Halt phosphatase inhibitor cocktail (#78420; Thermo Scientific, Loughborough,
1352 UK) and 5 μ M EDTA (Thermo Scientific, Loughborough, UK)) and homogenised on ice using a Potter-
1353 Elvehjem tissue grinder for 1 min using 20 strokes with the pestle, and sonicated on ice (3-5 pulses of
1354 5 sec, amplitude 40-50 x 25) using a Vibracell sonicator. Protein content was determined by
1355 bicinchoninic acid (BCA) assay (Sigma-Aldrich, Gillingham, UK). Tissue lysates were mixed with NuPAGE
1356 LDS Sample Buffer (Thermo Fisher Scientific) plus 2.5% 2-mercaptoethanol and denatured at 80°C for
1357 10 min. 20 μ g protein was run on NuPAGE Novex 10% Bis-Tris protein gels (Thermo Fisher Scientific,
1358 Loughborough, UK) using the Mini Protean III system (Bio-Rad, Watford, UK) and electro-transferred
1359 onto nitrocellulose blotting membrane (GE Healthcare Life Science, Amersham UK) using wet transfer
1360 in a Bio-Rad Mini Trans-Blot. The membranes were blocked in 5% bovine serum albumin/TBS-Tween-
1361 20 (#P2287; Sigma; 0.1%) then incubated with primary antibodies at 4°C overnight. Primary antibodies
1362 used were directed against total AKT (#2920; Cell Signaling Technology, UK), pAKT^{S473} (#4060; Cell
1363 Signaling Technology, UK) and β -actin (#sc-47778; Santa Cruz Biotechnology, UK) as a gel loading
1364 control. The next day, membranes were probed with IRDye fluorescence-tagged secondary antibodies

1365 (#926-32211 and #926-68020; LI-COR Biosciences, Ltd. UK) and imaged and quantified using the
1366 Odyssey imaging system (Image Studio Lite Ver 5.2; LI-COR Biosciences, Cambridge, UK).

1367

1368 ***In vivo* model of ischaemia reperfusion injury in mice**

1369 Male C57/BL6 mice weighing 25-30 g were used throughout. Animals received humane care in
1370 accordance with the United Kingdom Home Office Guide on the Operation of Animal (Scientific
1371 Procedures) Act 1986, Project Licence PPL70/15358.

1372 Animals were anaesthetised with intraperitoneal (i.p.) sodium pentobarbital at a dose of 100
1373 mg/kg. The mice were intubated by tracheotomy and ventilated with room air using a small animal
1374 ventilator (MinVent, Type 845, Hugo Sachs Elektronik, Harvard Apparatus). The mice were then placed
1375 on a heating pad and the rectal temperature monitored and maintained at ~37°C using a temperature
1376 controller. During the experiments, both ECG and heart rate were continuously recorded using a
1377 PowerLab (Adinstrument, USA). The chest was opened in the intercostal space between the 3rd and
1378 4th ribs to expose the heart, and a suture was placed around the left anterior descending (LAD)
1379 coronary artery followed by a snare to allow the occlusion and opening of the LAD. The left external
1380 jugular vein was cannulated for drug administration.

1381 By tightening the suture snare to occlude the LAD coronary artery, the hearts were subjected to
1382 40 min ischaemia, which was confirmed by both ST-segment elevation on the ECG and a change in
1383 heart colour. After 40 min, the snare was loosened and the heart allowed to reperfuse for the next
1384 120 min. 15 min prior to reperfusion, 50 µl of DMSO vehicle or 10 mg/kg 1938 compound in DMSO,
1385 was slowly injected via the jugular vein. The person carrying out the experiment was blinded to the
1386 treatment groups.

1387 After 120 min reperfusion, the chest was re-opened, the heart was removed and cannulated via
1388 the thoracic aorta, and blood within the heart was washed out with saline. The LAD coronary artery
1389 was then re-occluded with the suture that had been left loosely in place following ischaemia, and the
1390 hearts were injected with 2% Evans blue to delineate the area at risk. These hearts were then frozen
1391 at -80°C for ~10 min and subsequently cut into 5-6 slices of ~0.5 mm thickness. The heart slices were
1392 incubated in triphenyltetrazolium chloride (10 mg/ml) solution at 37°C, pH 7.4 for ~15 min to delineate
1393 viable (stained red) from the necrotic tissue (white regions). Slices were then transferred to 10%
1394 formalin solution and fixed overnight. The heart slices without right ventricular wall were then
1395 scanned using a Cannon digital scanner. The total area of myocardium, the non-ischaemic area (which
1396 is stained with Evans blue), and the infarct area (i.e. the white area) of each slice were measured using
1397 Image-J software. The “area at risk” was calculated by subtraction of the non-ischaemic area (blue
1398 area) from the whole slice area and expressed as “percentage of the left ventricle”, and “infarct size”
1399 calculated as infarct area as a percentage of the area at risk. 4 mice died during the experiment, before
1400 reperfusion (3 in DMSO group, 1 in 1938 group) and were excluded from analysis.

1401 Analysis of tissue samples by Western blotting was performed as follows. 50 µl of DMSO vehicle
1402 or 10 mg/kg 1938 compound in DMSO, was injected via the jugular vein of anaesthetized and
1403 intubated mice as described above. After 15 min, the chest was opened, and the heart removed and
1404 freeze-clamped in liquid nitrogen. Hearts were then homogenized in lysis buffer [100 mM Tris.HCl,
1405 300 mM NaCl, 1% IGEPAL, pH 7.4 supplemented with protease inhibitors (78438; Thermo Fisher
1406 Scientific) and phosphatase inhibitors (78427; Thermo Fisher Scientific)], by disruption using a pestle
1407 and mortar and sonicated on ice 5 times for 3 sec. The supernatant was then collected and after the
1408 addition of NuPAGE™ LDS Sample Buffer (4X) (Thermo Fisher Scientific), samples were boiled and
1409 stored at -80°C until SDS-polyacrylamide gel electrophoresis (SDS-PAGE) was performed. 20 µg of
1410 protein per well was loaded on a 10% NuPAGE Bis-Tris gel (Invitrogen), resolved by SDS-PAGE, and
1411 transferred to PVDF membranes (Millipore) for Western blot analysis. Membranes were incubated
1412 with primary antibodies in 5% BSA/TBS-0.1% Tween-20 overnight at 4°C, washed three times for 10
1413 min with TBS-0.1% Tween then incubated with secondary antibodies in 5% BSA/TBS-0.1% Tween for
1414 1 h, followed by washing three times for 10 min with TBS-0.1% Tween. Antibodies used were mouse
1415 monoclonal antibody to β-actin (Santa Cruz; sc-47778; used at 1:2000), mouse monoclonal antibody

1416 to total Akt (Cell Signaling Technology; CST2920; used at 1:1000) and rabbit antibodies from Cell
1417 Signaling Technology to phospho-Akt Ser473 (CST9271; used at 1:1000). Secondary antibodies used
1418 were IRDye 680LT goat anti-mouse and IRDye 800CW goat anti-rabbit (LI-COR Biosciences). Proteins
1419 were visualized and quantified using the Odyssey Imaging System (LI-COR Biosciences).

1420

1421 **Animals for neurological studies**

1422 Adult rats (Charles River, UK) were housed in groups of 4-5 per cage and maintained on a 14:10-h
1423 light/dark cycle with ad lib access to food and water. All experiments were conducted in accordance
1424 with the UK Animals (Scientific Procedures) Act (1986) and the European Communities Council
1425 Directives (86/609/EEC), with approval from the University College London Animal Welfare and Ethical
1426 Review Board.

1427

1428 **Quantification of neurite outgrowth**

1429 Dissociated adult rat dorsal root ganglion (DRG) cultures were used as an *in vitro* model for
1430 neuroregeneration^{80,81}. DRG neurons were isolated from adult male (>250g) Wistar rats as described,
1431 with DRGs from each rat cultured separately⁸¹. Following culling via schedule 1 (rising concentration
1432 of CO₂), the spinal column was removed and stored in PBS on ice. Cord tissue was removed to expose
1433 the DRGs and roots in the intervertebral foramen and the DRGs removed with forceps and scalpel
1434 under a dissecting microscope (Olympus SZ40). DRGs were manually cleaned by removal of roots,
1435 capsule and capillaries with forceps and then placed in DMEM supplemented with P/S. DRGs were
1436 treated with 0.125% collagenase type IV solution at 37°C for 90 min, and then mechanically dissociated
1437 by trituration using a 1 ml pipette. The collagenase solution was removed by 2 rounds of centrifugation
1438 in complete DMEM (DMEM with 1% P/S and 10% FBS) at 400 xg for 5 min, followed by resuspension
1439 of the DRG cell pellet in complete DMEM supplemented with 0.01 mM cytosine arabinoside. DRGs
1440 were plated in 75-cm² flasks coated with 0.1 mg/ml poly-D-lysine and incubated at 37°C, 5% CO₂. 24 h
1441 later, DRGs were resuspended by trypsinisation, and the trypsin was removed by centrifugation at 190
1442 xg for 4 min. The resultant cell pellet was resuspended by mechanical trituration in Neurobasal-A
1443 medium (Gibco #10888022) supplemented with B-27 (Gibco #17504044), 2 mM L-Glutamine (Merck
1444 #G7513) and 1% penicillin/streptomycin. DRGs were plated onto 0.1 mg/ml poly-D-lysine-coated clear
1445 bottom black-walled 384-well plates (Greiner #781090) at a density of 1,000 cells/well. Cells were
1446 incubated at 37°C, 5% CO₂ for 24 h. Prior to treatment, cells were washed with supplemented
1447 Neurobasal-A medium using a BRAVO liquid handler (Agilent) to a uniform volume. 1938 solubilised
1448 at 3 mM in DMSO was diluted 1:3 in an 8-point concentration response curve in DMSO. Drugs in
1449 concentration response curves were diluted in supplemented Neurobasal-A medium by transfer into
1450 intermediate plates using a BRAVO liquid handler. Intermediate plates were then used to treat cell
1451 plates using the BRAVO liquid handler (final concentration of 0.1% DMSO in the DRG cultures). The
1452 PI3K α inhibitor BYL-719 (final concentration of 500 nM in the DRG cultures) or vehicle (0.005% DMSO
1453 in supplemented Neurobasal-A medium) was added 15 min prior to the addition of the 1938
1454 concentration response curve (total concentration of 0.105% DMSO in the DRG cultures). After
1455 incubation for 72 h at 37°C and 5% CO₂, cells were fixed by addition of 4% paraformaldehyde for 20
1456 min. Wells were washed 3 times in PBS with 0.05% Tween-20 (PBST) before permeabilisation in PBS
1457 with 0.1% Triton X-100. Wells were washed 3 more times with PBST before blocking with fish skin
1458 gelatin/PBST for 1 h at room temperature. The wells were then incubated overnight at 4°C with
1459 primary antibody against the β -III tubulin neuronal marker; abcam #ab18207; 1:1000). The following
1460 day, cells were washed 3 times in PBST using the BRAVO liquid handler before incubation with anti-
1461 rabbit Alexafluor-488 (1:2000, A-11008) for 1 h at room temperature. Cells were washed 3 times with
1462 PBST using the BRAVO liquid handler before staining with Hoechst 33342 nucleic acid stain (Thermo
1463 Scientific #62249; 1:2000) for 20 min protected from light. Cells were washed another 3 times with
1464 PBST and 3 times with PBS and cell plates stored at 4°C protected from light before imaging. Image
1465 acquisition was performed using Opera (PerkinElmer) high-content screening system using the 20x
1466 water objective. Images of cell nuclei and β -III tubulin-positive cells were captured using

1467 excitation/emission wavelengths λ 380/455 and λ 490/518, respectively. 9 fields per well were
1468 captured and analysed using the CSIRO Neurite Analysis 2 logarithm in Columbus analysis software
1469 (Perkin Elmer). Neurites were defined using the following parameters: Smoothing window 0 pixels (px),
1470 Linear window 15 px, Contrast > 1.5, Diameter \geq 3 px, Gap closure distance \leq 17 px, Gap closure quality
1471 0, Debarb length \leq 40 px, Body thickening 1 px, Tree length \leq 0 px. Within each experiment treatments
1472 were performed in quadruplicate and data are represented as the average of biological repeats (n= 3)
1473 \pm standard error of the mean. Variable slope nonlinear regression (4 parameters) was performed in
1474 Prism 7. Whole well representative images were captured using Cytation 3 (Biotek) imaging plate
1475 reader using a 10X objective. A montage of images was captured before stitching and deconvolution
1476 in Gen 5 software (Biotek). Images of cell nuclei and β -III tubulin-positive cells were captured using
1477 excitation/emission wavelengths λ 380/455 and λ 490/518, respectively.
1478

1479 **Control experiments for nerve crush assays**

1480 Experiments to test the stability of 1938 in aqueous solution and the biological activity of 1938 on
1481 exposed rat sciatic nerves were performed as follows.

1482 Lyophilised 1938 was solubilised in autoclaved dH₂O to 100 μ M. Solubilisation required sonication
1483 at 30°C for 25 min before passing through a 0.22 μ m filter. Aliquots of 1938 (at 5 μ M and 100 μ M) or
1484 vehicle were frozen at -20°C in aliquots for later use on separate experimental days. An aliquot of 100
1485 μ M TRO-1938 and vehicle was defrosted and tested on A549 cells to test activity (**Extended Data Fig.**
1486 **8a, top panel**). Cells were seeded in 24-well plates at 200,000 cells/well in DMEM+Glutamax
1487 supplemented with 10% FBS and 1% Pen/Strep. Prior to treatment, cells were washed and incubated
1488 with serum-free DMEM+Glutamax. Cells were treated with an 8 point 1:3 dose response of 1938
1489 diluted in serum-free DMEM+Glutamax starting from 10 μ M for 15 min at 37°C. Cells were then
1490 washed in ice-cold PBS and lysed in RIPA buffer supplemented with protease and phosphatase
1491 inhibitors. Lysates were analysed by automated Western blot (Wes) (data shown in **Extended Data Fig.**
1492 **8a; top panel**).

1493 To assess if 1938 could induce pAkt generation in exposed rat sciatic nerves, adult male Sprague
1494 Dawley rats (>250g; n=2) were anaesthetised using isoflurane, the left sciatic nerve was exposed and
1495 injected with 2 μ l vehicle (sterile dH₂O) or 1938 (5 μ M in sterile dH₂O). Meanwhile the right sciatic
1496 nerve was exposed and bathed in 250 μ l of vehicle (sterile dH₂O) or 1938 (5 μ M in sterile dH₂O). Each
1497 animal received one vehicle and one compound treatment. The treatments were left on for 30 min
1498 prior to washing the bathed nerves with sterile PBS and culling via sodium pentobarbital injection
1499 according to local regulations. Nerves were then harvested, washed in fresh 4°C PBS and stored in a
1500 fresh vial before snap freezing in liquid nitrogen. Frozen sciatic nerves were homogenised in RIPA
1501 buffer supplemented with protease and phosphatase inhibitors using a mortar and pestle
1502 homogeniser. The subsequent crude lysates were centrifuged at 10,000xg for 10 min at 4°C, the
1503 supernatant harvested and stored at -80°C prior to automated western blot (Wes) analysis for pAkt
1504 and controls (**Extended Data Fig. 8a; bottom panel**).

1505

1506 **Rat sciatic nerve crush injury and 1938 treatment**

1507 We used the rat sciatic nerve crush model of peripheral nerve injury and regeneration⁸²⁻⁸⁴. Adult
1508 female Sprague Dawley rats (230-280 g, n=10, Charles River, UK) were anaesthetised by isoflurane
1509 inhalation in an induction chamber (5% isoflurane in O₂, 0.8 l/min). Anaesthesia was maintained with
1510 1.5-2.5% isoflurane inhalation, and the left sciatic nerve exposed at mid-thigh level.

1511 The nerve was crushed by application of constant pressure using fully closed sterile type 4
1512 tweezers (TAAB) for 15 sec. This was repeated two more times at the same point, with 45° rotation
1513 between each crush. The injury site was marked with a 10/0 epineurial non-absorbant suture (Ethicon).
1514 Following injury, a single 2 μ l injection of 1938 solution (5 μ M in sterile H₂O) or vehicle (sterile dH₂O)
1515 was administered proximal to the crush site with a 10 μ l Hamilton syringe. An osmotic minipump (Alzet
1516 1004, Charles River, UK) was also implanted between the muscle layers, adjacent to the nerve oriented
1517 with the outlet nearest to the crush site, loaded with 1938 solution (100 μ M in sterile H₂O) or vehicle

1518 (sterile H₂O). Animals were randomly assigned to groups (n=5 per group) and one experimenter was
1519 kept blind to condition for conducting functional and histological analyses. Overlying muscle layers
1520 were closed using 4/0 sutures (Ethicon) and the skin was closed with wound clips (Clay Adams).
1521 Animals were left to recover for 21 days.

1522

1523 **Functional assessment of muscle regeneration**

1524 At the end-point of the experiment (21 days), rats were anaesthetised and the sciatic nerve exposed
1525 as described above. A reference, ground (Natus) and recording electrode (Ambu Neuroline) were
1526 attached above the hip bone, into the tail, and into the tibialis anterior muscle respectively. A
1527 microchannel neurointerface (MNI) was placed approximately 2 mm proximal to the injury site and
1528 used to stimulate the nerve. The MNI was manufactured using a previously documented protocol⁸⁵.
1529 Electrode impedance of the MNI was 27.1 ±19.8 kΩ at 1k Hz. Compound muscle action potential
1530 (CMAP) was obtained by sciatic nerve stimulation with square wave pulses of 100 μsec with intensity
1531 from 1-10 mA. Stimulus was increased in 0.2 mA steps until muscle response amplitude no longer
1532 increased. CMAP amplitude was measured from peak to peak and recorded in triplicate for both the
1533 ipsilateral and contralateral side. The CMAP with the largest amplitude was selected for analysis.

1534 A modified multipoint stimulation technique was used to calculate Motor Unit Number Estimation
1535 (MUNE)⁸⁶⁻⁸⁸. Incremental responses were obtained by delivering a submaximal stimulation of 100 μsec
1536 duration at a frequency of 1Hz while increasing the stimulus intensity in increments of 0.02 mA to
1537 obtain minimal responses. The initial response was obtained with a stimulus intensity of between 0.21
1538 mA and 0.70 mA. If the initial response did not occur between these stimulus intensities, the
1539 stimulating electrode was adjusted to increase or decrease the stimulus intensity as required.
1540 Additional Single Motor Unit Potentials (SMUPs) were evoked by stimulation in increments of 0.02 mA
1541 to obtain a minimum of four additional increments. The position of the stimulating electrode and the
1542 location of the recording electrode was changed to allow the recording of SMUPs from a different site
1543 of the muscle. This process was repeated at least three times. The CMAP was divided by the mean
1544 magnitude of SMUPs to quantify MUNE.

1545

1546 **Sciatic nerve collection and processing**

1547 After electrophysiology recordings, animals were culled with sodium pentobarbital injection according
1548 to local regulations. Sciatic nerves, including the common peroneal branch, and tibialis anterior
1549 muscles were collected and placed in 4% paraformaldehyde (PFA). Nerve samples were fixed
1550 overnight in 4% PFA at 4°C before transferring to PBS. Nerve samples were divided into sciatic nerves
1551 including the crush site, and the common peroneal branch for sectioning. Nerve samples were
1552 immersed in 30% sucrose overnight at 4°C, then snap frozen in Neg-50 frozen section medium
1553 (Thermo Scientific) using liquid nitrogen cooled isopentane. Transverse sections (10 μm) were cut
1554 from the distal segment of the common peroneal nerve using a cryostat (HM535, Thermo Scientific).
1555 From the sciatic nerve, transverse cryosections (15 μm) were cut from 3 mm and 6 mm distal to the
1556 crush site. Sections were adhered to glass slides (Superfrost Plus, Thermo Fisher) for
1557 immunofluorescence staining.

1558 For immunofluorescence staining, all washes and dilutions were performed using immunostaining
1559 buffer (PBS with 0.002% sodium azide and 0.3% Triton-X 100). Slides were heated to 37°C for 20 min
1560 for antigen retrieval and then blocked with 5% normal horse serum for 40 min. Sections were then
1561 incubated in primary antibodies overnight at 4°C, followed by incubation for 45 min at room
1562 temperature in secondary antibodies. The following antibodies were used: mouse anti-neurofilament
1563 (Biolegend #835604, 1:500), goat anti-choline acetyltransferase (Millipore #AB144P, 1:50), DyLight
1564 anti-mouse IgG 549 (Vector #DI-2549, 1:300) and DyLight anti-goat IgG 488 (Vector DI-1488, 1:300).
1565 Slides were coverslipped with Vectashield Hardset mounting medium (Vector #H-1400).

1566 Fluorescence microscopy (Zeiss AxiolabA1, Axiocam Cm1) was carried out for quantification of
1567 motor axons (ChAT) in the distal segment of the common peroneal nerve. For analysis of sciatic nerve
1568 sections at 3 mm and 6 mm distal to the crush injury, confocal tile scans (Zeiss LSM 710, 20x

1569 magnification) were taken of each transverse section. Quantification of all neurofilament-positive
 1570 axons was performed using Velocity™ software (Perkin Elmer, Waltham, MA).

1571

1572 **Muscle collection and processing**

1573 Tibialis anterior muscles were fixed in 4% PFA for no longer than 15 min and then embedded in
 1574 Optimal Cutting Temperature (OCT) and snap-frozen on liquid nitrogen-cooled isopentane or left in
 1575 immunostaining buffer until ready to be processed. Transverse 20 µm cryosections were taken at 300
 1576 µm intervals. A minimum of 10 sections from each sample were obtained from the entire cross-section
 1577 of muscle and adhered to glass slides for immunofluorescence staining.

1578 All washes and dilutions were performed using immunostaining buffer (PBS containing 0.002%
 1579 sodium azide and 0.3% Triton-X100). Slides were heated to 42°C for 30 min with 20 µg/ml proteinase
 1580 K and then blocked with 10% goat serum for 40 min at room temperature. After washing, the sections
 1581 were incubated in primary antibody (neurofilament, Biolegend 835604, 1:500), washed, then
 1582 incubated with DyLight anti-mouse IgG 488 (Vector #DI-2488, 1:300) and alpha-bungarotoxin (Alexa
 1583 594 conjugate, ThermoFisher Scientific, 1:1000). Sections were mounted using Vectashield Hardset
 1584 mounting medium.

1585 Fluorescence microscopy (Zeiss AxioLabA1, AxioCam Cm1) was used to determine the proportion
 1586 of motor endplates (α-bungarotoxin) co-stained with neurofilament to quantify the percentage of
 1587 reinnervated motor endplates. For each sample, a minimum of 20 non-overlapping regions of the
 1588 entire muscle cross-section were analysed.

1589 For statistical analyses, data from 1938 and vehicle treated animals were compared by unpaired
 1590 t-tests (Graphpad Prism 8.0.0).

1591

1592 **Statistical methods**

1593 The statistical methods for the different types of experiments are included in each experimental
 1594 section above.

1595

1596 **Additional references associated with methods**

1597

1598 56 Lu, Y. *et al.* Rationally Designed PI3Kα Mutants to Mimic ATR and Their Use to Understand
 1599 Binding Specificity of ATR Inhibitors. *J Mol Biol* **429**, 1684-1704 (2017).
 1600 <https://doi.org/10.1016/j.jmb.2017.04.006>

1601 57 Anandapadamanaban, M. *et al.* Architecture of human Rag GTPase heterodimers and their
 1602 complex with mTORC1. *Science (New York, N.Y)* **366**, 203-210 (2019).
 1603 <https://doi.org/10.1126/science.aax3939>

1604 58 Masson, G. R. *et al.* Recommendations for performing, interpreting and reporting hydrogen
 1605 deuterium exchange mass spectrometry (HDX-MS) experiments. *Nat Methods* **16**, 595-602
 1606 (2019). <https://doi.org/10.1038/s41592-019-0459-y>

1607 59 Eid, S., Turk, S., Volkamer, A., Rippmann, F. & Fulle, S. KinMap: a web-based tool for interactive
 1608 navigation through human kinome data. *BMC Bioinformatics* **18**, 16 (2017).
 1609 <https://doi.org/10.1186/s12859-016-1433-7>

1610 60 Baretic, D. *et al.* Structures of closed and open conformations of dimeric human ATM. *Sci Adv*
 1611 **3**, e1700933 (2017). <https://doi.org/10.1126/sciadv.1700933>

1612 61 Guo, Z., Kozlov, S., Lavin, M. F., Person, M. D. & Paull, T. T. ATM activation by oxidative stress.
 1613 *Science (New York, N.Y)* **330**, 517-521 (2010). <https://doi.org/10.1126/science.1192912>

1614 62 Stock, D., Perisic, O. & Lowe, J. Robotic nanolitre protein crystallisation at the MRC Laboratory
 1615 of Molecular Biology. *Prog Biophys Mol Biol* **88**, 311-327 (2005).
 1616 <https://doi.org/10.1016/j.pbiomolbio.2004.07.009>

1617 63 Cianci, M. *et al.* P13, the EMBL macromolecular crystallography beamline at the low-
 1618 emittance PETRA III ring for high- and low-energy phasing with variable beam focusing. *J*
 1619 *Synchrotron Radiat* **24**, 323-332 (2017). <https://doi.org/10.1107/S1600577516016465>

- 1620 64 Kabsch, W. Xds. *Acta Crystallogr D Biol Crystallogr* **66**, 125-132 (2010).
1621 <https://doi.org:10.1107/S0907444909047337>
- 1622 65 Evans, P. R. & Murshudov, G. N. How good are my data and what is the resolution? *Acta*
1623 *Crystallogr D Biol Crystallogr* **69**, 1204-1214 (2013).
1624 <https://doi.org:10.1107/S0907444913000061>
- 1625 66 Vagin, A. & Teplyakov, A. Molecular replacement with MOLREP. *Acta Crystallogr D Biol*
1626 *Crystallogr* **66**, 22-25 (2010). <https://doi.org:10.1107/S0907444909042589>
- 1627 67 Adams, P. D. et al. PHENIX: a comprehensive Python-based system for macromolecular
1628 structure solution. *Acta Crystallogr D Biol Crystallogr* **66**, 213-221 (2010).
1629 <https://doi.org:10.1107/S0907444909052925>
- 1630 68 Emsley, P., Lohkamp, B., Scott, W. G. & Cowtan, K. Features and development of Coot. *Acta*
1631 *Crystallogr D Biol Crystallogr* **66**, 486-501 (2010).
1632 <https://doi.org:10.1107/S0907444910007493>
- 1633 69 Winter, G., Lobley, C. M. & Prince, S. M. Decision making in xia2. *Acta Crystallogr D Biol*
1634 *Crystallogr* **69**, 1260-1273 (2013). <https://doi.org:10.1107/S0907444913015308>
- 1635 70 Murshudov, G. N. et al. REFMAC5 for the refinement of macromolecular crystal structures.
1636 *Acta Crystallogr D Biol Crystallogr* **67**, 355-367 (2011).
1637 <https://doi.org:10.1107/S0907444911001314>
- 1638 71 Hsiao, T. et al. Inference of CRISPR Edits from Sanger Trace Data. *bioRxiv*, 251082 (2019).
1639 <https://doi.org:10.1101/251082>
- 1640 72 Cox, J. & Mann, M. MaxQuant enables high peptide identification rates, individualized p.p.b.-
1641 range mass accuracies and proteome-wide protein quantification. *Nat Biotechnol* **26**, 1367-
1642 1372 (2008). <https://doi.org:10.1038/nbt.1511>
- 1643 73 Choi, M. et al. MStats: an R package for statistical analysis of quantitative mass spectrometry-
1644 based proteomic experiments. *Bioinformatics* **30**, 2524-2526 (2014).
1645 <https://doi.org:10.1093/bioinformatics/btu305>
- 1646 74 Benjamini, Y. & Hochberg, Y. Controlling the False Discovery Rate - a Practical and Powerful
1647 Approach to Multiple Testing. *J R Stat Soc B* **57**, 289-300 (1995). <https://doi.org:DOI>
1648 10.1111/j.2517-6161.1995.tb02031.x
- 1649 75 Perez-Riverol, Y. et al. The PRIDE database and related tools and resources in 2019: improving
1650 support for quantification data. *Nucleic Acids Res* **47**, D442-D450 (2019).
1651 <https://doi.org:10.1093/nar/gky1106>
- 1652 76 Anderson, K. E., Juvin, V., Clark, J., Stephens, L. R. & Hawkins, P. T. Investigating the effect of
1653 arachidonate supplementation on the phosphoinositide content of MCF10a breast epithelial
1654 cells. *Advances in biological regulation* **62**, 18-24 (2016).
1655 <https://doi.org:10.1016/j.jbior.2015.11.002>
- 1656 77 Schindelin, J. et al. Fiji: an open-source platform for biological-image analysis. *Nat Methods* **9**,
1657 676-682 (2012). <https://doi.org:10.1038/nmeth.2019>
- 1658 78 Feoktistova, M., Gesserick, P. & Leverkus, M. Crystal Violet Assay for Determining Viability of
1659 Cultured Cells. *Cold Spring Harb Protoc* **2016**, pdb prot087379 (2016).
1660 <https://doi.org:10.1101/pdb.prot087379>
- 1661 79 Botker, H. E. et al. Practical guidelines for rigor and reproducibility in preclinical and clinical
1662 studies on cardioprotection. *Basic Res Cardiol* **113**, 39 (2018).
1663 <https://doi.org:10.1007/s00395-018-0696-8>
- 1664 80 Melli, G. & Hoke, A. Dorsal Root Ganglia Sensory Neuronal Cultures: a tool for drug discovery
1665 for peripheral neuropathies. *Expert Opin Drug Discov* **4**, 1035-1045 (2009).
1666 <https://doi.org:10.1517/17460440903266829>
- 1667 81 Rayner, M. L. D. et al. Developing an In Vitro Model to Screen Drugs for Nerve Regeneration.
1668 *Anatomical record* **301**, 1628-1637 (2018). <https://doi.org:10.1002/ar.23918>

- 1669 82 Wood, M. D., Kemp, S. W., Weber, C., Borschel, G. H. & Gordon, T. Outcome measures of
1670 peripheral nerve regeneration. *Ann Anat* **193**, 321-333 (2011).
1671 <https://doi.org:10.1016/j.aanat.2011.04.008>
- 1672 83 Caillaud, M., Richard, L., Vallat, J. M., Desmouliere, A. & Billet, F. Peripheral nerve regeneration
1673 and intraneural revascularization. *Neural Regen Res* **14**, 24-33 (2019).
1674 <https://doi.org:10.4103/1673-5374.243699>
- 1675 84 Alvites, R. *et al.* Peripheral nerve injury and axonotmesis: State of the art and recent advances.
1676 *Cogent Medicine* **5**, 1466404 (2018). <https://doi.org:10.1080/2331205X.2018.1466404>
- 1677 85 Lancashire, H. T. *et al.* Microchannel neural interface manufacture by stacking silicone and
1678 metal foil laminae. *J Neural Eng* **13**, 034001 (2016). [https://doi.org:10.1088/1741-](https://doi.org:10.1088/1741-2560/13/3/034001)
1679 [2560/13/3/034001](https://doi.org:10.1088/1741-2560/13/3/034001)
- 1680 86 Shefner, J. M., Cudkowicz, M. & Brown, R. H., Jr. Motor unit number estimation predicts
1681 disease onset and survival in a transgenic mouse model of amyotrophic lateral sclerosis.
1682 *Muscle & nerve* **34**, 603-607 (2006). <https://doi.org:10.1002/mus.20628>
- 1683 87 Jacobsen, A. B., Bostock, H. & Tankisi, H. CMAP Scan MUNE (MScan) - A Novel Motor Unit
1684 Number Estimation (MUNE) Method. *J Vis Exp* (2018). <https://doi.org:10.3791/56805>
- 1685 88 Arnold, W. D. *et al.* Electrophysiological Motor Unit Number Estimation (MUNE) Measuring
1686 Compound Muscle Action Potential (CMAP) in Mouse Hindlimb Muscles. *J Vis Exp* (2015).
1687 <https://doi.org:10.3791/52899>
- 1688 89 Berman, H. M. *et al.* The Protein Data Bank. *Nucleic Acids Research* **28**, 235-242 (2000).
1689 <https://doi.org:10.1093/nar/28.1.235>

1690 1691 **Acknowledgements**

1692 We thank Dusan Petrovic, Andy Davis, Garry Pairaudeau, Sabina Cosulich and Ralph Knoll (AstraZeneca)
1693 for advice and support, Chris Boshoff, David Lynch, Bryan Williams, David Miller, Nick McNally and Alan
1694 Holmes (UCL/UCLH) for support during the early stages of this work, Olga Perisic for help with cloning
1695 and protein expression (MRC-LMB), Sapna Arjun and Pelin Golforoush (The Hatter Cardiovascular
1696 Institute) for help with the analysis of the cardioprotection experiments, York Posor (UCL) and Gerry
1697 Hammond (University of Pittsburgh) for help and advice with TIRF microscopy, Fabrice Gorrec (MRC-
1698 LMB) for advice on crystallisation, Neil Vasan for gift of the Flag-PIK3R1 plasmid, Mariona Graupera
1699 (Barcelona), Ezra Aksoy (London), Lazaros Foukas (London) and Klaus Okkenhaug (Cambridge) for
1700 extensive feedback on manuscript, Jane Kinghorn and the other team members of the UCL
1701 Translational Research Office, Alex Sullivan and Veronica Dominguez for general support, and Dominic
1702 Leisi, Rachel Colman and Sara Garcia Gomez (UCLB) for business support. The authors would like to
1703 thank Diamond Light Source (DLS-UK) and EMBL-Hamburg (PETRA III/DESY, Germany) for beamtime
1704 (proposals mx23583 and mx28677 – DLS; and mx647- EMBL), the staff of beamlines i03 (DLS), i04 (DLS),
1705 i24 (DLS) and P13 (EMBL-Hamburg) for assistance with crystal testing and data collection, and the
1706 Diamond-CCP4 Data Collection and Structure Solution Workshop 2022 for training.

1707 1708 **Author contributions**

1709 B.V. provided the initial study conceptualization, with input from R.A., R.W., D.M.S., S.M.D. and D.Y.
1710 B.V. took the lead in writing the manuscript, with major input from G.Q.G., B.B., B.A., V.R., T.A., R.R.M.,
1711 S.E.C., S.M.D., J.B.P. and R.L.W., with other authors contributing to manuscript editing and finalisation.
1712 G.Q.G., B.B., B.A., G.R.M., V.R., T.A., S.O., R.R.M., S.E.C., D.B., O.N., Z.H., B.W., S.H.M., A.W.E.C., V.V.,
1713 K.E.A., N.P., E.L.-G. and J.B.P. designed and performed experiments and data analysis supporting the
1714 study, M.F., M.C., I.F. and A.M. supported the high throughput screen and drug modelling studies,
1715 D.M., A.B., S.S., M.W., A.H., C.P. and T.D.B. performed experiments and analysis, M.A.W. and M.K.
1716 provided general support, B.V., R.A., J.B.P. and R.W. supervised the study, with input from D.M.S.,
1717 D.M.Y., S.M.D., L.R.S. and P.T.H.

1718 1719 **Competing interests**

1720 B.V. is a consultant for iOnctura (Geneva, Switzerland), Venthera (Palo Alto, US), Pharming (Leiden,
 1721 the Netherlands) and Olema Pharmaceuticals (San Francisco, US), and has received speaker fees from
 1722 Gilead (Foster City, US). M.F., M.C., I.F., A.M. and D.M.S. are or were employees and shareholders in
 1723 AstraZeneca at the time of the work done. J.B.P. is co-Founder and Chief Scientific Officer of the UCL
 1724 spinout company Glialign Ltd. The other authors do not have competing interests to disclose. A patent
 1725 application GB 2113079.4, with relevance to this work has been filed by UCL Business and we want to
 1726 declare our relationship with this patent application.

1727

1728 Extended Figure legends

1729

1730 **Extended data Fig. 1 | Additional biochemical data on 1938.** **a**, Determination of K_d for the
 1731 dissociation of 1938 from p110 α /p85 α by surface plasmon resonance (SPR). SPR equilibrium response
 1732 titration of 1938 binding to immobilized p110 α /p85 α , yielding a dissociation constant $K_d = 36 \pm 5 \mu\text{M}$.
 1733 **b**, Determination of K_d for the dissociation of 1938 from p110 α /p85 α by differential scanning
 1734 fluorimetry (DSF). The first derivatives of the fluorescence change of p110 α /p85 α upon thermal
 1735 denaturation at the stated 1938 concentrations (*left panel*) were used to plot the melting temperature
 1736 (T_m) (*right panel*). Fits to data gave a $K_d = 16 \pm 2 \mu\text{M}$. K_d shown as mean \pm SD (n=3 independent
 1737 experiments). Representative experiment is shown. **c**, Effect of 1938 on the IC_{50} of BYL719 for PI3K α .
 1738 Data shown as mean \pm SEM (n=3 independent experiments). **d**, Activation of class IA PI3K isoforms by
 1739 a concentration range of pY using the ADP-Glo assay. Data shown as mean \pm SEM (n=3 independent
 1740 experiments).

1741

1742 **Extended data Fig. 2 | Additional data on HDX-MS and crystallography.** Structural changes induced
 1743 by BYL719 (**a**), or 1938 in combination with BYL719 (**b**), assessed by HDX-MS in full-length p110 α /p85 α ,
 1744 highlighted on the structure of p110 α (gray)/niSH2-p85 α (green) (PDB:4ZOP). Selection threshold for
 1745 significant peptides: a-b difference $\geq 2.5\%$, Da difference ≥ 0.25 , p-value < 0.05 (unpaired t-test). **c**,
 1746 Peptide uptake from HDX-MS. A selection of peptides (peptides 848-849, 532-551, 1002-1013 and
 1747 1006-1016 are from p110 α , peptide 555-570 is from p85 α) exhibiting significant differences in solvent
 1748 exchange rates on the addition of UCL-1938-TRO (red), BYL719 (green), both (purple) or neither (red).
 1749 Data presented here is from one of three biological replicates. Five time points were measured in
 1750 triplicate. Each point is the mean of one biological repeat. **d**, Omit map of ligand 1938 (mFo-DFc)
 1751 calculated at $\pm 3\sigma$ using phenix.polder. **e**, 1938 bound to p110 α shown in multiple orientations. **f**,
 1752 Effect of 1938 on catalytic activity of p110 α proteins with mutations in the 1938-binding pocket. Data
 1753 shown as mean \pm SEM (n=4 independent experiments).

1754

1755 **Extended data Fig. 3 | Additional data on 1938-driven signalling.** **a**, MEFs were stimulated for
 1756 different time points with 1938 (5 μM) or for 2 min with PDGF (20 ng/ml), followed by lipid extraction
 1757 and PI(3,4)P $_2$ measurement by mass spectrometry. **b**, MEFs were stimulated for 2 min with 1938 (30
 1758 μM) or PDGF (0.5 or 1 ng/ml), followed by lipid extraction and PI(3,4)P $_2$ measurement by mass
 1759 spectrometry. (**a,b**) n=independent experiments, shown in figure. Error bars represent SD. **c**, Control
 1760 TIRF microscopy data from DMSO-treated HeLa cells expressing the PIP $_3$ or the PI(3,4)P $_2$ reporter. HeLa
 1761 cells expressing the EGFP-tagged PIP $_3$ reporter PH-ARNO-I303Ex2 (ARNO) (*black lines*) or the PI(3,4)P $_2$
 1762 reporter mCherry-cPH-TAPP1x3 (*blue lines*) were stimulated with DMSO as indicated. Overlay plots
 1763 (mean \pm SEM) were generated by scaling to minimum and maximum values of the normalised
 1764 fluorescence intensity for each time point ($F_n(t)$). PIP $_3$ reporter data are representative of 2
 1765 experiments and 16 single cells. PI(3,4)P $_2$ reporter data are representative of 4 experiments and 29
 1766 single cells. Individual measurements were acquired every 2 min. **d**, pAKT^{S473} induction by 1938 in
 1767 PI3K α -KO MEFs transiently transfected with p110 α -WT or p110 α -mutants. Blot representative of n=2
 1768 experiments. **e**, Time course analysis of 1938-induced pAKT^{S473} in A549 by 1938+BYL719 or a saturating
 1769 insulin concentration. Blot representative of n=3 experiments. **f**, Time course analysis of 1938-induced
 1770 pAKT^{S473} and pS6^{S240/44} in MCF10A cells in the presence or absence of BYL719. Shown is a

1771 representative blot of n=2 independent experiments. **g**, Time course analysis of insulin- or 1938-
 1772 induced PI3K/AKT/mTORC1 signalling in A549, n=2 experiments.

1773

1774 **Extended data Fig. 4 | *In vitro* selectivity profile of 1938 (1 μ M) on 133 protein kinases and 7 lipid**
 1775 **kinases**, visualised as a waterfall plot (top panel) or KinMap (bottom panel). In the waterfall plot, the
 1776 protein and lipid kinases are labeled in black and red, respectively, with the dashed line delineating
 1777 25% of kinase inhibition.

1778

1779 **Extended data Fig. 5 | Effect of 1938 on *in vitro* kinase activity of the PI3K-related kinases ATM and**
 1780 **mTORC1 (mTOR/RAPTOR/LST8 complex)**. The kinases were incubated at 30°C for 30 min (ATM) or 3
 1781 h (mTORC1), with or without 200 μ M 1938 in the presence of their respective substrates (GST-p53 for
 1782 ATM and 4E-BP1 for mTORC1), followed by analysis and quantification as described in Methods. The
 1783 positive control for ATM was inclusion of the MRN complex (Mre11-Rad50-Nbs1), known to activate
 1784 ATM, in the kinase reaction. The positive control for mTORC1 was the use of a triple amount of
 1785 mTORC1 complex in the kinase reaction. Data show individual experiments (n=3), error bars represent
 1786 mean \pm SD.

1787

1788 **Extended data Fig. 6 | Phosphoproteomics experimental set-up and control data. a**, Experimental
 1789 design and workflow of phosphoproteomics experiment. PI3K α -WT and PI3K α -KO MEFs were serum-
 1790 starved overnight, stimulated with DMSO, 1938 (5 μ M) or insulin (100 nM) for 15 min or 4 h and
 1791 processed for phosphoproteomics analysis. 10,611 phosphosites from 3,093 proteins were analysed
 1792 by MSstats, the majority of which were pSer and pThr residues. **b**, Validation of phosphoproteomics
 1793 conditions. PI3K α -WT and PI3K α -KO MEFs were serum-starved overnight and stimulated with DMSO,
 1794 1938 (5 μ M) or insulin (100 nM) for 15 min or 4 h as indicated. Lysates were immunoblotted with
 1795 antibodies to pAKT^{S473}, pAKT^{T308}, total AKT, pPRAS40/AKT1S1^{S246}, pS6RP^{S240/244}, S6RP or GAPDH.
 1796 Samples were from a representative phosphoproteomics experiment. Representative of n=2
 1797 independent experiments. **c**, Volcano plot of phosphosites differentially regulated by 1938 (5 μ M)
 1798 relative to DMSO in PI3K α -WT MEFs. Note, these data are reproduced, enlarged and labelled from Fig.
 1799 4b. Red, upregulated phosphosites, Green, downregulated phospho-sites. Boxed phosphosites have
 1800 been previously reported to be regulated by PI3K signalling (PhosphoSitePlus). **d**, Insulin stimulation
 1801 induces phosphorylation of expected PI3K targets in PI3K α -WT MEFs. Volcano plot of Log₂(fold change)
 1802 versus -log₁₀(adjusted p-value) for phosphosites differentially regulated by (right) 15 min or (left) 4 h
 1803 100 nM insulin treatment in PI3K α -WT MEFs relative to DMSO-treated cells. **e**, High experimental
 1804 reproducibility of phosphoproteomics experiment. Quantified phosphopeptides were analysed within
 1805 the model-based statistical framework MSstats. Data were log₂ transformed, quantile normalised,
 1806 and a linear mixed-effects model was fitted to the data. The group comparison function was employed
 1807 to test for differential abundance between conditions. p-values were adjusted to control the FDR using
 1808 the Benjamini-Hochberg procedure. Multi-scatter plot of the Log₂(intensity) of signals obtained from
 1809 each replicate against the Log₂(intensity) of the same sample from all other replicates. Numbers
 1810 indicate the Pearson correlation coefficient for each pair.

1811

1812 **Extended data Fig. 7 | Additional data related to the functional activities of 1938 in cultured cells,**
 1813 **tissues and organisms. a**, Time-dependent dose-response of MEFs to 1938 as measured by CellTiter-
 1814 Glo[®]. PI3K α -WT and PI3K α -KO MEFs were serum starved for 4 h, followed by stimulation with a dose
 1815 range of 1938 in serum-free media for the indicated time points. Cellular metabolic activity was
 1816 assessed by measurement of cellular ATP content by CellTiter-Glo[®]. Luminescence normalised to
 1817 DMSO-only as 100% and 10 μ M bortezomib as 0%. Data shown from 2 individual experiments. **b**, MEFs
 1818 were serum-starved overnight, followed by 24h stimulation in serum-free medium with 1938+BYL719,
 1819 insulin, or culture medium containing 10% FBS, followed by measurement of cell number (crystal violet
 1820 staining). Data show 2 independent experiments. **c**, *Ex vivo* perfused Langendorff rat heart model.
 1821 Generation of pAKTS473 in ischaemic hearts treated with vehicle, 1938 or insulin upon reperfusion.

1822 Rat hearts were perfused for 10 min for stabilization, followed by 45 min global ischaemia and then
 1823 reperfused for 2 h. During the first 15 min of reperfusion, the buffer contained either vehicle (0.1%
 1824 DMSO), 1938 (5 μ M) or insulin (1 μ M). After 2 h, all hearts were freeze-clamped and frozen in liquid
 1825 nitrogen followed by tissue extraction in RIPA buffer, SDS-PAGE and immunoblotting with the
 1826 indicated antibodies. The quantification for this blot is shown in Fig. 5e. Statistics: 1-way ANOVA with
 1827 Tukey's post test. Each lane contains the extract of an individual heart: vehicle (n=5), 1938 (n=6) or
 1828 insulin (n=2). **d**, *In vivo* perfused mouse heart model. Left panel, area at risk in vehicle- and 1938-
 1829 treated hearts. Mice were subjected to 40 min coronary artery ligation followed by 2 h reperfusion.
 1830 15 min prior to reperfusion, 50 μ l of DMSO or 10 mg/kg 1938 in DMSO, was administered i.v., prior to
 1831 blinded assessment of infarct size by staining with tetrazolium chloride (this is shown in Fig. 5c). The
 1832 hearts were then excised, perfused with Evans Blue and the total ischaemic "area at risk" (AAR)
 1833 measured in serial slices. The AAR in each heart is indicated as a % of the total area of the left
 1834 ventricular (LV) myocardium. Since there was no significant difference in AAR between the two groups
 1835 (P=0.86), this control measurement demonstrates experimental consistency in suture positioning etc.
 1836 Statistics: Student's unpaired 2-sided t-test, data shown as mean \pm SEM. Right panel, generation of
 1837 pAKT^{S473} in ischaemic hearts treated with vehicle or 1938 upon reperfusion. 50 μ l of DMSO vehicle or
 1838 10 mg/kg 1938 in DMSO was injected i.v. into anaesthetized and intubated mice. After 15 min, the
 1839 chest was opened, the heart removed and immediately freeze-clamped in liquid nitrogen followed by
 1840 tissue extraction in RIPA buffer, SDS-PAGE and immunoblotting with the indicated antibodies. Each
 1841 lane contains the extract of an individual heart of mice treated with vehicle (n=4) or 1938 (n=4). The
 1842 quantification for this blot is shown in Fig. 5e, right panel.

1843

1844 **Extended data Fig. 8 | Additional and control studies for neuro-regeneration experiments.** **a**, *Top*
 1845 *panel*; Control experiment to test the biological activity of 1938 post-freezing. An aliquot of 100 μ M
 1846 1938 in dH₂O and vehicle was defrosted and tested for induction of pAKT^{S473} by 15 min treatment of
 1847 A549 cells, using insulin (1 μ M) or 1938 (10 μ M from control stocks in DMSO) as positive controls.
 1848 *Bottom panel*; pAKT^{S473} induction in exposed sciatic nerves, injected with vehicle (autoclaved H₂O) or
 1849 1938 (from stocks in autoclaved H₂O) or bathed in a solution of vehicle or 1938. After 30 min, the
 1850 nerves were washed and processed for analysis as described in Materials and Methods. Cell extracts
 1851 of MCF7 breast cancer cells stimulated for 15 min with 5 μ M 1938 or vehicle (DMSO) were loaded on
 1852 the gels as positive controls. n=1 experiment. **b**, Representative immunohistochemistry images of a
 1853 transverse section through the distal common peroneal rat nerve, showing ChAT- and neurofilament-
 1854 positive axons with tissue architecture typical of normal tissue. Scale bar = 50 μ m. **c**, Representative
 1855 immunohistochemistry images of rat TA muscle, showing a α -BTX-stained post-synaptic
 1856 neuromuscular structure with associated neurofilament-positive neurons. Scale bar = 20 μ m. n=5
 1857 animals.

1858

1859 **Extended data Fig. 9 | Additional data for methodology.** *Left panel*, Sanger sequencing of the
 1860 genomic *PIK3CA* locus of A549 cell clones subjected to CRISPR/Cas9 gene-targeting. *Lower traces*:
 1861 reference genomic *PIK3CA* sequence (wild-type), with the crispr RNA sequence underlined. *Top traces*:
 1862 DNA sequence of CRISPR/Cas9 gene-targeted or control-edited A549 clones. The *PIK3CA*-KO clone 12
 1863 shows a +1 bp insertion (arrow), leading to frameshift and the generation of 2 consecutive premature
 1864 stop-codons (asterisk) immediately downstream of the +1 bp insertion. Note that the first stop-codon
 1865 occurs 80 bp upstream from the 3' exon-exon junction and will therefore result in nonsense-mediated
 1866 decay of the mRNA. The *PIK3CA*-WT clone 9 shows wild-type genomic DNA sequence. *Right panel*,
 1867 Western blot for p110 α using antibody CST#4255.

1868

1869 **Grant funding:** This research was funded in part by the Wellcome Trust and UKRI [BBRSRC and MRC].
 1870 For the purpose of Open Access, the author has applied a CC BY public copyright licence to any Author
 1871 Accepted Manuscript version arising from this submission. Grant funding details are as follows: **UK**
 1872 **NIHR UCLH Biomedical Research Centre** (to B.V. [High Impact Experimental Medicine Initiative

1873 BRC80a/HI/TE/5995 and BRC80b/HI/TE/5995], to B.V. and R.A. [BRC504/CV/BV/101320,
 1874 BRC732/JK/101400 and RCF309/BVH/101440/2017] and to the UCL Drug Discovery Group
 1875 [BRC247/HI/DM/101440 and BRC454/HI/JK/104360]); **MRC** (to R.L.W. [MC_U105184308]; to B.V. and
 1876 R.A. [UCL Proximity to Discovery Fund (MC_PC_15063, MC_PC_16087 and MC_PC_17202); MRC
 1877 Confidence in Concept [MC_PC_16063 and MC_PC_18063]; to G.R.M. and V.V. [MRC iCase
 1878 Studentship (MR/R01579/1)]; to G.R.M. and R.L.W. [Blue Sky collaboration MRC Laboratory of
 1879 Molecular Biology and AstraZeneca (BSF33)]; **Rosetrees Trust** (to V.R. [Rosetrees Trust Seedcorn 2020
 1880 (100049)] and J.B.P. [UCL Rosetrees Stoneygate Prize 2018; M827]); **Cancer Research UK** (to B.V.
 1881 [C23338/A29269 and C23338/A25722]); **BBSRC** (to R.A. and B.V. [BBSRC Global Challenges Research
 1882 Fund Impact Acceleration Account GCRF-IAA], to G.R.M. (BBSRC Capital Equipment Grant
 1883 BB/V019635/1), and to L.R.S, P.T.H. and K.E.A. [BBSRC Institute Strategic Programme Grant
 1884 BB/PO13384/1]); **British Heart Foundation** (to S.D., D.Y., B.V. and R.A. [PG/18/44/33790]); **Fidelity**
 1885 **Foundation** (to T.B. and M.K. [180348]) and the **UCL Enterprise HEIF Knowledge Exchange and**
 1886 **Innovation Fund** (to R.A. [KEI2017-05-18]). The UCL Drug Discovery Group received additional support
 1887 from the **Wellcome Trust** (Institutional Strategic Support Fund; awarded to UCL [105604/Z/14/Z and
 1888 204841/Z/16/Z], with subaward to the Drug Discovery Group [ISSF2/H17RCO/033 and
 1889 ISSF3/H17RCO/006]). A.B. is supported by the CRUK Cancer Immunotherapy Network Accelerator
 1890 (CITA) Award [C33499/A20265] and CRUK UCL Centre award [C416/A25145]. S.S. and the UCL Cancer
 1891 Institute Translational Technology Platforms are supported by the CRUK UCL Centre Award
 1892 [C416/A25145].

1893

1894 **Personal fellowships** were from EU Marie Skłodowska-Curie (to G.G. [contract number 839032] and
 1895 S.E.C. [contract number 838559]) and Wellcome Trust (to R.M., 220464/Z/20/Z). G.R.M. was
 1896 supported by the AstraZeneca/LMB Blue Sky Initiative [MC-A024-5PF9G to R.L.W.] and a Henslow
 1897 Research Fellowship from The Cambridge Philosophical Society and St Catharine's College, Cambridge,
 1898 UK.

1899

1900 **Data Availability**

1901 All raw images for the TIRF experiments are provided via the Open Science Framework
 1902 (https://osf.io/gzxfm/?view_only=8de666831f5b444087a0ab7c6cf3a636). Mass spectrometry data
 1903 (raw and processed data) have been deposited to the ProteomeXchange Consortium via the PRIDE
 1904 partner repository⁷⁵, with the dataset identifier PXD037721. The mass spectrometry proteomics data
 1905 have been deposited to the ProteomeXchange Consortium via the PRIDE partner repository with the
 1906 dataset identifier PXD027993. Crystallography data have been deposited in PDB Protein Database⁸⁹
 1907 (<https://www.rcsb.org/>) with the following PDB IDs: 8BFU (apo p110 α), 8BFV (p110 α /1938 complex),
 1908 7PG5 (apo p110 α /p85 α) and 7PG6 (BYL719-p110 α /p85 α). Protein structures used for analysis are
 1909 available from the PDB database (4JPS, 4ZOP, 4OVV). Protein sequences (*PIK3CA*, *PIK3CB* and *PIK3CD*)
 1910 are obtained from the UniProt database (<https://www.uniprot.org/>). The other data that support the
 1911 findings in this study are available from the corresponding author upon request.

1912

1913 **Code Availability**

1914 All macros and R analysis scripts for the TIRF experiments are provided via the Open Science
 1915 Framework (https://osf.io/gzxfm/?view_only=8de666831f5b444087a0ab7c6cf3a636). Mass
 1916 spectrometry scripts have been deposited to the ProteomeXchange Consortium via the PRIDE partner
 1917 repository⁷⁵, with the dataset identifier PXD037721.

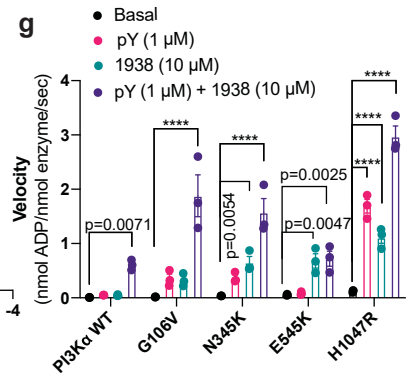
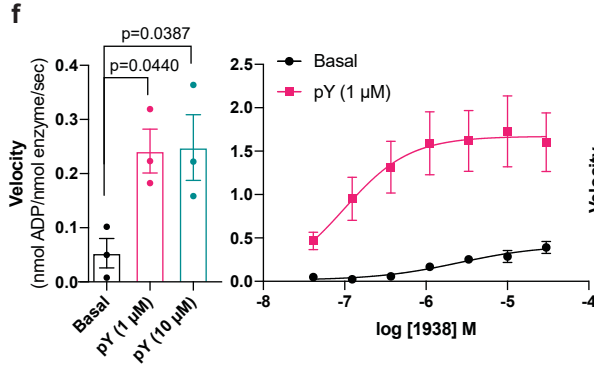
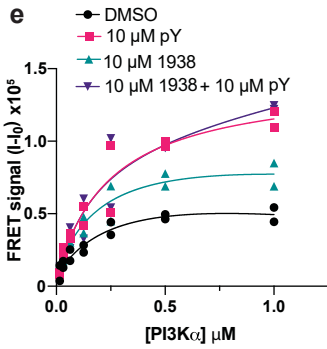
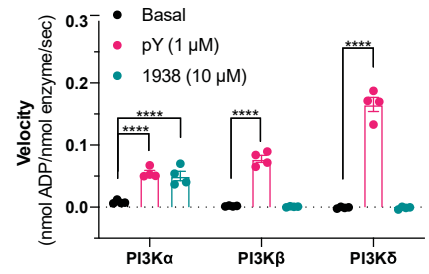
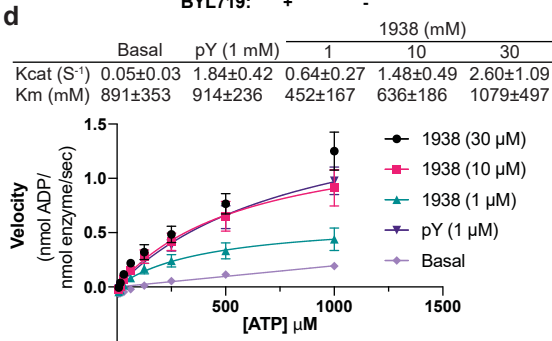
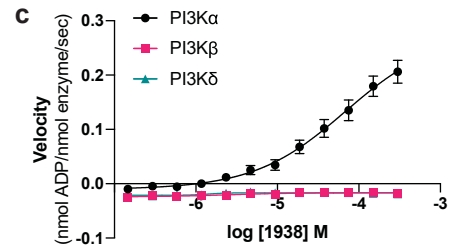
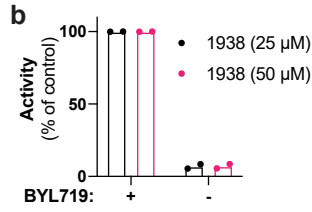
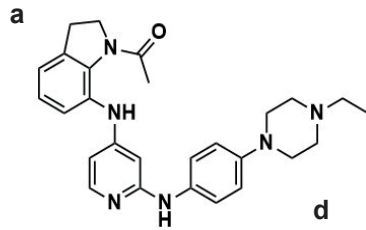
1918

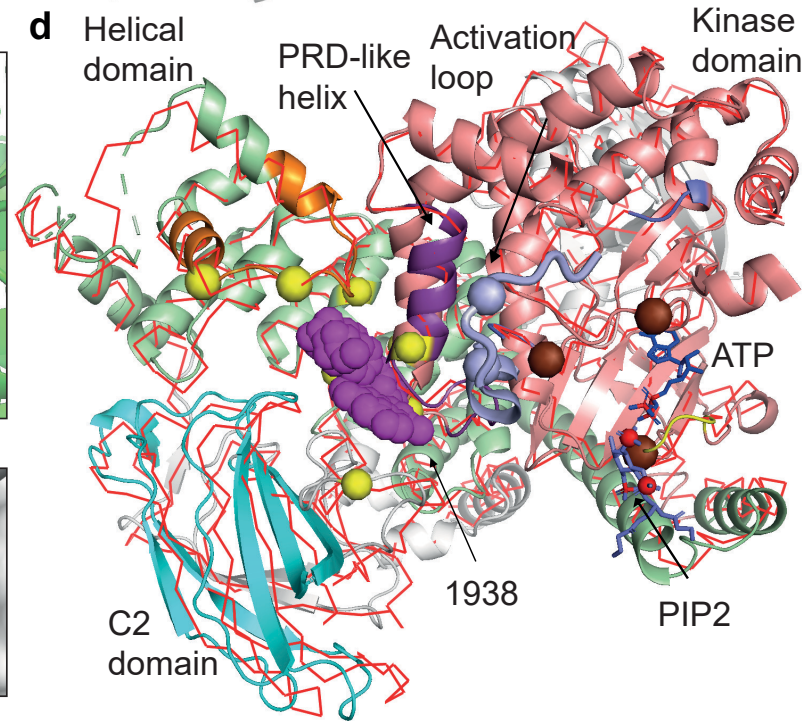
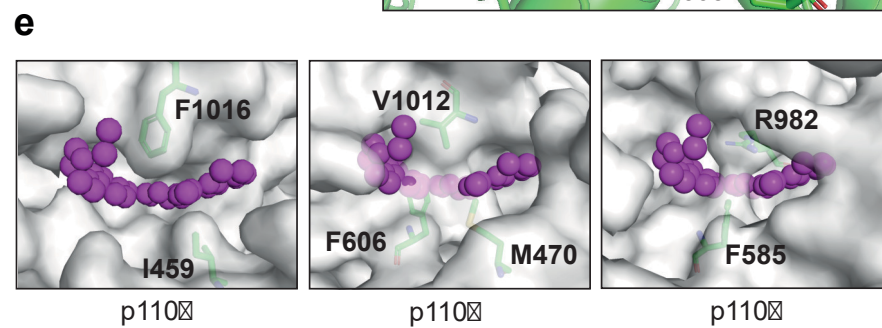
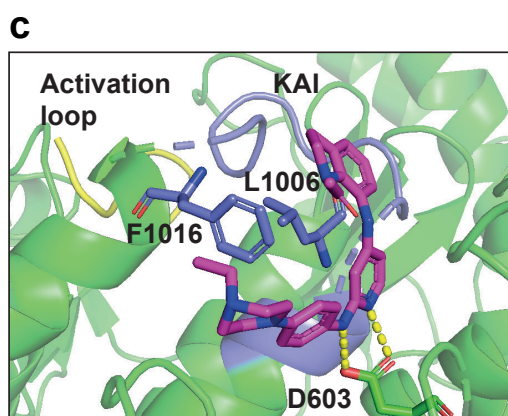
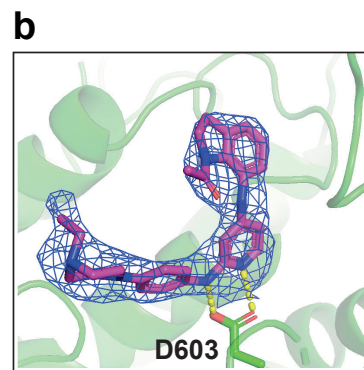
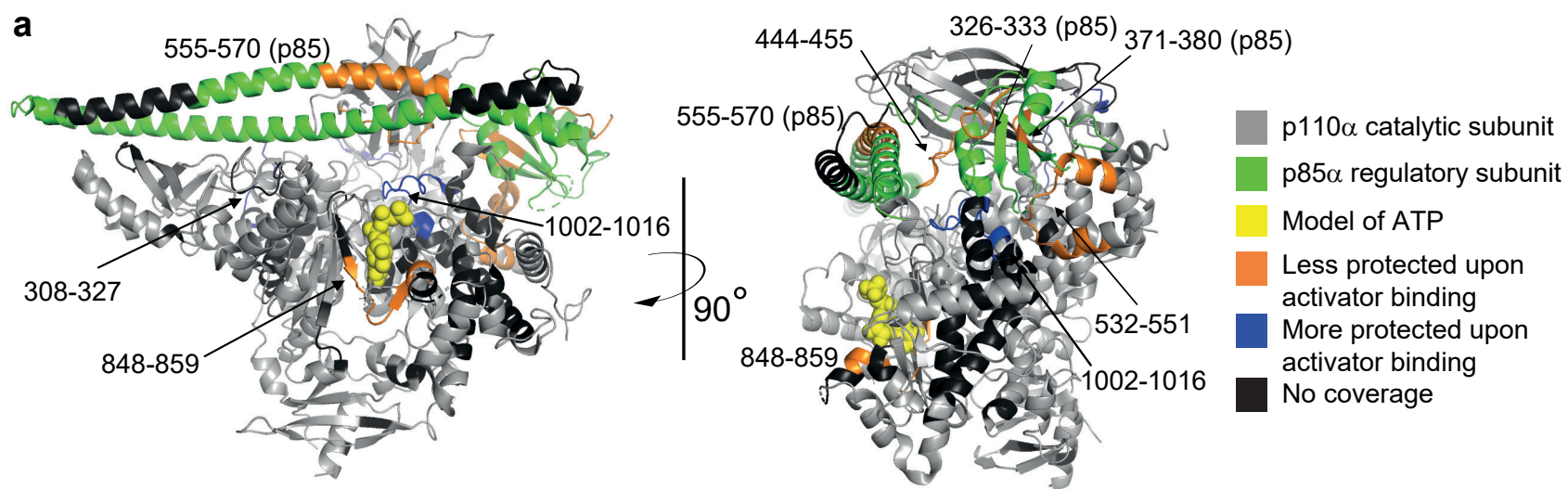
1919 **Keywords:** PI3K / PI3K α / *PIK3CA* / kinase / small molecule / allosteric / activator / regeneration / drug
 1920 development / cell protection / modulator / signalling / HDX-MS / crystallography / neuron / cardiac
 1921 / heart / ischaemia reperfusion injury

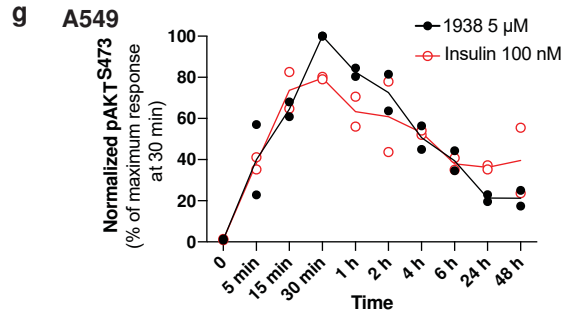
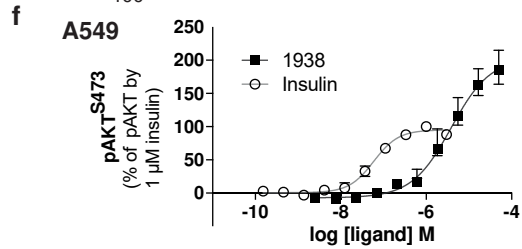
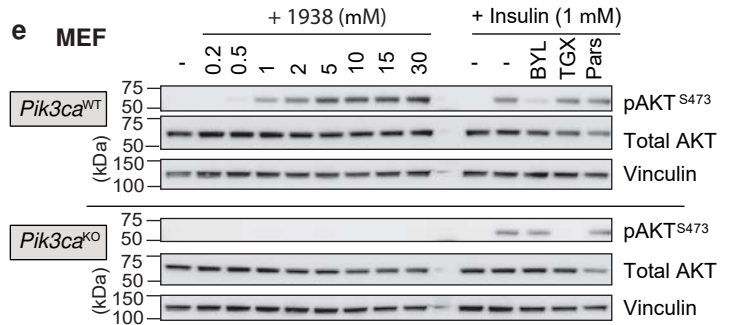
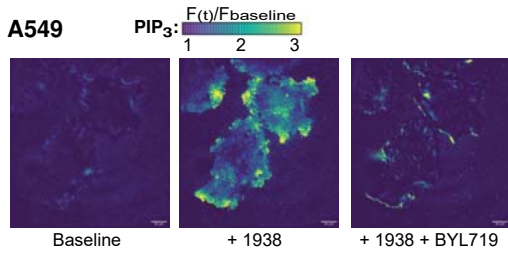
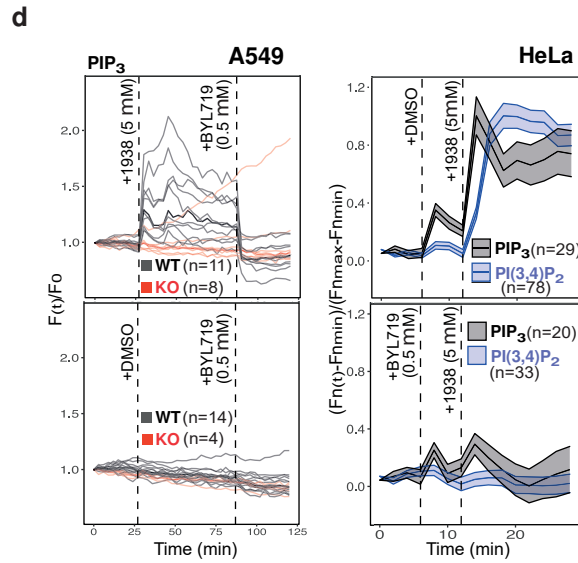
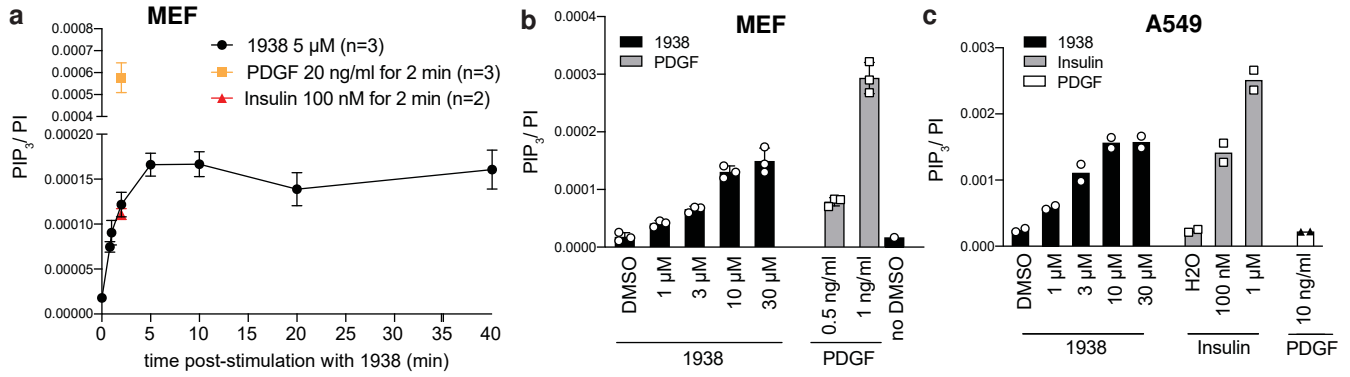
1922

1923 **Online content**

1924	1. Extended Data Figures 1-9
1925	2. Supplementary Figure 1-2
1926	3. Supplementary Tables 1-9
1927	4. Supplementary Videos 1-4







a Phosphosites reported to be regulated by:

- insulin / PI3K (LY294002) or AKT (MK2206) inhibitor
- mTOR inhibition
- △ PDK1 inhibition (GSK2334470)

